Alteration of Subsurface Basaltic Rocks and Glasses: Implications of Environmental, Chemical and Structural Properties on Fe Mobilization

Von der Naturwissenschaftlichen Fakultät der

Gottfried Wilhelm Leibniz Universität Hannover

zur Erlangung des Grades

Doktor der Naturwissenschaften (Dr. rer. nat.)

genehmigte Dissertation

von

Marius Stranghöner, M. Sc.

[2019]

Referent:	Prof. Dr. Harald Behrens (Leibniz Universität Hannover)
Korreferenten:	Prof. Dr. Axel Schippers (BGR, Hannover)
	PD. Dr. Stefan Dultz (Leibniz Universität Hannover)
Tag der Promotion:	07.08.2019

Acknowledgements

Abstract

Weathering of basaltic rocks and glasses plays a key role for the transport and geochemical cycling of elements between lithosphere and hydrosphere. Despite the vast number of scientific literature devoted to shed light on the complex mechanisms governing the alteration of silicate rocks and glasses and their significance for biotic and abiotic processes, some questions still remain unanswered. Within this dissertation the importance of volcanic islands for a potential high release of soluble Fe to ocean surface water is highlighted. It is furthermore demonstrated that microbial activity significantly contributes to the dissolution of basaltic rocks and glasses under certain environmental and substrate conditions and a strong relationship between the Fe redox state and thermal history of basaltic glasses and their dissolution behavior is emphasized.

The abundance of fresh and highly reactive rocks and glasses on volcanic islands together with their exposed location and high weathering rates make them candidates for increased supply of soluble Fe to surrounding ocean surface waters. Based on a case study on the island of Hawaii differentially altered subsurface basaltic rocks of the HSDP2 ICDP drill core were characterized with respect to Fe containing solid phases and their potential Fe release. It is shown that aging of secondary Fe solid phases in subsurface basaltic rocks of Hawaii is suppressed by adsorption of dissolved Si and other anionic species preserving their high reactivity towards dissolution. Based on this observation a high release of soluble Fe from subsurface rocks of Hawaii and potentially also from other volcanic islands is expected and thought to locally impact on the primary productivity in ocean surface waters.

The microbial alteration and Fe mobilization from the HSDP2 basaltic rocks was investigated using a single strain of *Burkholderia fungorum* as a model organism. Nutrient deficiency and attachment of microbial cells on basaltic glass surfaces promoted the microbial mediated dissolution. Moreover, quenched basaltic glasses showed increased dissolution during microbial alteration. Further investigations into the effect of thermal history on dissolution of basaltic glasses revealed that organic ligands are able to enhance in particular the dissolution of quenched basaltic glasses relative to annealed glasses of the same composition. Furthermore, it is shown that dissolution of basaltic glasses is affected by the Fe redox state and increases with increasing Fe(III) content. These findings allow for a better understanding of the relationship between the composition / structure of basaltic glasses and their dissolution behavior under certain (biotic and abiotic) environmental conditions.

Zusammenfassung

Die Verwitterung basaltischer Gesteine und Gläser spielt eine Schlüsselrolle für den Transport und den geochemischen Kreislauf der Elemente zwischen Lithosphäre und Hydrosphäre. Trotz der großen Anzahl an wissenschaftlicher Literatur, die sich mit den komplexen Mechanismen der Basaltverwitterung und ihrer Bedeutung für biotische und abiotische Prozesse befasst bleiben einige Fragen offen. Im Zuge dieser Dissertation wird die Bedeutung vulkanischer Inseln für eine potentiell hohe Freisetzung von gelöstem Fe in das Oberflächenwasser der Ozeane aufgezeigt. Weiterhin wird gezeigt, dass die mikrobielle Aktivität unter bestimmten Umgebungs- und Substratbedingungen erheblich zur Auflösung von basaltischen Gesteinen und Gläsern beiträgt. Dies legt einen starken Zusammenhang zwischen dem Fe Redoxzustand und der thermischen Vorgeschichte von Basaltgläsern mit ihrem Auflösungsverhalten nahe.

Vulkaninseln bestehen zum großen Teil aus frischen, sehr reaktiven basaltischen Gesteinen und Gläsern die sie in Kombination mit ihrer exponierten Lage und den damit verbundenen hohen Verwitterungsraten zu einer Lokalität für eine erhöhte Freisetzung von gelöstem Fe in das umgebende Oberflächenwasser der Ozeane machen. Basierend auf einer Fallstudie an der Insel Hawaii wurden unterschiedlich stark verwitterte Basaltgesteine des HSDP2 ICDP Bohrkerns im Hinblick auf Fe-haltige Festphasen und die potentielle Fe Freisetzung charakterisiert. Es wird gezeigt, dass die Alteration sekundärer Fe-haltiger Festphasen in Basaltgesteinen aus dem Untergrund von Hawaii durch Adsorption von gelöstem Si und anderen anionischen Spezies unterdrückt wird und dadurch ihre hohe Reaktivität gegenüber der Auflösung erhalten wird. Basierend auf dieser Beobachtung wird eine erhöhte Freisetzung von löslichem Fe aus Untergrundgesteinen von Hawaii und potentiell auch anderen vulkanischen Inseln erwartet, wodurch lokal die Primärproduktivität in Oberflächenwassern der Ozeane angetrieben wird.

Die mikrobielle Alteration und Fe Mobilisierung von HSDP2 Basaltgesteinen wurde unter Verwendung eines einzelnen Stammes des Bakteriums *Burkholderia fungorum* als Modellorganismus untersucht. Es wurde gezeigt, dass Nährstoffmangel und die Anhaftung von mikrobiellen Zellen auf Basaltglasoberflächen die Auflösung fördern. Weiterhin zeigten gequenchte Basaltgläser eine stärkere Auflösung während der mikrobiellen Alteration. Weiterführende Untersuchungen zum Einfluss der thermischen Vorgeschichte auf die Auflösung von Basaltgläsern zeigten, dass organische Liganden speziell die Auflösung von

gequenchten Basaltgläsern im Vergleich zu getemperten Gläsern der gleichen Zusammensetzung verstärken können. Es wurde ferner gezeigt, dass die Auflösung von Basaltgläsern durch den Fe Redoxzustand beeinflusst wird und mit zunehmendem Fe(III) Gehalt zunimmt. Diese Ergebnisse ermöglichen ein besseres Verständnis des Zusammenhangs zwischen der Zusammensetzung / Struktur von Basaltgläsern und ihrem Auflösungsverhalten unter bestimmten (biotischen und abiotischen) Umgebungsbedingungen.

Table of Contents

General Introduction

Weathering of silicate rocks and glasses has been extensively studied over the last decades but the entirety of participating processes and mechanisms and how they influence each other are yet not fully understood. The contribution of silicate rock weathering and its influence on geochemical element cycles [1], the chemical mass balance of the oceans [2,3], microbial life in the deep biosphere [4] atmospheric CO_2 drawdown [5], and soil formation [6] is of great significance and well documented. Furthermore, detailed knowledge of the processes governing silicate rock and glass dissolution is also of importance for industrial applications such as the geological storage of CO_2 [7,8], for the prediction of long term durability of nuclear waste glass [9,10] or fertilization of soils and ocean surface waters [11].

Volcanic Islands

Volcanic islands are widespread on the earth surface and their occurrence is coupled to volcanism at plate boundaries (e.g., mid-ocean ridges), subduction zones (e.g., Aeolian islands), and hot spots (e.g., Hawaii emperor chain). Taking all these volcanic settings together, an annual global extrusive magma production rate of 6-8 km³ is proposed of which 1 km³ is basaltic glass [12,13]. Young volcanic islands such as Hawaii comprise fresh and highly reactive volcanic rocks and glasses that are susceptible to weathering [5]. The lifetime of volcanic islands is strongly coupled to the magma supply from depth and can be divided in 7 stages of development [14]. The island of Hawaii is supposed to be in stage 5 with continuous declining volcanic activity [15]. As soon as the erosion rate exceeds the growth rate the volcanic island submerges (stage 6) and remains as a seamount (stage 7).

In high nitrate, low chlorophyll regions such as the Southern Pacific Ocean the primary productivity is limited by Fe deficiency [16]. The supply of growth limiting nutrients (e.g. Fe) to this regions strongly influences the primary productivity and facilitate seasonal phytoplankton blooms which in turn control atmospheric CO_2 drawdown into the oceans [17,18]. Among the major sources discussed for the supply of soluble Fe to the oceans are volcanic ashes and seasonal dust storms [19], hydrothermal activity [20], and advection from continental margins [21]. However, increased supply of soluble Fe to ocean surface waters was also observed in the vicinity of volcanic islands such as Hawaii in the Pacific Ocean and Kerguelen and Crozet in the Indian Ocean [22–24]. Here subsurface weathering of the rocks predominate since surface erosion by streams is ephemeral [25]. This is supported by Schopka and Derry [26] who proposed that the majority of weathering products on young volcanic islands are transported via

submarine groundwater discharge to the ocean. However, the contribution of volcanic islands for at least local supply of soluble Fe to ocean surface waters is still under debate and not fully understood.

Basaltic Rocks and Glasses

Among the silicate rocks, basalts are the dominant rock type covering about 60% of the earth surface [27]. Basaltic rocks usually consist of SiO_2 < 55 wt.% and FeO_{tot} > 10 wt.% and their composition can range between 100% glass to fully crystallized basalts with fine grained plagioclase, pyroxene and olivine being the dominant mineral phases. Furthermore, their morphology changes depending on the conditions during eruption from dense basaltic flows (low vesicular) to highly porous scoria (highly vesicular). When cooling of the hot lava is fast enough (e.g., in contact with water), crystallization is suppressed and basaltic glass is formed. Basaltic rocks with high glass contents are pillow basalts and hyaloclastites. Staudigel and Hart [28] predicted that ~20% of the upper oceanic crust are made up by basaltic glass.

Besides of environmental influences the composition and thermal history of basaltic glasses have important controls on their dissolution behavior. Basaltic glasses are mainly built up by the network forming cations Si, Al and Fe(III) which cross-link the network by formation of Si-O-Si, T-O-Si and T-O-T bonds (T = Al, Fe(III)) and polymerize the glass structure. Thus, it is hardly surprising that dissolution rates of silicate glasses increase with increasing SiO_2 content from basaltic (< 55 wt.% SiO_2) to rhyolitic (> 70 wt.% SiO_2) compositions [29]. However, an increase in the Al and Fe(III) content of the glass does not necessarily increase its chemical stability [30]. Alkali (K, Na) and alkaline earth metals (Ca, Mg) as well as Fe(II) act as network modifiers that first charge compensate AlO_4^- and FeO_4^- tetrahedral sites and, upon their saturation, induce the disruption of the glass network structure by formation of non-bridging oxygens [31].

The thermal history has important controls on the molecular structure of glasses e.g., lower density, higher structural disorder and strained chemical bonds for rapidly quenched glasses [32,33]. Natural basaltic glasses show a wide range of cooling rates from 0.1-2.3 K/s for glassy surfaces of air quenched lava flows [34] and 0.1-72 K/s for submarine hyaloclastites and glassy margins of pillow basalts [35] up to $10^{5.31}$ K/s for hyperquenched basaltic glass from Loihi Seamount [36]. The influence of the cooling rate on dissolution of basaltic glasses is poorly determined. However, some literature for technical glasses such as soda-lime and borosilicate

compositions exist and has recently demonstrated a decreased glass durability with increasing cooling rates from annealed to quenched glasses [37–39].

Iron (Fe)

Fe is the fourth most abundant element in the earth crust and an essential nutrient for all living organisms. In nature, it occurs predominantly in its two oxidation states as either Fe(II) or Fe(III). Fe(II) is found in primary (magmatic) minerals such as olivine [Mg,Fe(II)]$_2$SiO$_4$ and pyroxene [Ca,Mg,Fe(II)]$_2$Si$_2$O$_6$, but also in secondary minerals such as pyrite FeS. Despite of Fe(III) bearing primary minerals such as magnetite Fe$_3$O$_4$, Fe(III) is most abundant in secondary minerals (e.g., hematite Fe$_2$O$_3$, goethite FeO[OH]). In basaltic glasses Fe occurs in its two oxidation states Fe(II) and Fe(III) with mean Fe(II)/Fe$_{tot}$ ratios from 0.93 to 0.85 ($\pm$0.03) [40]. As a result of its two oxidation states and its high abundance on the earth surface, the Fe(II)-Fe(III) redox couple is of great importance for biological and chemical processes [41]. However, under natural conditions dissolved Fe(II) and Fe(III) are not stable under oxic conditions and elevated pH, respectively. Complexation with organic ligands increases the (bio)availability which is shown to occur for 99.9% of the dissolved Fe in natural waters [42,43]. In natural ocean waters the (bio)availability of Fe is nevertheless limited with mean concentrations in the range of a few nM to tens of nM and strongly influenced by mineral species and particle size [24,44].

Weathering of Basaltic Rocks and Glasses

Volcanic rocks are thermodynamically unstable under ambient conditions and in aqueous environments and their alteration strongly impact on element transfers in aquatic and terrestrial systems. Weathering of basaltic glass is about 10 times faster compared to crystalline basalt [45]. Dissolution of silicate minerals and glasses proceeds via a multiple step mechanism [46]: (i) the fast removal of alkali (Na, K) and alkaline earth (Ca, Mg) metals by a metal-proton exchange reaction (particularly H$^+$ at low pH) and formation of a leached layer followed by (ii) protonation of network forming species (Al, Fe(III)) and break-up of T-O-Si bonds (T = Al, Fe(III)) and formation of partially liberated Si tetrahedra and (iii) the transport of hydrolyzed species to solution leading to the destruction of the glass network. However, the rate limiting step for the complete dissolution of the glass is the breakup of the slowest breaking bond which, for silicate glasses are Si-O-Si bonds [46]. In aqueous environments formation of a hydrous Si-rich alteration layer (called palagonite) is often observed on surfaces of glasses that

has a protective effect and dramatically slows down dissolution rates [9,10,47,48]. The process is most affected by the mineralogy of the rock [49] and the availability of pathways for the transport of the solution in- and dissolved elements out of the rock [50,51]. Fractures inside rocks together with high connected porosities facilitate fast movement of waters and accelerate mineral and glass dissolution but limit secondary phase precipitation [52]. Moreover, environmental influences such as solution composition, pH/Eh, temperature, and organic ligands control the bulk chemical exchange between the rock and environment [53–57].

Depending on the environmental conditions and the extent of weathering dissolved elements are either leached or precipitated as secondary phases. For instance, Fe released at circumneutral pH from the dissolving basalt is precipitated in the form of Fe (oxyhydr)oxides. Typical alteration products are various types of smectites, zeolites and Ca-silicates (e.g., phillipsite) with variable crystallinities [58–60]. Palagonite, the common alteration product evolving at the glass-water interface of pillow basalts, is a hydrous and heterogeneous Fe-rich material consisting of mixtures of amorphous to poorly crystalline clays, zeolites and (oxyhydr)oxides [61]. The mobility of Fe from these secondary phases is controlled by their crystallinity (= reactivity) that changes with time due to aging and structural rearrangement into thermodynamically more stable phases [62]. With an increase in the structural order of the secondary phases the susceptibility of Fe for the transfer to solution decreases. However, the high reactivity of secondary phases towards dissolution can be preserved by adsorption of anions and organic ligands which are highly abundant in seawater [63,64].

Microbial Alteration

Over the past 20 years the deep biosphere within the oceanic crust has gained increasing attention and, since then, the knowledge has steadily expanded [65]. Microorganisms are ubiquitous on the earth surface and their contribution to silicate rock and glass alteration processes is widely accepted. Granular and tubular alteration textures along preexisting cracks were observed in young (6 Ma) as well as old (70 Ma) basaltic rocks of the oceanic crust and interpreted as remnants of microbial activity [66]. Moreover, the dimension of these granular alteration textures is often congruent with the size of bacterial cells [65]. Recently, Fisk et al., [67] proposed that microbial cells act as gateways in tubular alteration textures and facilitate the flux of protons and ions between the solution and glass. Despite of these findings there is still controversy about the biotic origin of such textures [68]. Active sub-seafloor endolithic microbial communities in the oceanic crust were observed to extent to depth of at least 380 mbsf and

temperatures up to 100°C contributing to about 60 to 85% of the total glass alteration [65,69]. Microbial alteration features have also been witnessed in basaltic glasses of subsurface volcanic rocks of the HSDP2 drill core [70]. The effectiveness of microbial mediated dissolution depends on several factors such as the chemical composition of the host rock [71], its porosity and specific surface area [65,72] as well as temperature and solution properties [73].

Redox sensitive elements such as Fe and Mn play a key role for energy yielding microbial metabolic reactions. Chemolithoautotrophic microorganisms are able to gain energy through either the use of Fe(II) as an electron donor (FeOB) and Fe(III) as an electron acceptor (DIRB) which causes the Fe to be mobilized or precipitated, respectively, depending on the environmental conditions [74–76]. Laboratory experiments and field observations have shown that basaltic rocks, enriched in bio-essential nutrients such as Fe(II) and Mn(II), are a potential energy source for a variety of microorganisms [75,77]. Moreover, it is well known from laboratory experiments that microorganisms attach to glass surfaces and produce microenvironments in which the pH conditions are dramatically different from the surrounding environment [78]. Here, organic acids and siderophores are of great importance as they chemically modify the rock matrix, increase reaction rates and accelerate glass and mineral dissolution [79–82]. This finding is in accordance with observation from seafloor basalts of which the abundance of cells is by 3-4 orders of magnitude higher than in the surrounding seawater suggesting that they actively participate in rock weathering rather than using elements released during abiotic weathering [83,84].

Outline of the Study

Despite of its great importance the mechanisms by which Fe is released from basaltic rocks and glasses under biotic and abiotic conditions and its transport to the environment are complex and yet not fully understood. The objectives of this dissertation were the investigation of differentially altered rock samples of the HSDP2 ICDP drill core together with synthetic basaltic glasses of the same composition addressed to the following questions:

I.   How do environmental influences affect the secondary phases assemblage of differentially altered subsurface basaltic rocks? What is the capacity of these rocks with respect to the release of soluble Fe to ocean surface waters?

II.   What is the possible contribution of microorganisms to the Fe mobilization from basaltic rocks and glasses? Does a relationship between the chemistry / structure of the substrate and microbial activity exist?

III.   What are the effects of varying Fe redox states and thermal histories on basaltic glass dissolution at far from equilibrium conditions and in the presence of organic ligands?

Referring to these questions, the dissertation comprises three chapters (all with Marius Stranghöner as first author) including one publication published in a peer-reviewed journal and two manuscripts being prepared for submission.

Chapter I - Implications of Subsurface Basaltic Rock Alteration on the Supply of Soluble Fe to Ocean Surface Waters - a Study on ICDP Site Hawaii.

Chapter I offers insights into the potential release of soluble Fe from secondary Fe solid phases of subsurface basaltic rocks of an active volcanic ocean island (Hawaii). A sequential extraction was performed on 83 natural basaltic rocks and the results related to rock specific parameters such as the Fe redox state and specific surface area. About 2/3 of the Hawaii Scientific Drilling Project Phase2 (HSDP2) drill core rocks comprised elevated contents of easy mobilizable Fe located in free Fe (oxyhydr)oxides. A potential (local) contribution of volcanic islands for the supply of soluble Fe to ocean surfaces waters is suggested.

> *Chapter I („Implications of subsurface basaltic rock alteration on the supply of soluble Fe to ocean surface waters - a study on ICDP site Hawaii”) is currently being prepared for publication with **Marius Stranghoener** as first author. Stefan Dultz, Harald Behrens and Axel Schippers represent co-authors.*

Chapter II - Experimental Microbial Alteration and Fe Mobilization from Basaltic Rocks of the ICDP HSDP2 Drill Core, Hilo, Hawaii.

Chapter II is aimed towards a better understanding of the contribution of microorganisms to the alteration of basaltic rocks and glasses. On the basis of biotic and abiotic batch dissolution experiments a strong relationship between environmental influences (e.g., nutrient-limiting conditions) and surface attachment of microbial cells is emphasized. Moreover, it is shown that *Burkholderia fungorum* is capable of obtaining essential nutrients directly from the basaltic glasses and demonstrate that the substrate chemical and structural composition can influence microbe-surface interactions.

> ***Stranghoener, M***., *Schippers, A., Dultz, S., Behrens, H. (2018): Experimental microbial alteration and Fe mobilization from basaltic rocks of the ICDP HSDP2 drill core, Hilo, Hawaii. Front. Microbiol. 9:1252. doi:10.3389/fmicb.2018.01252.*

Chapter III - Far from Equilibrium Basaltic Glass Alteration: The Effect of Fe Redox State and Thermal History on Dissolution Rates.

Chapter III makes an attempt to relate structural and chemical properties of basaltic glasses to their dissolution behavior. Percolation experiments at far from equilibrium conditions were performed with synthetic basaltic glasses of varying Fe redox states and thermal histories. The dissolution of these glasses with respect to Fe(II)- and Fe(III)-rich compositions was investigated and the importance of the thermal history for the long term dissolution of basaltic glasses in the presence of organic ligands highlighted.

> *Chapter III („Far from equilibrium basaltic glass alteration: The effect of Fe redox state and thermal history on dissolution rate") is currently being prepared for publication with **Marius Stranghoener** as first author. Stefan Dultz, Harald Behrens and Axel Schippers represent co-authors.*

Chapter I

Implications of Subsurface Basaltic Rock Alteration on the Supply of Soluble Fe to Ocean Surface Waters - a Study on ICDP site Hawaii.

Marius Stranghoener[1], Stefan Dultz[2] and Harald Behrens[1], Axel Schippers[3]

[1] *Institute of Mineralogy, Leibniz Universität Hannover, Hanover, Germany*
[2] *Institute of Soil Science, Leibniz Universität Hannover, Hanover, Germany*
[3] *Geomicrobiology, Federal Institute for Geosciences and Natural Resources, Hanover, Germany*

Abstract

The potential for the release of Fe from subsurface basaltic rocks of the Hawaii Scientific Drilling Project Phase 2 (HSDP2) drill core was investigated to elucidate the contribution of volcanic islands to the geochemical Fe budget of ocean surface waters. Rock specific parameters possibly governing Fe release such as Fe redox state, the specific surface area (SSA) and connected porosity were determined. Furthermore, a four step sequential extraction with increasing strength of the extractant (from deionized H_2O (Fe_{H2O}) and solutions of citrate bicarbonate (Fe_{CB}), oxalate (Fe_o), and dithionite citrate bicarbonate (Fe_d)) was applied. With this method the type of chemical bonding of Fe was determined that is a prerequisite for its release from the basaltic rocks. Amorphous and crystalline, free Fe (oxyhydr)oxides were identified by their Fe_o/Fe_d ratio.

Basaltic rocks with different weathering degree showed elevated Fe(III) contents with $Fe(II)/Fe_{tot}$ ratios ranging from 0.82 to 0.42. Highest SSAs, increasing with depth, were observed for hyaloclastites with maximum values of 70 m²/g. Both parameters depended mainly on the alteration state that is more strongly affected by the fluid chemistry (freshwater↔seawater) than by the age of the rocks. The extractions revealed that submarine rocks comprise elevated amounts of Fe_{H2O} as well as Fe_o in comparison to rocks exposed to freshwater. In contrast, the latter showed secondary phases of higher crystallinity (Fe_d). Indication was obtained that aging of secondary Fe phases was suppressed in submarine rocks most probably by the adsorption of anions stemming from the meteoric- or seawater. Here, extractions indicated a strong interaction of silica with secondary phases.

Hyaloclastites and pillow basalts showed highest contents of Fe located in free Fe (oxyhydr)oxides with up to 19% and 16% of the total Fe content of the rock, respectively. The investigations revealed the presence of (i) highly reactive Fe phases ($Fe_o/Fe_d > 0.85$) within basaltic rocks altered by seawater and (ii) Fe phases of higher crystallinity ($Fe_o/Fe_d < 0.70$) for freshwater altered rocks. Thus, a potential high Fe release from basaltic rocks altered under seawater dominated conditions can be expected. It is therefore likely that subsurface basaltic rocks of volcanic ocean islands that were altered in the submarine environment are, so far, an underestimated and additional source for increased Fe supply to ocean surface waters.

1.1 Introduction

The processes of subsurface basalt weathering under various environmental conditions and the release of chemical constituents are of great importance for the geochemical cycles between hydrosphere, lithosphere and atmosphere. Basaltic rocks, covering about 60% of the Earth's surface [27], are Fe rich (up to 15 wt.% FeO) and are by far more susceptible to alteration than felsic rocks due to their relatively low SiO_2 content [29]. Furthermore, basaltic rocks can contain large amounts of basaltic glass that formed during rapid cooling of the erupted lava by contact with water or air and is more vulnerable to chemical weathering. Hence, weathering and chemical fluxes of solutes from crystalline rocks (e.g., massive basalts) are different to those containing glass (e.g., pillow basalts, hyaloclastites) [49].

Fe is known to be a limiting nutrient for microbial and especially phytoplankton growth and, hence, influencing CO_2 sequestration into the oceans [16,79,85]. The solubility of Fe in natural fresh- and seawaters and therefore its mobility depends on several environmental factors (e.g., pH, oxygen availability, redox potential, the presence of organic ligands) and the petrographic characteristics of the source, (e.g., rock type, secondary mineral assemblage, porosity, pore connectivity). Despite the various sources effective for Fe supply to the ocean surface waters (e.g., aeolian dust, hydrothermal activity), volcanic islands comprising fresh, porous, and chemically reactive basaltic rocks are together with their water cycles a potential source for increased Fe release and supply to ocean surface waters. Here it is assumed that Fe acts as a growth limiting nutrient causing annual algae blooms in the oceans [17,22]. However, subsurface rock alteration is the major source for the transport of chemical constituents of volcanic islands and seamounts to the oceans but their contribution to the global chemical budget of the hydrosphere is poorly understood [18,25,26].

9

Alteration of basaltic rocks is mainly affected by the mineralogy of the primary rock [49,59,86], its specific surface area (SSA), and connected porosity [87–89] as well as the chemistry and flow rate of the interacting fluid [7,90,91]. In addition to inorganic effects, microorganisms have also been shown to contribute to subsurface weathering processes of basaltic rocks and glasses [4,69,92]. Fe(II) released from primary minerals and glasses during weathering under oxygenated conditions is rapidly oxidized to Fe(III) and precipitated in the form of secondary (mainly amorphous) Fe bearing solid phases. Once bound, the mobility of Fe is controlled by the solubility of the secondary mineral phases [49]. Early Fe bearing phases (e.g., ferrihydrite) have high SSA comprising highly reactive sites for the sorption of metals, organic matter or nutrients [93]. However, as they are thermodynamically unstable, transformation into more stable and ordered crystalline Fe oxides such as goethite/hematite takes place and therefore decreases their reactivity and hereby also the susceptibility of Fe release to solution [94]. This process is known as Ostwald ripening sequence [62].

The transformation pathway could be altered depending on changing environmental conditions such as the solution chemistry (e.g., freshwater↔seawater). It is well known that anionic organic ligands, having a high affinity for Fe oxide surfaces, can impede crystallization of ferrihydrite by adsorption on reactive surface sites preventing hereby crystallization and/or dissolution [63,95,96]. Besides of organic ligands, silica was shown to inhibit the Fe(II) catalyzed transformation of instable Fe(III) (oxyhydr)oxides and hereby preserving its high reactivity [97]. In the presence of sulfate which is abundant in seawater, the formation of poorly ordered Fe (oxyhydr)oxides is favored [64]. Furthermore, Tomaszewski et al., [98] and Thompson et al., [99] have shown that even in the absence of stabilizing agents (e.g., silicic acid), ferrihydrite can persist under dynamic redox conditions (e.g., wetlands, tidal areas) providing reactive surfaces, e.g., for sorption of nutrients such as phosphate anions.

Based on the type of chemical bonding secondary phases can be distinguished into easily soluble, amorphous/weakly crystalline and well crystalline species. Characterization of the type of chemical bonding of Fe in secondary phases thus allows estimations on its reactivity and potential release to the environment. In this context, Canfield [100] defined and used the term "reactive Fe" to describe the reactivity of various Fe bearing phases toward sulfide in marine sediments. Furthermore, sequential extraction schemes have been developed to provide information on the potential Fe release from different secondary phases under simulated environmental conditions ([101] and literature therein). Here, the ratio of amorphous to crystalline Fe (oxyhydr)oxides, defined as activity of free Fe oxides (Fe_o/Fe_d), is often used as

an important measure for the progress of weathering and the reactivity of Fe in secondary Fe bearing solid phases [44,100]. The amount of Fe that is possibly available can be estimated by comparing Fe released during the sequential extraction to the total amount of Fe in the rock.

Despite that numerous studies have been devoted to weathering of basaltic rocks [46,102,103] the chemical budget of fluid-rock interactions [28,104] and secondary mineral formation [56,59,90], little is known about the potential subsurface Fe release from volcanic islands and the transfer to ocean surface waters. Within this study, the potential Fe release from different subsurface basaltic rocks of an active volcanic island (Hawaii) was investigated considering hereby freshwater as well as seawater conditions. Furthermore, different Fe-containing secondary phases were characterized along the entire length of the Hawaii Scientific Drilling Project Phase 2 (HSDP2) drill core and elucidated how different rock specific parameters (crystallinity of secondary phases, SSA, Fe redox state, porosity) contribute to- and influence the release of Fe from these subsurface rocks.

1.2 Site Description

The island of Hawaii is part of the Hawaiian emperor chain comprising the five main islands and more than 100 seamounts. All of them are of volcanic origin, formed by mantle plume activity. The island of Hawaii is the youngest, largest and the only one with active volcanism. Fig. 1-1a shows a simplified overview of the drilled lithologies of the International Continental Scientific Drilling Program (ICDP) HSDP2 drill core [105]. The hole was drilled to a total depth of 3098 meter below sea level (mbsl) including subaerial (from surface to 1079 mbsl) and submarine (from 1079 to 3098 mbsl) erupted volcanic rocks. Subaerial rocks can be distinguished by `a`a-, pahoehoe- and transitional lavas (in the following summarized as basaltic flows) and to a minor extend massive basalts. Below the subaerial/submarine transition basaltic flows are absent and massive basalts, pillow basalts and hyaloclastites dominate with some minor intrusive rocks.

The oldest lavas close to the bottom of the borehole at 2798 mbsl have, based on ^{40}Ar-^{39}Ar dating, an estimated age of 683±82 kyr [106]. Despite of their age, basaltic rocks from the drill core are relatively fresh (= moderately altered) based on the presence of less stable olivine and basaltic glass [58]. Alteration of core rocks is mostly restricted to fractures and vesicles with abundant neoformation of smectite (± Fe (oxyhydr)oxides) and various types of zeolites [58,105].

The majority of dissolved products from weathering reactions on the island of Hawaii are not transported via rivers to the ocean but by submarine groundwater discharge as a consequence of highly permeable volcanic rocks [26]. The subsurface fluid flow of Hawaii through the different lithological units (i), (ii), and (iii) is complex and yet no fully understood (Figure 1-1b). The freshwater-seawater boundary was found at ~600 mbsl and describes a major change in the fluid chemistry. However, some of the deep aquifers had salinities lower than seawater [107] and are assumed to result from topographically driven downward flow of freshwater to greater depth, which is common for volcanic ocean islands with high elevation differences [108]. This indicates that a connection exist with the surface near freshwater system [109]. Hypersaline aquifers are present and discussed to result from less permeable units or are entrapped by dikes [26,109].

In general, the fluid flow in unit (i) is directed primarily downward whereas fluids in units (ii) and (iii) flow upward due to heating and buoyancy differences. Subaerial erupted rocks from surface to 1079 mbsl are highly vesicular and fluids (mainly from meteoric recharge) are

transported relatively unimpeded (i). With transition to the submarine erupted rocks at 1079 mbsl fluid transport is mainly controlled by the porosity of the hyaloclastites and the abundance of less permeable massive basalts and, at greater depth, also dense intrusive rocks that can act as fluid barriers (ii). Pathways and flow rates can slow down by either complete cementation or partially clogging of pores due to secondary mineral precipitation. At depth > 2000 mbsl fluids are transported mainly through fracture systems within pillow basalts (iii).

Bore hole temperatures measured during drilling where found to be surprisingly low with ~13°C at depth of 1600 mbsl. Below this depth the temperature gradient slowly increased with 19 °C/km to 45°C at depth of ~3098 mbsl (Figure 1-1c). Such low temperatures indicate fast exchange in the circulating groundwater systems that may be responsible for the moderate alteration of rocks observed in the drill core [58,107].
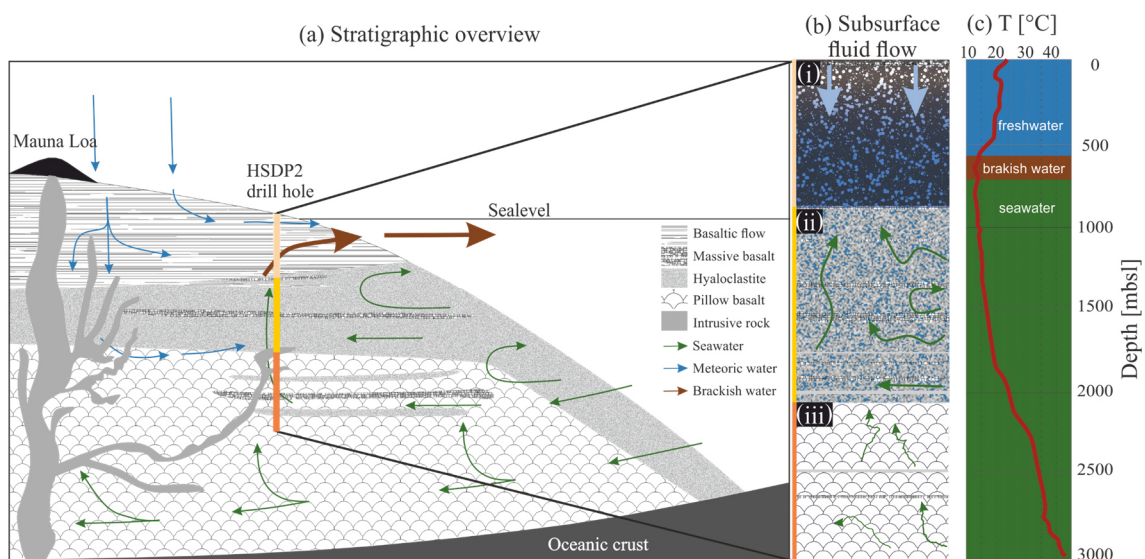
FIGURE 1-1: *Scheme of the island of Hawaii showing the stratigraphy and subsurface fluid flow and temperatures. (a) Stratigraphic overview with the bore hole location, main lithologies and groundwater flow. (b) Different subsurface fluid flows through (i) highly vesicular basaltic flows, (ii) porous and partially cemented hyaloclastites and (iii) fractured pillow basalts. (c) Downhole temperatures measured in the HSDP2 bore hole (modified after [105]).*

1.3 Material and Methods

1.3.1 Primary Minerals and Textures

Samples of the ICDP HSDP2 drill core were achieved from the repository at the American Museum of Natural History in New York. 83 different basaltic rock samples of various sampling depths comprising all major lithology's were investigated.

A detailed petrographic description of mineral abundances and textures of HSDP2 drill core samples is given by Garcia et al., [105]. Regardless of the rock types, all samples contain olivine, plagioclase and clinopyroxene pheno- and microphenocrysts in different proportions. Mg-rich olivine (with 9-18% Fe_2SiO_4) is by volume the dominant mineral phase within the phenocrysts in all rock types with highly variable contents but means of 6.9 vol.% (intrusive rocks), 9.7 vol.% (hyaloclastites), 12.6 vol.% (pillow basalts), 12.7 vol.% (basaltic flows), and 16.5 vol.% (massive basalts) [105]. Plagioclase and clinopyroxene pheno- and microphenocrysts are present but their proportions are usually < 1 vol.% in all rock types. Thus, the proportion of groundmass in the rocks depends mainly on the olivine abundance and is therefore highest for intrusive rocks (Ø 93 vol.%) with low phenocryst contents. The groundmass is composed either of cryptocrystalline plagioclase ± Fe-Ti oxides (basaltic flows, massive basalts, intrusive rocks) or basaltic glass (hyaloclastite, pillow basalts). Vesicularity ranges from highly vesicular basaltic flows (Ø 9.7 vol.%) to medium vesicular hyaloclastites (Ø 3.5 vol.%) to low vesicular intrusive rocks (Ø 0.7 vol.%) [105]. Despite mineralogical and textural differences between the rock types, the Fe content is relatively constant and ranges between 12 to 14 wt.% Fe_2O_3 [110].

1.3.2 Alteration and Secondary Minerals

Garcia et al., [105] also described the alteration of HSDP2 core rocks by using an alteration index (AI) after Quane et al., [111] which (1) refers to unaltered rocks and (5) to extensive matrix alteration and complete replacement of olivine by iddingsite. Subaerial rocks are somewhat less altered than submarine rocks, which could be easily explained by their age. However, there is no clear trend for increasing alteration with core depth. Alteration is mostly restricted to fractures (pillow basalts) or vesicles (basaltic flows) leaving major portions of the rocks relatively fresh to moderately altered. Low groundwater temperatures and short residence times of the rocks at the surface made significant contributions to the low alteration state of the basaltic rocks [58,105].

Walton and Schiffman [58] were the first to describe the alteration of the HSDP2 core rocks with special emphasis on hyaloclastites. Based on the first occurrence of secondary mineral paragenesis, hyaloclastites were divided in zones of incipient (1080 to 1335 mbsl), smectitic (1405 to 1573 mbsl), and palagonitic (or normal) (1573 to the deepest sample) alteration. Palagonite is usually known to be an intermediate phase in the evolution of basaltic glass to smectite [61]. Here, on the other hand, smectites formed by replacing olivine and plagioclase

grains without evidence of extensive palagonite rim development during smectitic alteration. Fe released during alteration of primary minerals is either retained in secondary phases or transferred to solution. Typical alteration products throughout the drill core are various forms of smectites (13.34±4.33 wt.% Fe_2O_3), palagonite (14.88±4.24 wt.% Fe_2O_3), and zeolites such as chabazite and phillipsite [2]. Furthermore, indications for microbial activity in hyaloclastites of the HSDP2 drill core were obtained based on tubules between unaltered glass and secondary phases that possibly have formed by microbial activity during the incipient stage of alteration [58,112].

1.3.3 Preparation of Core Rocks

Basaltic rock samples were gently crushed in an agate mortar. In this way it was tried to carefully break down the samples into small particles < 2 mm without grinding to avoid generation of fresh cleavage planes that might induce high Fe release not observed in the original samples [113]. The crushed samples were dry sieved to obtain 0.063-2 mm grain fractions for determination of soluble Fe fractions and SSA. It has to be noted that fine particles, which might adhere to the surface of larger grains were not removed by washing the samples with H_2O as the first step of the sequential extraction involves the determination of the water soluble fraction. Part of the 0.063-2 mm fraction was ground further for the Fe(II)/Fe_{tot} determination in an agate mortar to produce a fine and homogeneous rock powder sieved to grain sizes < 63 μm. Grinding was done shortly before measurements to prevent oxidation of the sample material due to the high reactive surfaces. For the molten alloy intrusion large pieces of selected samples were used and obtained either by drilling of small (Ø 7 mm) cores or, for brittle samples, by using larger fragments.

1.3.4 Fe Redox State, Specific Surface Area and Pore Space Characteristics

The redox state of the samples was determined by a wet chemistry method according to Schuessler et al., [114]. Samples were decomposed in a solution of 40% HF, 1 M H_2SO_4 and ~14.1 μmol NH_4VO_3. The reaction of released Fe(II) with V^{5+} follows Eq. 1-1

$$Fe^{2+} + 2H^+ + VO_2^+ \rightleftharpoons Fe^{3+} + H_2O + VO^{2+} \qquad \text{Eq. 1-1}$$
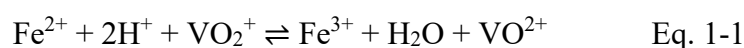
The V^{5+} is used as an oxidant for released Fe(II) preventing its uncontrolled oxidation due to free oxygen. After complete dissolution, the pH was increased shifting the equilibrium of Eq. 1-1 to the left side. Thereafter, 2,2′-bipyridine was added forming a coloured

Fe(II) bipyridine-complex whose absorption was used to measure the Fe(II) content. The total Fe (Fe$_{tot}$) was determined in the same solution after complete reduction of Fe(III) by hydroxylamine hydrochloride. Bulk rock samples including Fe derived from basaltic glass, minerals (e.g., olivine) and secondary alteration phases were used for this analysis. The absorbance measurements of the solutions were done with a SHIMADZU UV-1800 Spectrometer. The Fe redox state of each sample was measured from three individual batches and a standard deviation was calculated.

The SSA of core samples was determined using a multi-point N$_2$ adsorption BET isotherm. The 0.063-2 mm fraction was degassed at 65°C for ~24 h under vacuum and subsequently mounted on the instrument for measurement (Quantachrome Nova 4000e).

Visualization of the connective pore space (pores > 5 nm), and secondary phases in pores was done by intrusion of a molten alloy. Using Wood's metal, an alloy composed of Bi$_{50}$Pb$_{25}$Zn$_{12.5}$Cd$_{12.5}$ has the advantage of a low melting point (78°C), which can therefore be easily liquefied/solidified at low temperatures [115]. Representative samples of each rock type were selected based on the following criteria: the alteration index (AI), the SSA and the total amount of Fe released during the sequential extractions. The sample was placed in a small Teflon tube, spilled with the molten alloy, loaded in an autoclave, evacuated and the molten alloy intruded at ~100°C by applying an argon pressure of ~550 bar for 10 minutes. Samples were isobarically cooled < 40°C and polished sections prepared for further analysis by scanning electron microscopy (SEM type JEOL JSM-7610FPlus). Quantification of the intruded pore space was done on the BSE images using the software ImageJ.

1.3.5 Sequential Extractions

A four-step sequential extraction modified after [113] was used to characterize the type of chemical bonding of Fe, Si, Al, and Mn within secondary phases of basaltic rocks from the HSDP2 drill core. Sequential extractions are routinely used in soil science for the characterization of element mobility in soils, sediments or mine tailings [113,116,117]. As it was shown by many authors, the outcome of an extraction procedure is strongly influenced by the sample pretreatment (storage, grinding), the duration and the temperature at which the extraction is performed as well as the solid/solution ratio of the extracting agent and the sample material [113,116]. These influences were minimized by applying exactly the same experimental conditions including sample preparation for all samples. The steps involved extraction of 1 g

of basaltic rocks of the 0.063-2 mm fraction with (i) deionized H_2O, (ii) sodium citrate bicarbonate, (iii) ammonium oxalate, and (iv) dithionite citrate bicarbonate (Table 1-1).

Extractions (i)-(iii) were carried out on a horizontal shaking table at 105 rpm for different time intervals. After each extraction step the samples were centrifuged and the clear supernatant decanted in volumetric flasks. The residue from (i), (ii), and (iii) was washed with deionized H_2O and 0.1 M $MgSO_4$ solution for (iv). After centrifugation, the supernatant was added to the initial extract. For the last step (iv) the tubes were placed in a water bath, heated to 75°C and each 0.5 g sodium dithionite powder were added and thoroughly stirred. After 15 min the samples were centrifuged and the supernatant decanted. The whole procedure was repeated twice and the solutions combined. Released Fe, Si, Al, and Mn were measured for all extractions by Inductively Coupled Plasma Optical Emission Spectroscopy (ICP-OES, Varian 725-ES). Extractions for selected samples were performed in duplicates and deviations between individual extractions were found to be < 5%.

TABLE 1-1: *Sequential extraction procedure after* [113].

Extraction	Fraction	Extractant	Volume [ml]	Time [h]	T [°C]
X_{H2O}*	(i) Water soluble	Deionized H_2O	20	2	25
X_{CB}	(ii) Exchangeable	0.3 M trisodium citrate + 0.1 M sodium bicarbonate	20	20	25
X_{Ox}	(iii) Bound to amorphous Fe oxides	0.2 M oxalic acid + 0.2 M ammonium oxalate	10	2	25
X_{DCB}	(iv) Bound to crystalline Fe oxides	0.3 M trisodium citrate + 0.1 M sodium bicarbonate + 0.5 g sodium dithionite	2x 25	2x 0.25	75

*X refers to Fe, Si, Al or Mn

1.4 Results

1.4.1 Fe Redox State, Specific Surface Area and Pore Space Geometry

From the diagram of the mean Fe redox state vs. depth it could be deduced that the majority of basaltic rocks showed incipient to moderate degrees of alteration (Figure 1-2a; igneous $Fe(II)/Fe_{tot}$ after [118]). Samples from subaerial erupted basaltic flows showed a wide range of Fe redox states with some being close to primary igneous values ($Fe(II)/Fe_{tot} = 0.89$) and others relatively oxidized ($Fe(II)/Fe_{tot} = 0.38$). The most oxidized samples were located in the freshwater saturated zone. Submarine erupted massive basalts ranged between $Fe(II)/Fe_{tot} = 0.79$ to 0.59. There was no distinctive trend for massive basalts, pillow basalts and intrusive rocks to become more oxidized with increasing sample depth. The Fe redox state of these rocks ranged between 0.89 to 0.55. A distinct trend was only observed for hyaloclastites. Here, the $Fe(II)/Fe_{tot}$ ratio decreased with increasing sample depth from 0.82 (1250 mbsl) to 0.57 (2780 mbsl).

The SSA of subaerial erupted basaltic flows ranged between 1 and 46 m²/g (Figure 1-2b). There was no relationship between the SSA and the sample depth for basaltic flows but for some of the samples the SSA noticeable increased in the freshwater saturated zone. The SSA of massive basalts did not significantly change with depth and ranged between 1 and 9 m²/g. Considering hyaloclastites, the SSA generally increased with sampling depth from 4 m²/g (1233 mbsl) to 69 m²/g (2893 mbsl). The increase was not steady and some hyaloclastites had the same SSA even if they were located far from each other in the drill core. Intrusive rocks and pillow basalts did not show any systematic changes with sample depth. The SSA of intrusive rocks and pillow basalts ranged between 1 and 15 m²/g with one pillow basalt having a SSA of 54 m²/g. Comparing the AI (see 1.3.2) with the measured SSAs shows that both are correlated for basaltic flows, massive basalts, intrusive rocks and pillow basalts. With progressive alteration (based on the AI) the SSA of basaltic flows constantly increased from 1 m²/g (AI = 1) to 17 m²/g (AI = 3), from 2 m²/g (AI = 1) to 9 m²/g (AI = 4.5) for massive basalts, from 2 m²/g (AI = 1) to 8 m²/g (AI = 5) for intrusive rocks and from 2 m²/g (AI = 1) to 12 m²/g (AI = 4.5) for pillow basalts. No correlation between the SSA and AI was found for hyaloclastites.

Basaltic flows showed a homogeneous distribution of connected pore space visualized by the intrusion of the molten alloy, whereby the alloy was abundant along fractures and grain boundaries (Figure 1-3a,b; enlarged section) and the interior of phenocrysts was mainly not

18

intruded (Figure 1-3b; red arrow). Vesicles (Ø 0.5-2 mm) were completely filled with the molten alloy (not shown). The amount of alloy intruded in basaltic flows increased with the degree of alteration from AI = 2 to AI = 3 (Figure 1-3a→1-3b) for samples located in the freshwater saturated zone (Figure 1-3b). In comparison to basaltic flows, massive basalts are denser, less porous and no alloy along grain boundaries was observed (Figure 1-3c). The connected porosity increased with alteration from AI = 3 to AI = 4.5. Intrusive rocks were comparable to massive basalts but with even lower alloy abundances. No correlation between the connected porosity and the AI was observed.
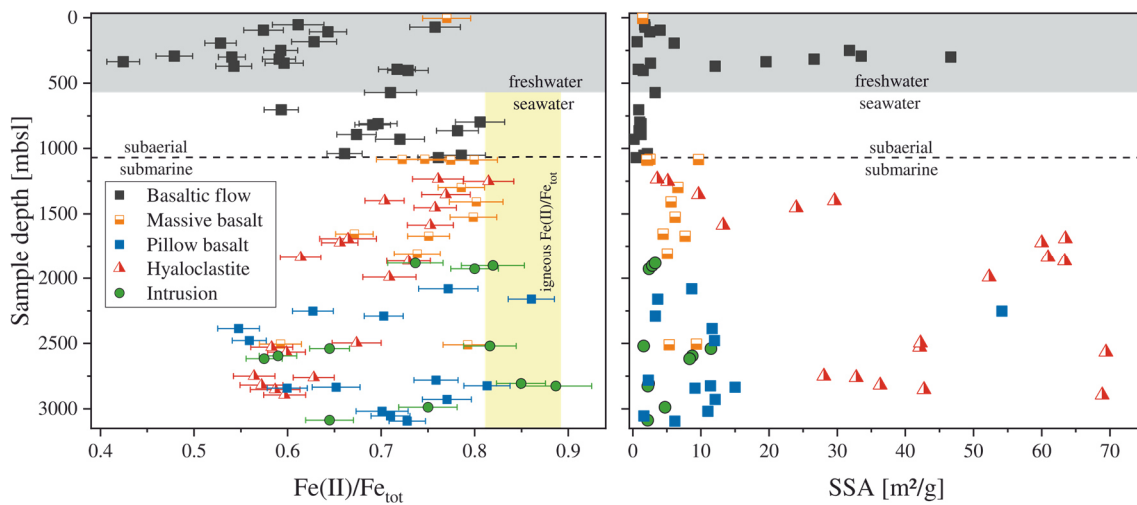
FIGURE 1-2: *Fe redox state **(a)** and SSA **(b)** of different HSDP2 basaltic rocks vs depth of the drill core. Standard deviations for **(a)** were calculated based on three independent measurements. Grey colored area indicates the freshwater saturated zone. Yellow striped area **(a)** shows the primary igneous Fe redox state after [118].*

The distribution of the alloy within hyaloclastites was heterogeneous and mainly weathered olivine phenocrysts and fractures were intruded with the glass being almost unaffected (Figure 1-3d). Here, it has to be noted that pores with a diameter < 5 nm were not accessible by the molten alloy and might lead to an underestimation of the total pore space for weathered rocks with high shares of fine pores due to the presence of clay minerals (e.g., hyaloclastites) [87]. Artifacts, such as secondary fractures and holes were observed that originated before (due to drilling) or after metal intrusion by polishing for SEM (Figure 1-3d; black arrow). However, secondary fractures can be easily distinguished by the absence of alteration phases that are only present in primary fractures.

Intrusion of the alloy within glassy parts of pillow basalts was also heterogeneous and mainly along fractures (Figure 1-3e; red arrow). The abundance of fractures significantly increased with increasing AI (not shown here). Some of the fractures in pillow basalts showed

evidence of crack lining palagonite (Figure 1-3e; white arrow). EDX analysis confirmed that the molten alloy was intruded in those secondary phases. A close-up image of a vesicle in a pillow basalt showed a zoned filling that consisted of smectites and zeolites (Figure 1-3f). The smectites were divided in sm1 and sm2 due to their appearance in BSE images. Sm1 seemed to be dense and no alloy was observed whereas alloy was abundant (possibly) between sheets of sm2 (Figure 1-3f; red arrow). The zeolites, filling the inner part of the vesicle, were again dense and not intruded. The boundary between palagonite and sm1 was ~10 µm wide and filled with alloy and secondary phases.
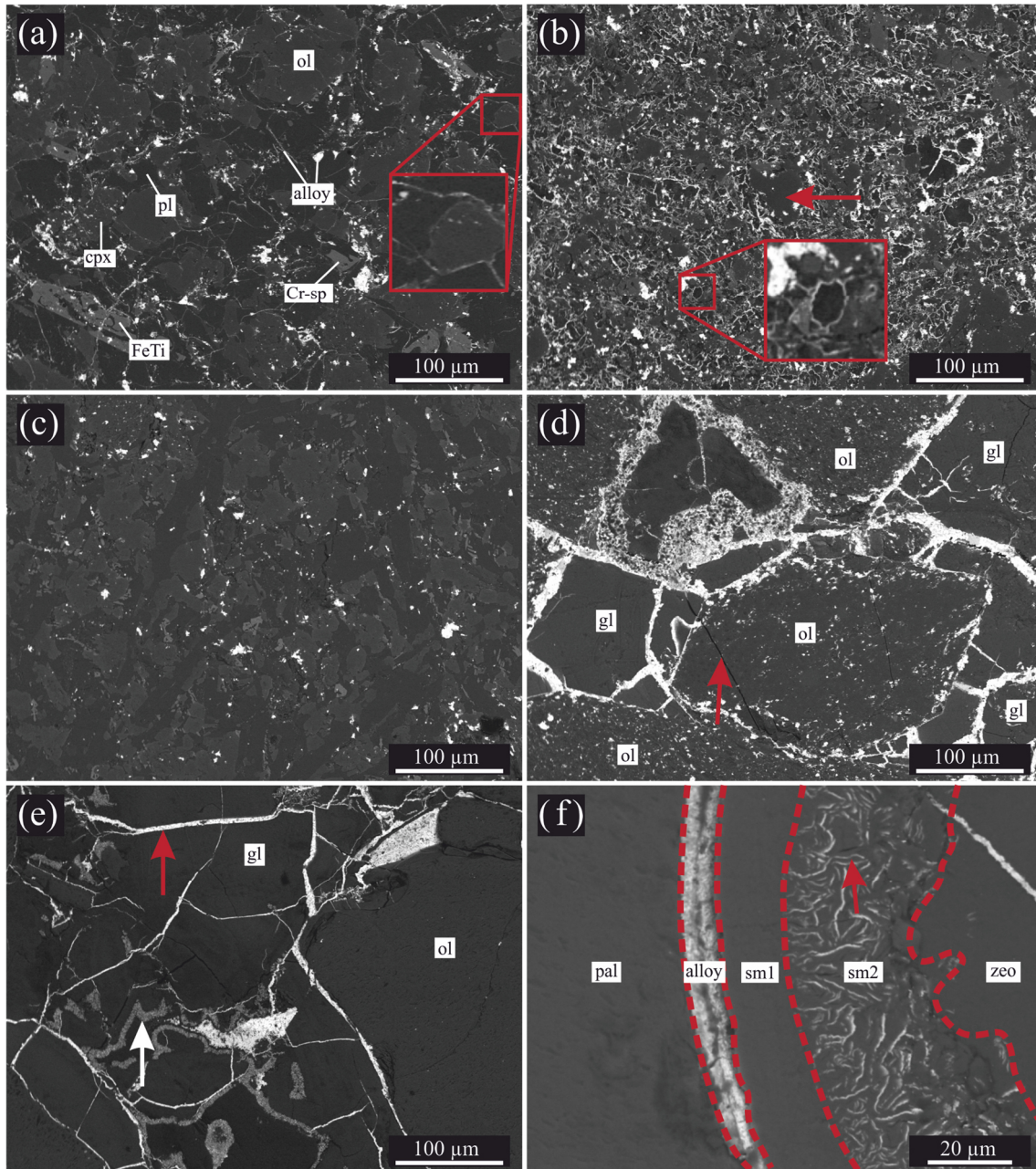
FIGURE 1-3*: Back scattered electron images of selected typical samples used for visualization of connected pores by intrusion of a molten alloy (Wood`s metal). The alloy appears bright in the images. **(a)***: basaltic flow from 893 mbsl (AI = 2; SSA = 1.2 m²/g). Enlarged section (red) shows the alloy around mineral grain boundaries. ***(b)****: basaltic flow from 300 mbsl (AI = 3; SSA = 46.6 m²/g). Red arrow: unaltered mineral grain not intruded by the molten alloy. Enlarged section (red) shows molten alloy in open spaces along grain boundaries. **(c)***: massive basalt from 1087 mbsl (AI = 3; SSA = 2 m²/g). The amount of alloy intruded is much less compared to ***(a)*** and ***(b)***. ***(d)****: hyaloclastite from 1587 mbsl (AI = 3.5; SSA = 13.2 m²/g). Altered olivine phenocrysts were intruded by the molten alloy adjacent to basaltic glass that seemed to be mostly unaltered. Red arrow: unfilled fracture as a relic from polishing after metal intrusion. **(e)***: pillow basalt from 2251 mbsl (AI = 4; SSA = 54.1 m²/g). Red arrow: crack in the glass filled by the alloy. White arrow: crack filled by secondary minerals. EDX analysis revealed that the alloy intruded also the fractures filled with secondary phases. ***(f)****: vesicle in pillow basalt from 3054 mbsl (AI = 1.5; SSA = 1.6 m²/g). The vesicle showed a zoned filling with secondary smectites and zeolites. Dashed lines separate the different zones (rim-left, core-right). The space between pal and sm1 is about 10 µm wide and intruded by the molten alloy. Sm1 and zeo seemed to be dense and not intruded by the alloy whereas sm2 showed distribution of the alloy possibly between sheets (red arrow). Abbreviations: ol = olivine; pl = plagioclase; cpx = clinopyroxene; FeTi = Fe-Ti oxides; Cr-sp = Cr-Spinel, pal = palagonite, sm = smectite, zeo = zeolite.*

21

1.4.2 Sequential Extraction on Fe, Si, Al and Mn

A general observation for almost all extractions and measured elements (except Fe_{H2O}, Al_{Ox} and Si_{Ox}) was a definite maximum in the amount of released Fe, Si, Al, and Mn from basaltic flows in the freshwater saturated zone (Figure 1-4 grey area; surface to ~600 mbsl). The amount of released elements increased by a factor of 2 to 5 relative to rocks affected by brackish- and seawater in the range ~600 to 1079 mbsl.

Considering Fe, a relatively high release of easy exchangeable Fe (Fe_{H2O}; Fe_{CB}) from massive basalts, hyaloclastites, pillow basalts and intrusive rocks increasing with depth up to 3.5 µmol/g was observed. Amorphous and weakly crystalline bound Fe (Fe_{Ox}) increased for hyaloclastites with depth whereas it remained low for massive basalts and intrusive rocks. A sudden increased Fe release (Fe_{H2O}; Fe_{Ox}) was apparent for pillow basalts at ~2400 mbsl followed by a subsequent drop to lower values. In contrast, well crystalline bound Fe (Fe_{DCB}) was low for all rocks below the subaerial-submarine transition (1079 mbsl).

Easy exchangeable as well as amorphous and weakly crystalline bound Si (Si_{H2O}; Si_{CB}; Si_{Ox}) increased comparable to Fe below the subaerial-submarine transition but with concentrations twice as high (e.g., Fe_{Ox} max. 200 µmol/g Fe and Si_{Ox} up to 400 µmol/g Si). In contrast to Fe, Si content in well crystalline phases (Si_{DCB}) was elevated for all rocks below 1079 mbsl. Hyaloclastites showed highest Si release that increased from 1200 to 1750 mbsl and remained high at greater depth. For all other rock types, Si released from well crystalline phases did not vary considerably with increasing depth but a peak was apparent at ~2400 mbsl.

The Al and Mn release was comparable throughout the various extractions. Easily exchangeable as well as amorphous and weakly crystalline bound Al and Mn (Al/Mn_{H2O}; Al/Mn_{Ox}) increased for hyaloclastites from 1200 to ~1750 mbsl. For massive and pillow basalts the release of Al and Mn remained low with increasing depth but showed a peak around ~2400 mbsl (for Al/Mn_{H2O}; Al/Mn_{Ox}) similar to Fe and Si. Concentrations of CB and DCB extractable Al and Mn were low and did not noticeably increase with depth.
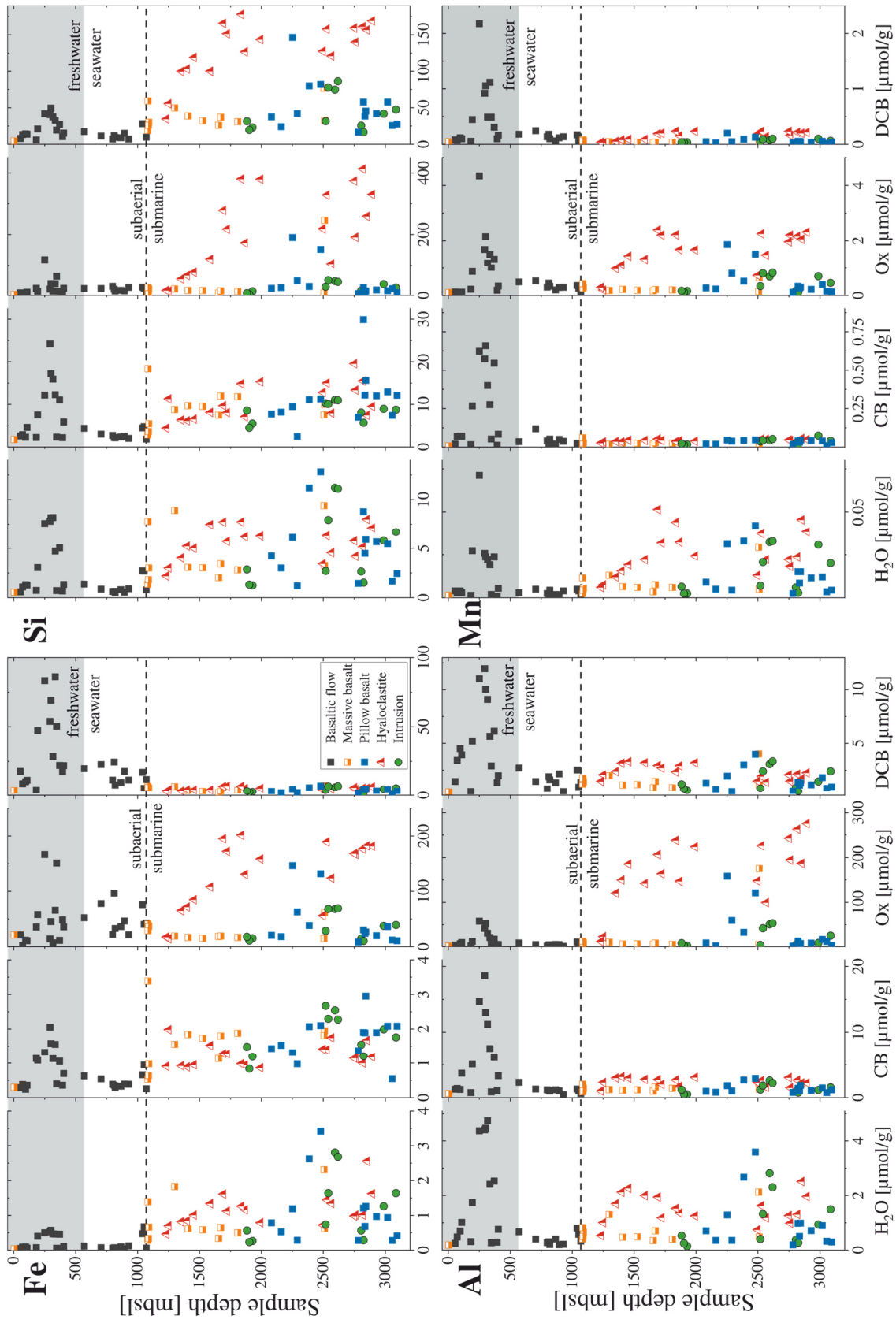
FIGURE 1-4: *Released amounts of Fe, Si, Al and Mn from different HSDP2 basaltic rocks during the four-step sequential extraction procedure vs depth of the drill core. H₂O/CB = easily exchangeable; Ox = amorphous to weakly crystalline bound; DCB = well crystalline bound. Grey colored area indicates the freshwater saturated zone.*

1.5 Discussion

1.5.1 Alteration State of HSDP2 Basaltic Rocks

For understanding the release behavior of Fe from basaltic rocks it is necessary to characterize the degree of alteration of the basaltic rocks and estimate the influence of varying environmental conditions on secondary phase formation. Alteration of HSDP2 core rocks is mostly restricted to fractures and vesicles and significantly more abundant in the submarine portion (1079 to 3098 mbsl) of the drill core [119]. Here, smectites (either grain replacing or in palagonite) are most abundant alteration phases with variable structural Fe contents and compositions between saponite and nontronite [120].

Besides from petrographic observations an estimation on the extent of alteration of the whole drill core can be done by comparing elements that behave mobile (e.g., K) to those that are relatively immobile (e.g., P) during weathering [121]. Unaltered Hawaiian basalts have primary igneous K_2O/P_2O_5 ratios between 1.5-2.0 [119]. With progressive weathering of the basaltic rocks this ratio is shifted < 1 [122]. Another useful tool providing information on the alteration state of basaltic rocks is the loss on ignition (LOI) due to dehydration of alteration phases. Rhodes and Vollinger [110] investigated 289 basaltic rocks of the HSDP2 drill core and measured whole rock chemical compositions by XRF and the H_2O content by weight loss following ignition at ~1000°C (LOI).

K_2O/P_2O_5 ratios remarkably decreased (< 1) in the freshwater saturated zone (surface to ~600 mbsl) and increased towards the subaerial/submarine boundary at 1079 mbsl (Figure 1-5). The stronger alteration in the freshwater saturated zone was only partly reflected by the LOI. With the beginning of the submarine erupted rocks at 1079 mbsl no distinctive trends were present but K_2O/P_2O_5 ratios were constantly below primary igneous values. This was also reflected by higher LOI values indicating significant hydration of submarine basaltic rocks and the presence of hydrous secondary phases (e.g., Fe (oxyhydr)oxides). For subaerial rocks (above 1079 mbsl), the K_2O/P_2O_5 ratio and the LOI values are contradictory. K_2O/P_2O_5 ratios indicate strong alteration in the freshwater saturated zone whereas hydration is negligible for those rocks.

Comparison with the Fe(II)/Fe$_{tot}$ ratios (Figure 1-2a) support the observations from K_2O/P_2O_5. This suggests that secondary phases within rocks above 1079 mbsl are less hydrous possibly due to ripening and dehydration of secondary phases. Furthermore, Fig. 1-5 clearly shows that the progress of alteration of HSDP2 basaltic rocks is highly variable even on small

scales for adjacent rocks. Similar observations were made by Walton and Schiffman [58] based on alteration features observed within hyaloclastites. Here, it was suggested that the rocks must have been affected by at least four different alteration processes, namely dissolution (with or without formation of secondary phases), biotic and abiotic driven replacement of olivine and plagioclase by smectites and formation of palagonite from basaltic glass. Walton and Schiffman [58] assumed that geochemical thresholds have led to the observed varieties of differentially altered rocks. In summary of the results, alteration of HSDP2 core rocks is highly heterogeneous and not directly linked to the age with some rocks being relatively fresh and others moderately altered.
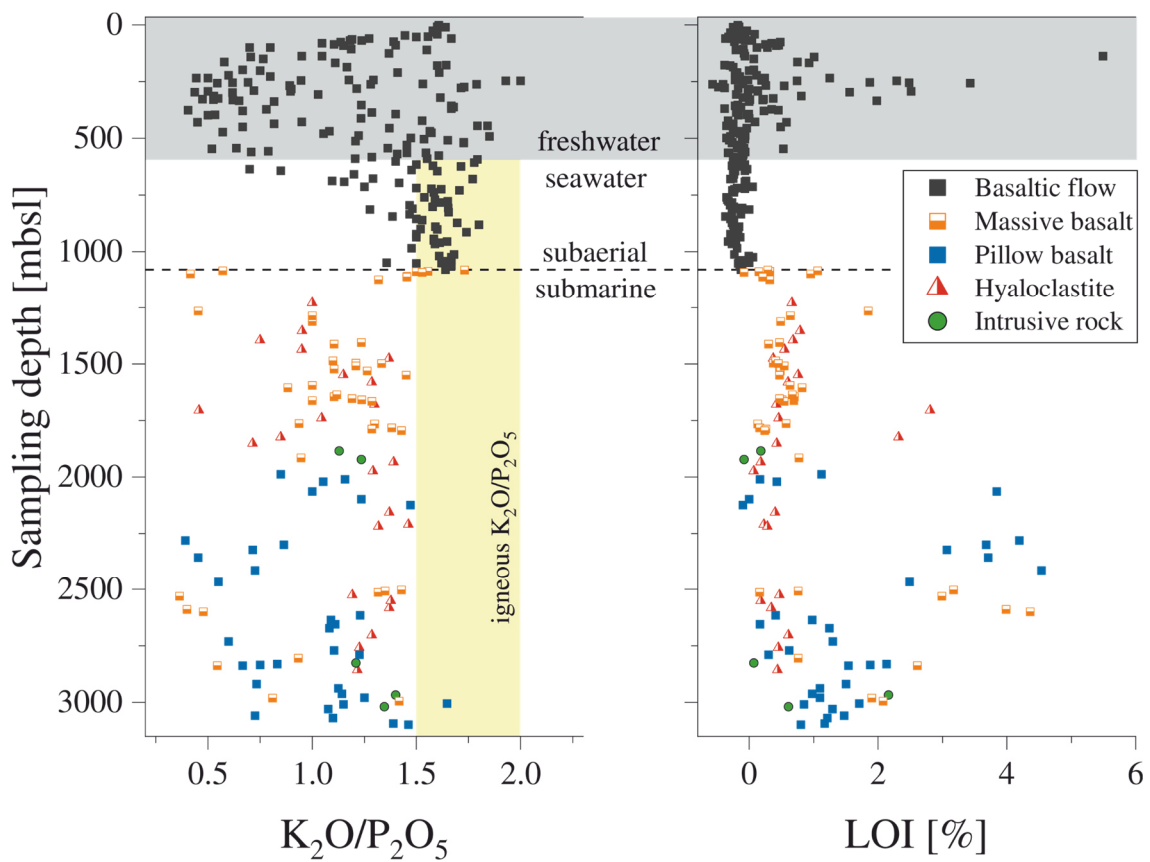
FIGURE 1-5: *Alteration state of different HSDP2 basaltic rocks based on K_2O/P_2O_5 ratios and LOI values vs depth of the drill core (data points from supplemental material of [110]). K_2O and P_2O_5 were determined by XRF and LOI values by heating of the rocks. Grey colored area indicates the freshwater saturated zone. Yellow colored area shows the primary igneous K_2O/P_2O_5 ratio.*

1.5.2 Connected Porosity and Implications for Fluid Flow

The connected porosity of a rock is a prerequisite for the intensity of alteration providing pathways inside rocks where fluids can circulate and, thus, affects weathering reactions and the chemical composition of pore water. Furthermore, it is the only possibility for the transport of solutes (e.g., Fe) to the environment. The connected porosity of a rock can change with progressive alteration, e.g., by partially clogging of pores by secondary phases or compaction of weakly consolidated rocks such as hyaloclastites [123,124]. This implies that the permeability and therefore the susceptibility of a rock for alteration by penetrating fluids can slow down with progressive alteration. However, the opposite is the case when fractures evolve in the rocks, e.g., due to strain in glassy rims of pillow basalts and pore volume is increased by dissolution of minerals and loss of solutes by circulating fluids. Here, the newly formed pathways in basaltic glass provide access to otherwise inaccessible portions of the rocks (see Figure 1-3f).

BSE images of rocks intruded with the molten alloy showed that the connected porosity drastically changed within the same rock type and that different kinds of pathways (fractures, vesicle, grain boundaries) within the rocks exist (Figure 1-3a). The mean connected porosity (determined by image analysis without vesicles) in basaltic flows increased with increasing AI (AI = 2→AI = 3) and SSA (1.2 m²/g→46 m²/g) from ~8 vol.% to 24 vol.% for freshwater influenced rocks (Figure 1-3a;b). For massive basalts, fractures were rare and mean porosities lower (~6 vol.%) compared to basaltic flows. Intrusive rocks showed the lowest but homogeneous porosities (2 to 3 vol.%) that mainly depend on the number of fractures in the rocks. The porosity of hyaloclastites and pillow basalts was highly variable and not fully characterized due to high shares of fine pores (< 5 nm) as identified by Woods metal intrusion. Pathways for fluids in hyaloclastites were restricted to weathered olivine phenocrysts and fractures whereas glassy parts rarely showed any substantial porosity (Figure 1-3d). The amount of alloy intruded seemed to decrease with depth which is in agreement with findings of Walton and Schiffman [58] and Moore [125] that hyaloclastites lose their porosity due to compaction and cementation.

This has important implications for the hydrological system of Hawaii and the solute transport of Fe since hyaloclastites change from a fluid conductor at shallow to a fluid barrier at greater depth. However, pathways for fluids in greater depth are provided by fractures within pillow basalts whose abundance increased during alteration. Vesicles in pillow basalts were zoned and filled with secondary phases (smectites and zeolites) of various structural

morphologies (Figure 1-3f). This observation elucidates that the conditions of alteration and therefore the secondary phase assemblage can be versatile on small scales and is comparable to what was observed for the degree of alteration (see Figure 1-5).

Transferring these observations to the hydrological system of Hawaii and the subsurface fluid flow implies that meteoric waters can pass relatively unimpeded through basaltic flows and flow downward towards the seawater saturated rocks. Furthermore, the basaltic flows located in the freshwater saturated zone show increased porosities compared to those influenced by seawater indicating that leached elements are mainly transported with the fluids rather than being directly precipitated as secondary phases. With increasing depth, the fluid flow may progressively slow down and mainly depend on the hydraulic conductivity of the different lithological units. In hyaloclastites, for example, the transport mechanism changes with depth from convective-dominated in unconsolidated to diffusion-dominated in cemented materials. Convective flow, however, is maintained in greater depth by fractures within pillow basalts. Furthermore, the occurrence of freshwater in depth > 2000 mbsl shows that decreasing porosities are no insuperable barrier for circulation of fluids through the whole volcanic complex.

1.5.3 Reactivity of Secondary Fe bearing Solid Phases

Weathering of basaltic rocks implies primary mineral dissolution going along with element release where some parts are lost to the surrounding pore solution and others immobilized by the formation of secondary mineral phases. Freshly precipitated oxides are predominantly amorphous, highly reactive but thermodynamically unstable which favors recrystallization or dissolution/precipitation into more crystalline and stable phases. In this context the ratio of amorphous to crystalline Fe (oxyhydr)oxides (Fe_o/Fe_d), defined as activity of free Fe oxides, can be used to estimate the reactivity of Fe bearing secondary phases [44]. The Fe_o/Fe_d ratio was calculated as follows: $Fe_o = Fe_{H2O}+Fe_{CB}+Fe_{Ox}$ and $Fe_d = Fe_{H2O}+Fe_{CB}+Fe_{Ox}+Fe_{DCB}$ and ranges between 0 and 1. With ripening (aging) of amorphous to structurally more ordered crystalline secondary phases the ratio is shifted from 1 to almost 0 (e.g., transformation of ferrihydrite to better crystalline oxides).

The Fe_o/Fe_d to identify lithological units with highly reactive Fe bearing solid phases within the subsurface basaltic rocks (Figure 1-6). A general trend observed for basaltic rocks of the HSDP2 drill core was an increased Fe_o/Fe_d ratio with depth. Subaerial basaltic flows influenced by freshwater (surface to ~600 mbsl) showed Fe_o/Fe_d ratios between 0.25 and 0.9.

However, most of the samples showed $Fe_o/Fe_d < 0.75$ and possibly reflect association of mixtures of amorphous and better crystalline phases. With increasing depth towards the subaerial-submarine boundary (1079 mbsl) ratios slightly increased again. From 1079 to 3098 mbsl, the Fe_o/Fe_d ratios varied from 0.8 to 0.98 but were noticeable higher compared to rocks above the subaerial-submarine boundary. Highest ratios were observed for hyaloclastites below 1300 mbsl. The other rock types showed larger scatter but no significant trends were observed. In general, below 1079 mbsl in the submarine environment elevated amounts of oxalate extractable Fe, Al, Si and Mn were present suggesting that these rocks comprise large amounts of amorphous to weakly crystalline, highly reactive secondary solid phases (compare Figure 1-4).
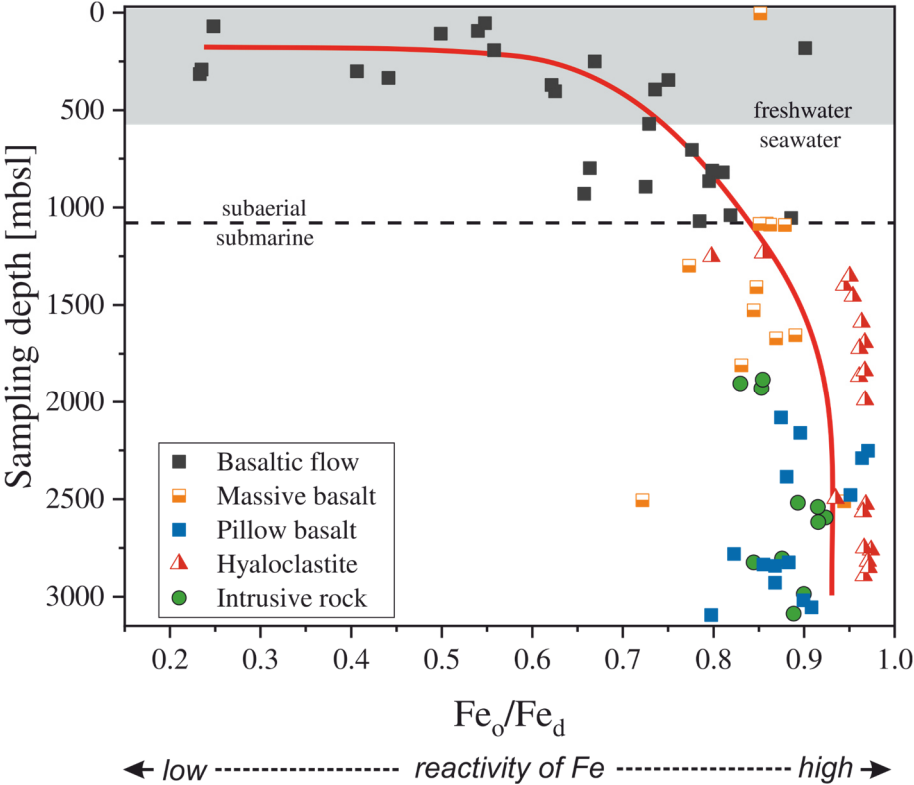
FIGURE 1-6: Fe_o/Fe_d ratio of different HSDP2 basaltic rocks vs depth of the drill core. $Fe_o = Fe_{H2O}+Fe_{CB}+Fe_{Ox}$; $Fe_d = Fe_{H2O}+Fe_{CB}+Fe_{Ox}+Fe_{DCB}$. Solid line shows the trend in Fe_o/Fe_d with depth. Grey colored area indicates the freshwater saturated zone. Red line only guides the eye.

Canfield, [100] and Raiswell at el., [126] used buffered dithionite and HCl solutions to investigate the reactivity of Fe from various Fe (oxyhydr)oxides toward sulfide anions under anoxic conditions in marine sediments. It was observed that amorphous Fe (oxyhydr)oxides such as ferrihydrite comprise large fractions of reactive Fe that rapidly reacts with sulfide anions to form pyrite and hence influences pore water chemistry. The reactive Fe fraction decreased

toward more crystalline phases such as hematite [126]. Even if the concept of reactive Fe introduced by Canfield, [100] is not directly adaptable to the investigations of this study it nevertheless underlines that the majority of secondary Fe bearing solid phases within submarine altered HSDP2 core rocks are potentially highly reactive.

Reconsidering that ripening of first alteration products involves their partly dehydration, one would expect the basaltic flows under subaerial conditions to have lower LOI values compared to the submarine rocks. Comparison of the Fe_o/Fe_d ratios with the LOI values (Figure 1-5) shows that they are in good agreement for subaerial and submarine rocks reflecting the higher crystalline (anhydrous) secondary phases above- as well as the amorphous (hydrous) secondary phases below 1079 mbsl. However, the LOI values always show the sum of H_2O that is bound in or adsorbed on surfaces of secondary phases such as clay minerals and a clear differentiation is only possible with more specific methods (e.g., determination of water content by Karl-Fischer titration). Besides of this, the LOI values alone without the information from the sequential extraction would lead to the conclusion that subaerial basaltic flows are by far less or completely unaltered. The K_2O/P_2O_5 ratios, on the other hand, clearly show that at least freshwater influenced subaerial basaltic flows (surface to ~600 mbsl) are strongly altered.

However, the observation that highly reactive Fe bearing solid phases persist in the submarine portion of the HSDP2 drill core is somehow surprising. The Fe_o/Fe_d ratio is usually expected to decrease with time as a consequence of progressive weathering [44,127]. Early formed Fe (oxyhydr)oxides such as ferrihydrite transform into more stable crystalline phases either by dehydration (e.g., hematite) or dissolution and recrystallization (e.g., goethite). The findings show an opposing trend towards less crystalline Fe bearing solid phases with increasing depth (= increasing age). All these observations imply that major portions of the HSDP2 drill core (about 2/3) comprise highly reactive secondary Fe bearing solid phases. The release of Fe from these phases is assumed to be relatively constant and might be a long-lasting source of Fe supply to the hydrosphere.

1.5.4 Possible Controls on Transformation of Fe bearing Solid Phase

It was demonstrated in chapter 1.5.1 and 1.5.3 that highly reactive amorphous Fe oxides are abundant in basaltic rocks of the HSDP2 drill core and prevail especially at depth > 1079 mbsl under saline conditions in the region of the seawater cycle. With respect to ripening of secondary Fe bearing solid phases, subaerial basaltic flows influenced by freshwater have an advanced ripening progress compared to rocks affected by seawater (Figure 1-6).

There are several reasons that might have influenced or suppressed ripening of secondary phases, e.g., intensity of weathering and interaction with dissolved species (cations/anions, dissolved organic matter), connected porosity, temperature and redox conditions [90,99,128,129].

The intensity of weathering changed during the postshield stage of the Island of Hawaii when lava accumulation rates significantly decreased from 8.6±3.1 m/kyr (for rocks below 1079 mbsl) to about 0.9±0.4 m/kyr for rocks at ~250 mbsl [106]. This had important implications for the upper subaerial erupted rocks as they have undergone more intense alteration by penetrating meteoric waters compared to rocks closer to 1079 mbsl. In the latter case rocks were covered much faster by new lava flows and, thus, characterized by intermittent alteration only. The longer exposure time of the subaerial erupted rocks was sufficient enough for the development of some soils interbedded between the lava flows [105]. Comparison with laterites, a soil common in hot and wet tropical areas with strong leaching conditions shows the same tendency of decreasing crystallinity with soil depth. In such soils, large amounts of silica are mobilized from the top and transported with the migrating fluid downward to greater depth [130].

High concentrations of aqueous Si can stabilize Fe(III) by the formation of Fe-Si complexes and, thus, slow down nucleation and growth of solid Fe(III) (oxyhydr)oxides keeping hereby Fe(III) mobilities high [131,132]. Furthermore, precipitation of silica during nucleation of goethite can inhibit its crystallization and therefore strongly affect the crystallinity of the secondary Fe bearing solid phases [97]. Intense Si leaching and redistribution due to subaerial weathering of a volcanic island was also assumed for basaltic rocks of the Nintoku seamount sampled during ODP Leg 197 on Site 1205 [104]. In addition to dissolved silica transported downward with meteoric waters, seawater inflow at greater depth through the sediment-covered flanks of Hawaii can be an additional source for various anions (e.g., SO_4^{2-}; CO_3^{2-}) and dissolved organic matter.

The connected porosity provides pathways for fluids and controls the fluid/rock ratio. Alteration rates slow down as the porosity decreases and the fluid flow changes from convection to diffusion, e.g., due to secondary minerals precipitating in pores and fractures [133]. The porosity of HSDP2 core rocks strongly depends on the rock typ. Subaerial basaltic flows ('a'a, pahoehoe, transitional) are highly vesicular (Ø 9.7 vol.%) whereas intrusive rocks are among the lowest vesicular (Ø 0.7 vol.%). Within the hyaloclastites, porosity decreases downhole from initially 40-45 vol.% at 1080 mbsl to < 4 vol.% at 1573 mbsl [58]. Indication was obtained from the Wood´s metal intrusion experiment that the porosity of rocks below the

subaerial/submarine boundary is significantly lower compared to subaerial rocks, e.g., the properties of hyaloclastites change with increasing depth from a fluid conductor to a barrier that locally impedes fluid flow. The observed amounts of weakly ordered Fe bearing solid phases in the submarine rocks can be partly explained by supersaturation of the fluid due to cementation and consolidation and consequently fast nucleation and crystal growth. This, in turn, is known to favor the formation of disordered and poorly crystalline phases [90].

It seems reasonable to us that neither the temperature nor the subsurface redox conditions significantly influenced ripening of secondary Fe bearing phases. Temperatures in the borehole ranged between ~9 to 45°C and differentially altered hyaloclastites were found in direct vicinity to each other (= equal temperatures) [58]. The low temperatures also indicate that the subsurface fluid flow is fast enough to supply "fresh" oxygen thereby maintaining aerobe conditions. This is also evidenced by elevated $Fe(III)/Fe_{tot}$ ratios throughout all rocks of the drill core compared to primary igneous values (see Figure 1-2a).

It was osberved that dissolved silica strongly influences ripening of secondary Fe bearing solid phases. Besides of aqueous Si, the affinity of SO_4^{2-} for adsorption on positive charged surface sites of goethite and hematite was experimentally shown by Walsch and Dultz, [134]. Adsorbed sulfate anions are known to prevent the transformation of early Fe (oxyhydr)oxides to better crystalline phases [64]. Furthermore, coprecipitating dissolved organic matter drastically decreases the crystallinity of precipitating ferrihydrite and prevented formation of better crystalline Fe oxides [135]. This implies that besides silica, other dissolved species provided by the penetrating seawater can have similar effects on transformation of secondary Fe bearing solid phases. It is therefore reasonable to assume that the rocks above 1079 mbsl have been intensively altered by meteoric waters as a consequence of longer exposure at the surface before being buried. The leached constituents (e.g., silica) were then transported downward with the fluid flow where they progressively accumulated due to decreasing porosities and interacted with the secondary Fe bearing solid phases.

This conclusion is also supported by work of Schopka and Derry [26]. It was shown that surface drainage (e.g., by streams) is ephemeral on the island of Hawaii and that about 79% of the total precipitation percolates uninterrupted through the highly porous rocks towards the groundwater table. Dissolved silica (and other anions such as SO_4^{2-} and CO_3^{2-}) as well as organic matter were additionally provided from seawater that penetrated the submarine erupted rocks. Low Fe_o/Si_o ratios support this hypothesis and provide evidence for high amounts of amorphous Si within submarine erupted rocks (Figure 1-7). For subaerial rocks above

1079 mbsl the ratio varies between 0.22 and 7.6 whereas below the subaerial/submarine boundary the Fe_o/Si_o ratio is always < 1.3. This indicates that Fe bearing solid phases below 1079 mbsl are progressively associated with amorphous Si. Secondary phases in natural environments are seldom pure and often contain impurities such as Si in siliceous 2-line ferrihydrite that dramatically lowers the rate of transformation to better crystalline oxides [136,137]. Proof whether the Si in the samples is directly associated with Fe bearing solid phases as Fe-Si (oxyhydr)oxides or precipitated in the form of amorphous Si inhibiting ripening of Fe (oxyhydr)oxides is, at this point, not possible.
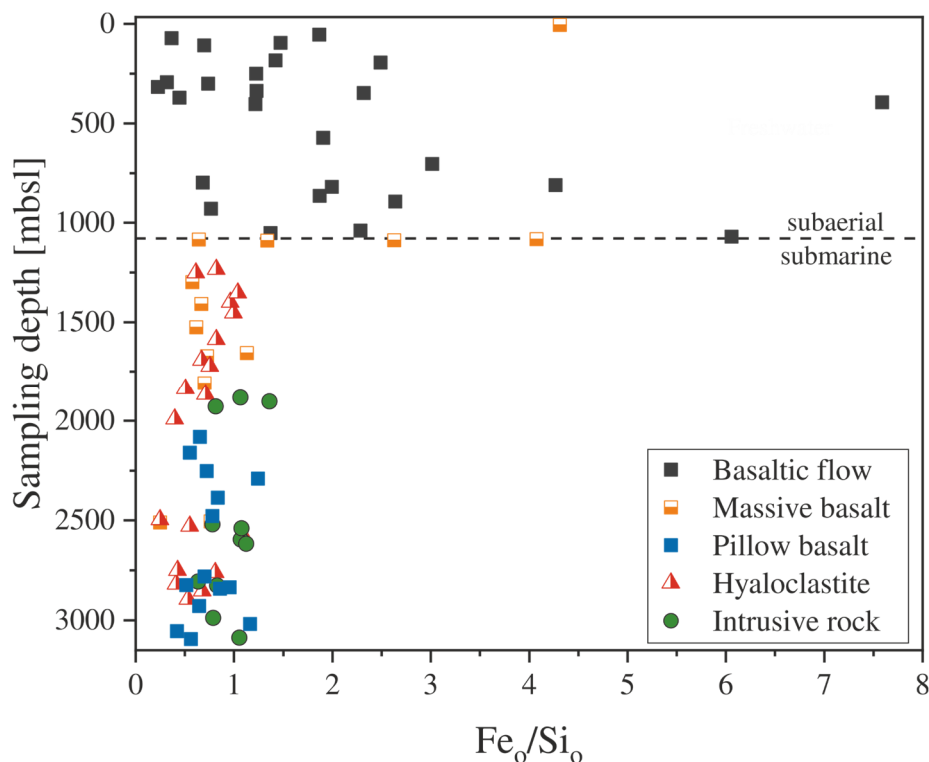
FIGURE 1-7: Fe_o/Si_o ratio of different HSDP2 basaltic rocks vs depth of the drill core. The ratio sharply declines for submarine rocks at the subaerial/submarine boundary (1079 mbsl; dotted line).

1.5.5 Fe Mobility as a Function of the Fe Redox State

The mobility of Fe from basaltic rocks and glasses is known to be much lower compared to alkali and alkaline earth elements [49]. Fe in unweathered basaltic rocks and glasses is predominantly in the form of Fe(II). Upon weathering oxidation of Fe(II)→Fe(III) and precipitation in the form of Fe(III) (oxyhydr)oxides is fast at circumneutral pH, oxygenated conditions and in the absence of complexing agents [138]. In this context, the ratio of Fe(II) to total Fe can be used as an indicator for the alteration state of the basaltic rocks. A continuous

conversion of Fe(II)→Fe(III) due to oxidation of structurally bound Fe or dissolution of primary silicates going along with Fe release and oxidation/precipitation of secondary phases should shift the Fe(II)/Fe$_{tot}$ ratio to lower values with progressive weathering (see. Figure 1-2a) [56].

To test whether this shift influences the Fe release from basaltic rocks, the mobility of Fe, given as the ratio of Fe released from secondary phases during the extractions (Fe$_d$) to the total Fe content of the rocks (Fe$_{tot}$) (Fe$_{tot}$ measured according to section 1.3.4) was calculated. This Fe$_d$/Fe$_{tot}$ ratio describes the amount of Fe that is (possibly) available from secondary phases. HSDP2 basaltic rocks comprise a wide range of Fe mobilities from < 2% for some pillow basalts to > 18% for some hyaloclastites (Figure 1-8). Distinctive trends for increased Fe mobility with decreasing Fe(II)/Fe$_{tot}$ were observed for hyaloclastites and intrusive rocks (e.g., from 2% (Fe(II)/Fe$_{tot}$ = 0.82) to 17% (Fe(II)/Fe$_{tot}$ = 0.59)). The mobility of Fe from subaerial basaltic flows and pillow basalts showed larger scatter (r^2 = 0.25 and 0.33) but a tendency for increased Fe mobilities is apparent. No distinctive trend for increased Fe release with changing Fe redox state was observed for massive basalts.

FIGURE 1-8: *Fe mobility (Fe$_d$/Fe$_{tot}$) vs Fe redox state of different HSDP2 basaltic rocks. Dotted lines show linear fits and corresponding r^2. Massive basalts did not show a trend and were not fitted.*

It is obvious from Fig. 1-8 that for hyaloclastites and intrusive rocks the Fe mobility increase with decreasing $Fe(II)/Fe_{tot}$ (= progressive alteration) whereas basaltic flows and pillow basalts show a weak dependency only. Assuming that Fe is not lost to the solution, this suggests that Fe is incorporated and/or passively accumulated in secondary phases such as ferrihydrite and palagonite, respectively. Further evidence for this is provided by increasing amounts of released Fe with increasing K_2O loss during alteration (compare Figure 1-5). Passive accumulation of Fe during the conversion of basaltic glass/sideromelane to palagonite, for example, is a well-known feature during rock-water interaction [28,139]. Fe that is bound in amorphous secondary solid phases (e.g smectite, ferrihydrite) is, because of high SSA, weak ordering, more mobile compared to Fe from primary Fe bearing phases (olivine, pyroxene, glass) and more easily available for microorganisms or the transfer to solution [70].

1.5.6 Link between Fe_o/Fe_d and Fe Mobility

It was observed in chapter 1.5.3 that the Fe_o/Fe_d strongly increased from subaerial to submarine rocks (Figure 1-6). The Fe mobility (Fe_d/Fe_{tot}) was shown to correlate with the Fe redox state for hyaloclastites and intrusive rocks whereas pillow basalts and massive basalts showed weak correlation (see Figure 1-8). Assuming that more Fe can be mobilized from amorphous compared to crystalline Fe bearing solid phases, the Fe mobility should strongly depend on the Fe_o/Fe_d. Fig. 1-9a clearly shows that Fe mobilities decreased with decreasing Fe_o/Fe_d for hyaloclastites from 19% ($Fe_o/Fe_d = 0.97$) to 2% ($Fe_o/Fe_d = 0.85$), for pillow basalts from 16% ($Fe_o/Fe_d = 0.97$) to 1% ($Fe_o/Fe_d = 0.80$), for massive basalts from 6% ($Fe_o/Fe_d = 0.94$) to 2% ($Fe_o/Fe_d = 0.84$), and from 8% ($Fe_o/Fe_d = 0.92$) to 2% ($Fe_o/Fe_d = 0.83$) for intrusive rocks. No correlation was observed for basaltic flows but Fe mobilities tend to slightly decline with decreasing Fe_o/Fe_d from 15% ($Fe_o/Fe_d = 0.75$) to 3% ($Fe_o/Fe_d = 0.23$) (Figure 1-9b).

Surprisingly, the Fe mobilities decreased to values below 5% for all rocks within a narrow range of Fe_o/Fe_d (0.97 to 0.90), except for basaltic flows. Here the Fe mobility remained high over a much wider range of Fe_o/Fe_d (from ~0.8 to 0.4). The majority of basaltic flows showed intermediate Fe mobilities (between 5 to 10%) comparable to massive basalts and intrusive rocks. However, the fact that such intermediate Fe mobilities are preserved over a much wider range of Fe_o/Fe_d is an important implication for the Fe availability from these rocks. Subaerial basaltic flows are exposed to periodically changing weathering conditions with periods of high recharge and intense leaching followed by dry periods which leads to secondary Fe oxides with variable crystallinities [99].

In contrast, submarine rocks are not affected by periodically changing weathering conditions as they are permanently water saturated. Furthermore, submarine rocks are influenced by fluids that contain high amounts of dissolved anionic species stemming from (i) the leached basaltic flows or (ii) the penetrating seawater, both influencing the formation and kind of secondary Fe bearing solid phase (see 1.5.4). This is in accordance with Walton and Schiffman [2], who showed that palagonitization of hyaloclastites alone did not provide sufficient elements necessary for the amount of secondary minerals (e.g., smectites) formed within this rocks. It was proposed that additional sources (e.g., fluids saturated with dissolved elements) must have provided elements for smectite formation within hyaloclastites. The observations from Fig. 1-9 suggest that little changes in the Fe_o/Fe_d of submarine rocks significantly influence the Fe mobility and therefore the amount of Fe that can be released to the environment. For subaerial rocks above 1079 mbsl, on the other hand, the Fe mobility is less dependent on the Fe_o/Fe_d possibly due to higher crystalline Fe bearing phases.

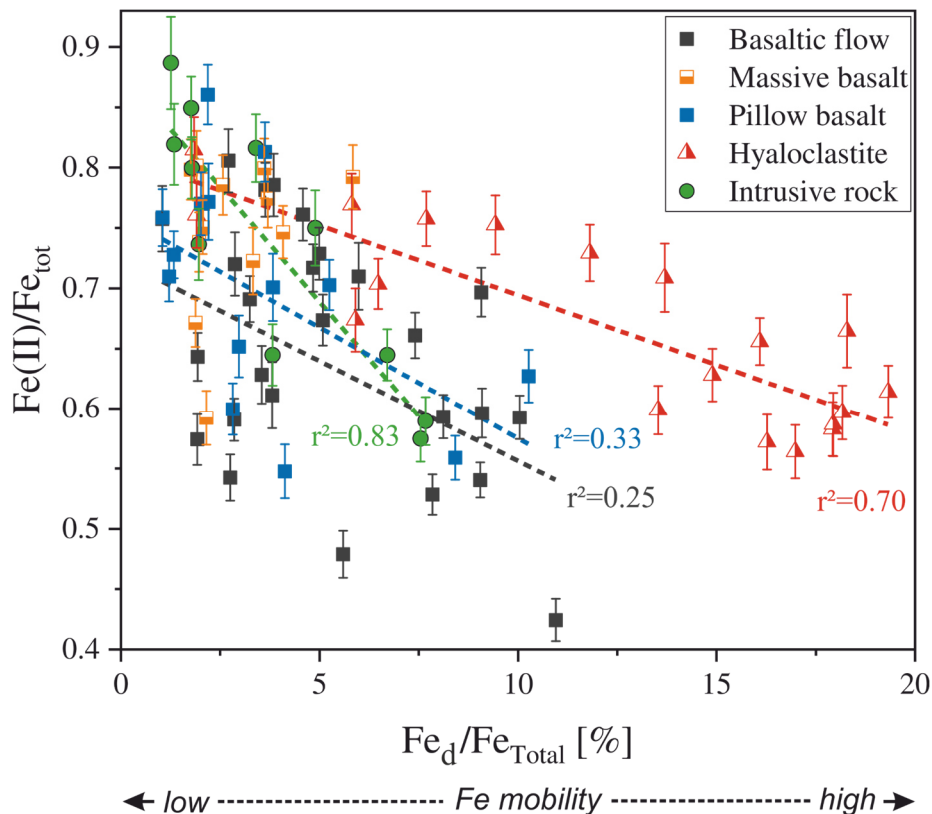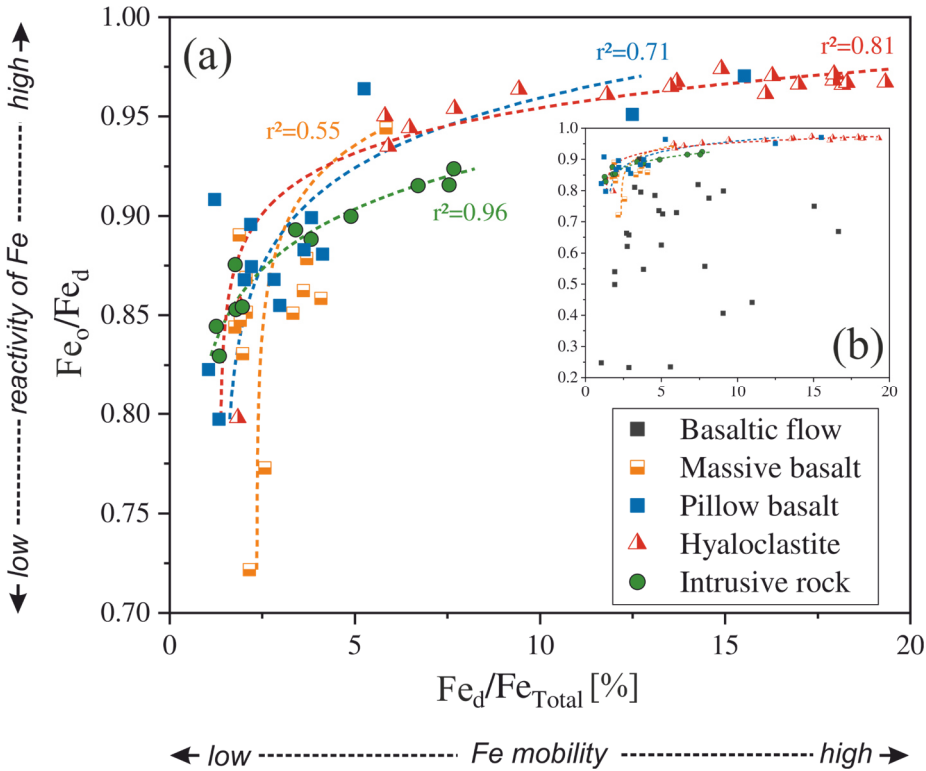**FIGURE 1-9**: *(a) Fe_o/Fe_d vs Fe mobility (Fe_d/Fe_{tot}) of different HSDP2 basaltic rocks. Dotted lines show linear fits and corresponding r^2. (b) Subaerial basaltic flows are separately shown and were not fitted due to their large scatter.*

1.6 Conclusions

There is still controversy about the contribution of volcanic islands to the global Fe budged of ocean surface waters. Here it is shown that subsurface basaltic rocks of volcanic islands have the potential for high Fe release that can significantly contribute to the geochemical Fe budged of the oceans, at least on local scale. Alteration of HSDP2 basaltic rocks is heterogeneous even on a μm scale and the release of Fe is closer related to the fluid composition, from freshwater to seawater, and less to the nature of the rocks. Extractions on Fe (oxyhydr)oxides and quantification of total Fe content revealed that large shares of Fe released during alteration are locally bound in secondary phases such as smectites and Fe (oxyhydr)oxides. For submarine rocks altered under seawater dominated conditions high $Fe_o/Fe_d > 0.85$, also confirmed by high SSAs, indicated that amorphous, oxalate soluble Fe phases dominate. Based on the observations it is likely that aging of Fe (oxyhydr)oxides is strongly hindered in the submarine environment under seawater conditions by adsorption of silica. Considering the high ionic strength of seawater, a contribution of other anions such as SO_4^{2-}, supressing the transformation from amorphous to crystalline Fe (oxyhydr)oxides is also suggested. Basaltic rocks, where weathering is dominated by meteoric waters showed $Fe_o/Fe_d < 0.70$ suggesting that crystalline Fe (oxyhydr)oxides were abundant.

A comparison of the Fe_o/Fe_d ratio with the Fe mobility (Fe_d/Fe_{tot}) was used to identify lithological units of which high Fe release can be expected. For submarine rocks, the Fe release was highest for rocks with high shares of oxalate soluble Fe ($Fe_o/Fe_d > 0.95$). The amount of released Fe increased in the order massive basalts < intrusive rocks < pillow basalts < hyaloclastites. For subaerial rocks under freshwater conditions elevated Fe release was observed also at $Fe_o/Fe_d < 0.5$.

It is therefore concluded that subsurface basaltic rocks of Hawaii especially those exposed to seawater comprise large amounts of highly reactive Fe bearing phases of which the potential Fe release is high. It is likely that this phenomenon is typical also for other volcanic ocean islands and seamounts but further investigations are needed to clarify the impact of e.g., rock composition, temperature, availability of dissolved silica and age. The findings on the properties of Fe (oxyhydr)oxides in marine systems have likely also strong implications for other geological settings such as Mid Ocean Ridge systems, where large amounts of basaltic rocks are in direct contact with seawater that circulates within the oceanic crust inducing rock alteration and governing hereby mobility of released Fe.

Chapter II

Experimental Microbial Alteration and Fe Mobilization from Basaltic Rocks of the ICDP HSDP2 Drill Core, Hilo, Hawaii.

Marius Stranghoener[1], Axel Schippers[2], Stefan Dultz[3] and Harald Behrens[1]

[1] *Institute of Mineralogy, Leibniz Universität Hannover, Hanover, Germany*
[2] *Geomicrobiology, Federal Institute for Geosciences and Natural Resources, Hanover, Germany*
[3] *Institute of Soil Science, Leibniz Universität Hannover, Hanover,Germany*

Abstract

The interaction of a single bacterial species (*Burkholderia fungorum*) with basaltic rocks from the ICDP HSDP2 drill core and synthetic basaltic glasses was investigated in batch laboratory experiments to better understand the role of microbial activity on rock alteration and Fe mobilization. Incubation experiments were performed with drill core basaltic rock samples to investigate differences in the solution chemistry during biotic and abiotic alteration. Additionally, colonization experiments with synthetic basaltic glasses of different Fe redox states and residual stresses were performed to evaluate their influence on microbial activity and surface attachment of cells. In biotic incubation experiments bacterial growth was observed and the release of Fe and other major elements from drill core basaltic rocks to solution exceeded that of abiotic controls only when the rock sample assay was nutrient depleted. The concentration of dissolved major elements in solution in biotic colonization experiments with synthetic basaltic glasses increased with increasing residual stress and Fe(II) content. Furthermore, the concentration of dissolved Fe and Al increased similarly in biotic colonization experiments indicating that their dissolution might be triggered by microbial activity. Surface morphology imaging by SEM revealed that cells on basaltic rocks in incubation experiments were most abundant on the glass and surfaces with high roughness and almost absent on minerals. In colonization experiments, basaltic glasses with residual stress and high Fe(II) content were intensely covered with a cellular biofilm. In contrast, glasses with high Fe(III) content and no residual stress were sparsely colonized. It is therefore concluded that

structurally bound Fe is most probably used by *B. fungorum* as a nutrient. Furthermore, it is assumed that microbial activity overall increased rock dissolution as soon as the environment becomes nutrient depleted. The results show that besides compositional effects, other factors such as redox state and residual stress can control microbial alteration of basaltic glasses.

2.1 Introduction

Weathering of volcanic rocks is a key factor for the transport and geochemical cycling of elements between lithosphere and hydrosphere. The oceanic crust is composed mainly of glassy or massive basaltic lava flows that cover 60% of the earth's surface [27]. Volcanic rocks often show high contents of glass when erupted in contact with water due to rapid cooling. The corresponding rocks can be composed of small glass fragments (hyaloclastites) or have a glassy rim and a partially crystallized interior (pillow basalts). As a relic from rapid cooling, such glasses show residual stress weakening their structure and making them more vulnerable to alteration [28]. Environmental influences such as water, temperature and atmospheric gases induce weathering and alter the chemical composition by the dissolution of primary and formation of secondary mineral phases. Basaltic rocks are in general less resistant to weathering when compared with other volcanic (e.g., rhyolites) or intrusive rocks (e.g., granites) due to their low silica and high glass content, respectively [29]. Young volcanic islands comprising relatively fresh and chemically reactive basaltic rocks are a potential source for increased Fe supply to ocean surface waters. Dissolved Fe in the Pacific surface waters was found to increase near the Hawaiian Islands from 0.1 nM to 0.6 nM with a maximum of 1.56 nM close to the Kauai Coast [22].

The mechanisms of chemical glass and rock alteration have been extensively studied in the past [46,90,102,103,140–142]. However, we are still beginning to understand the contribution of microorganisms to these processes. Microbial activity in natural basaltic rocks is evident from alteration textures, major element chemistry and geochemical tracers at temperatures up to 100°C and as deep as 380 meter below seafloor [65,69,70,143–145]. Biologically mediated alteration of volcanic glasses was also observed in samples from ICDP/IODP drilling sites making a major contribution of up to 75% to total alteration [4,65]. Hyaloclastites from HSDP (Hawaii Scientific Drilling Project) drill hole indicate microbial activity in rocks to depth of 1.9 km and possibly deeper [112]. Nevertheless, there are only a few studies that have investigated dissolution mechanisms of basaltic glasses under the action of microorganisms.

Bacteria collected near deep sea hydrothermal vents are capable of inducing the release of Fe and Mn from basaltic rocks and contribute to the geochemical cycling of these elements [146]. Bailey et al., [147] have shown in laboratory experiments that microbes are able to obtain beneficial nutrients from basaltic glasses in a nutrient- and energy limiting environment. Furthermore, basaltic glasses are a potential habitat for Fe(II)-oxidizing microorganisms using Fe(II) in basaltic glasses as an energy source [75,148]. Microbial oxidation of Fe(II) by different strains of Fe-oxidizing bacteria (FeOB) was found to enhance the dissolution of basaltic rocks by six to eight times over abiotic rates [149]. Wu et al., [150] also observed elevated elemental release rates during microbial alteration of basaltic rocks relative to inorganic conditions. In contrast, other studies reported small to negligible effects of microbial activity on basaltic glass dissolution rates [151]. Such discrepancies are believed to result from different experimental approaches and initial nutritional status of the bacteria [81].

Fe is a micronutrient for most organisms and as such essential for a variety of enzymatic processes [79]. It is found in nature in its two oxidations states as Fe(II) and Fe(III). The solubility of Fe in natural fresh- and seawaters and therefore its bioavailability depends on several parameters such as pH, oxygen availability, redox potential, and the presence of organic ligands. At neutral pH and in oxygen rich environments, Fe is mostly present as insoluble Fe(III) forming Fe oxy(hydroxides). However, microorganisms have developed strategies to overcome this problem by creating reactive microenvironments at the mineral or glass surface. The most important are (i) complexation or oxidation/reduction of ions changing the equilibrium of the system [88,151] and (ii) bacterial acid production and proton consumption that change the solution pH and in this way enhancing dissolution and release of limiting nutrients (e.g., Fe, P) [150].

The majority (> 99%) of microorganisms in aqueous and soil environments are attached to surfaces and alteration studies have shown that surface attached microorganisms are by far more effective in dissolution of nutritional elements than unattached microorganisms [80]. Furthermore, the abundance of microorganisms is positively correlated with the age and alteration state of basaltic rocks [152]. It is known from field studies that microbial colonization and alteration is restricted to minerals and glasses containing beneficial elements (e.g., Fe, P) [79]. A loss of Fe(II) and Mn(II) and oxidation of residual Fe in subseafloor basaltic glasses was evidenced close to microbial alteration features [153]. In addition, Templeton et al., [77] found Mn(II) oxidizing bacteria on pillow basalts from Loihi Seamount, which supports a biological catalysis of Mn(II) oxidation during basalt weathering.

The microbial release of Fe and Mn from rocks into solution is also assumed to be relevant for the formation of Mn-nodules on deep sea sediments [154].

In this study, batch experiments were performed with a single bacterial species (*Burkholderia fungorum*) under laboratory conditions to investigate the potential role of microorganisms in the alteration and Fe mobilization from different natural basaltic rocks from the ICDP HSDP2 drill core. In addition, synthetic basaltic glasses were used as an analogue to specifically study the importance of the Fe redox state and residual stress on microbial activity. Biotic and abiotic control experiments were performed in a nutrient depleted medium and changes in solution chemistry were continuously monitored. Surface morphological features were analyzed after 41/42 days by environmental scanning microscopy and laser microscopy. The hypothesis was tested that microbial activity results in increased Fe mobilization and element release relative to abiotic conditions when the microorganisms are forced to actively scavenge nutrients from the basaltic rocks.

2.2 Materials and Methods

2.2.1 Site Description

The Hawaiian emperor chain comprises five main islands and more than 100 sea mounts. All of them are of volcanic origin, formed by mantle plume activity. The island of Hawaii is the youngest, largest, and the only one with active volcanism. The hydrology of the island is complex as it is not solely composed of a surface near freshwater aquifer overlaying seawater derived saline fluids but also by alternating layers of fresh- and seawater in greater depth [109]. Exchange in the circulating seawater system is fast enough to keep temperatures of ~9°C to depth of 1600 mbsl (mbsl = meter below sea level), which may be responsible for the relatively unaltered rocks observed in the drill core [58,107]. Below this depth, the temperature gradient slowly increases with 19 °C/km to 45°C at depth of ~3 km. The majority of weathering products on the island of Hawaii are transported via submarine groundwater discharge to the ocean as a consequence of highly permeable volcanic rocks [26]. This is shown in Fig. 2-1 where cold seawater penetrates the highly porous rocks and flows landwards. The seawater then rises towards the freshwater lens, mixes, and discharges as brackish water to the ocean surface waters.
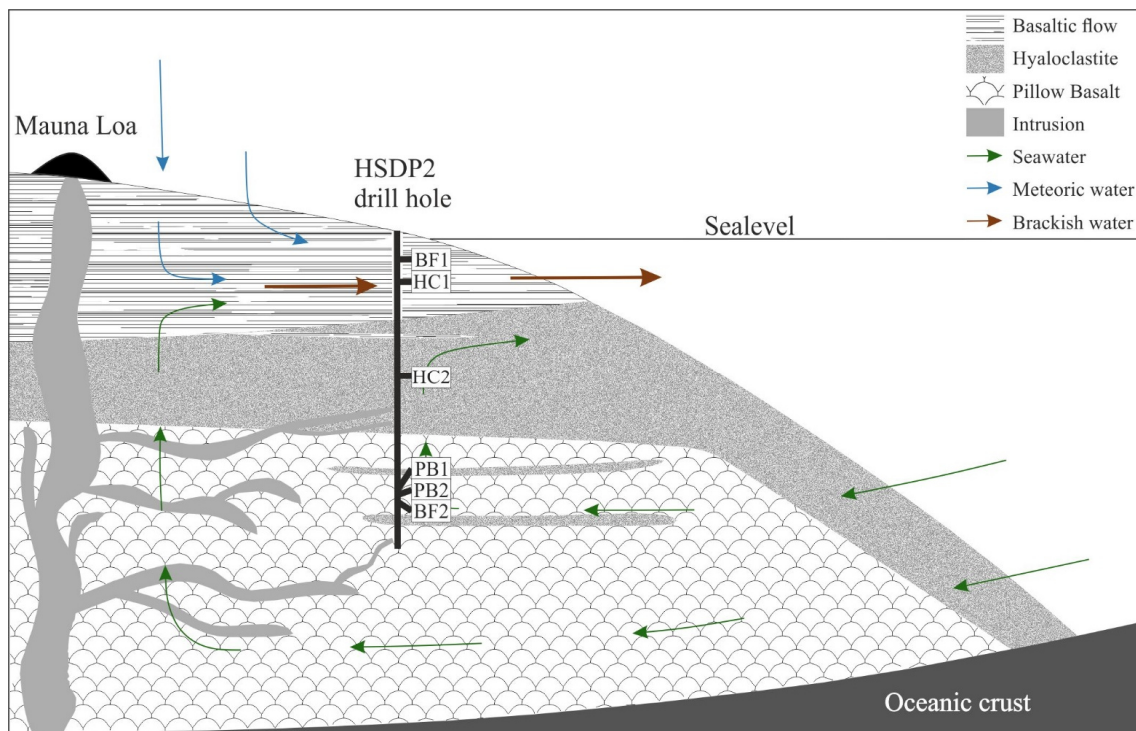
FIGURE 2-1: *Schematic overview of the drilling site. Shown are the main lithologies found in the drill core and a simplified illustration for the hydrology of the island of Hawaii. The relative sample depth of the natural basaltic rocks used in incubation experiments are shown as well (modified after [110]).*

Fig. 2-1 also shows a schematic overview of the drilled lithologies as well as the hydrological conditions and the relative sample locations in the ICDP HSDP2 drill core [105]. The core was drilled to a total depth of 3098 mbsl including subaerial (= erupted above sea level; from surface to 1079 mbsl) and submarine (= erupted below sealevel; from 1079 mbsl to total depth) volcanic rocks. The rock types included hyaloclastites, pillow basalts, basaltic flows, and to a lesser extent, intrusive rocks. Hyaloclastites are classified as a breccia composed mainly of glass with olivine phenocrysts and minor amounts of plagioclase and pyroxene [2]. Pillow lavas are characterized by glassy margins originated from submarine quenching and lower olivine contents compared to basaltic flows. Intrusive rocks occurred only at depth > 1883 mbsl and were petrographically and geochemically distinct from other core rocks [110,119]. Alteration of core rocks was in general less pronounced and mostly restricted to fractures, vesicles and olivines, leaving major portions of the rocks relatively fresh [105].

2.2.2 HSDP2 Core Rocks

Samples of the ICDP HSDP2 drill core were achieved from the repository at the American Museum of Natural History in New York. Six different basaltic rock samples of various sampling depths were chosen for the experiments, namely two basaltic flows (BF1: 604 mbsl; BF2: 2399 mbsl), two hyaloclastites (HC1: 732 mbsl; HC2: 1904 mbsl), and two pillow basalts (PB1: 2377 mbsl; PB2: 2385 mbsl). The samples were analyzed by polarization microscopy for their mineral content and texture (Figure 2-2). Considering their petrography, all samples contained olivine- $[Mg,Fe(II)]_2SiO_4$ and clinopyroxene $[Mg,Fe(II),Mn(II)]$ $[Mg,Fe(II),Mn(II),Ca]Si_2O_6$ phenocrysts in different proportions (5-20 vol.% olivine; 5-15 vol.% clinopyroxene). Plagioclase $[Ca,Al]_2Si_2O_8$ and/or $[Na,Al]_2Si_3O_8$ phenocrysts were present in samples BF1, HC1, and HC2 (5-20 vol.%). Secondary minerals such as phillipsite $[K,Na,Ca_{0.5}]_6Al_6Si_{10}O_{32}*12H_2O$ were observed in both pillow basalts PB1 and PB2 (veins) and sample BF2 (vesicles).

In most samples, the matrix was composed of glass (60-90 vol.%) with some showing small quench crystals of plagioclase (BF2, PB1, PB2). The glass was partially altered to palagonite along fractures. Samples BF1 and HC1 were the only samples with a cryptocrystalline matrix that was composed of different proportions of plagioclase, olivines, clinopyroxenes, and Fe-Ti-oxides and only minor interstitial glass.
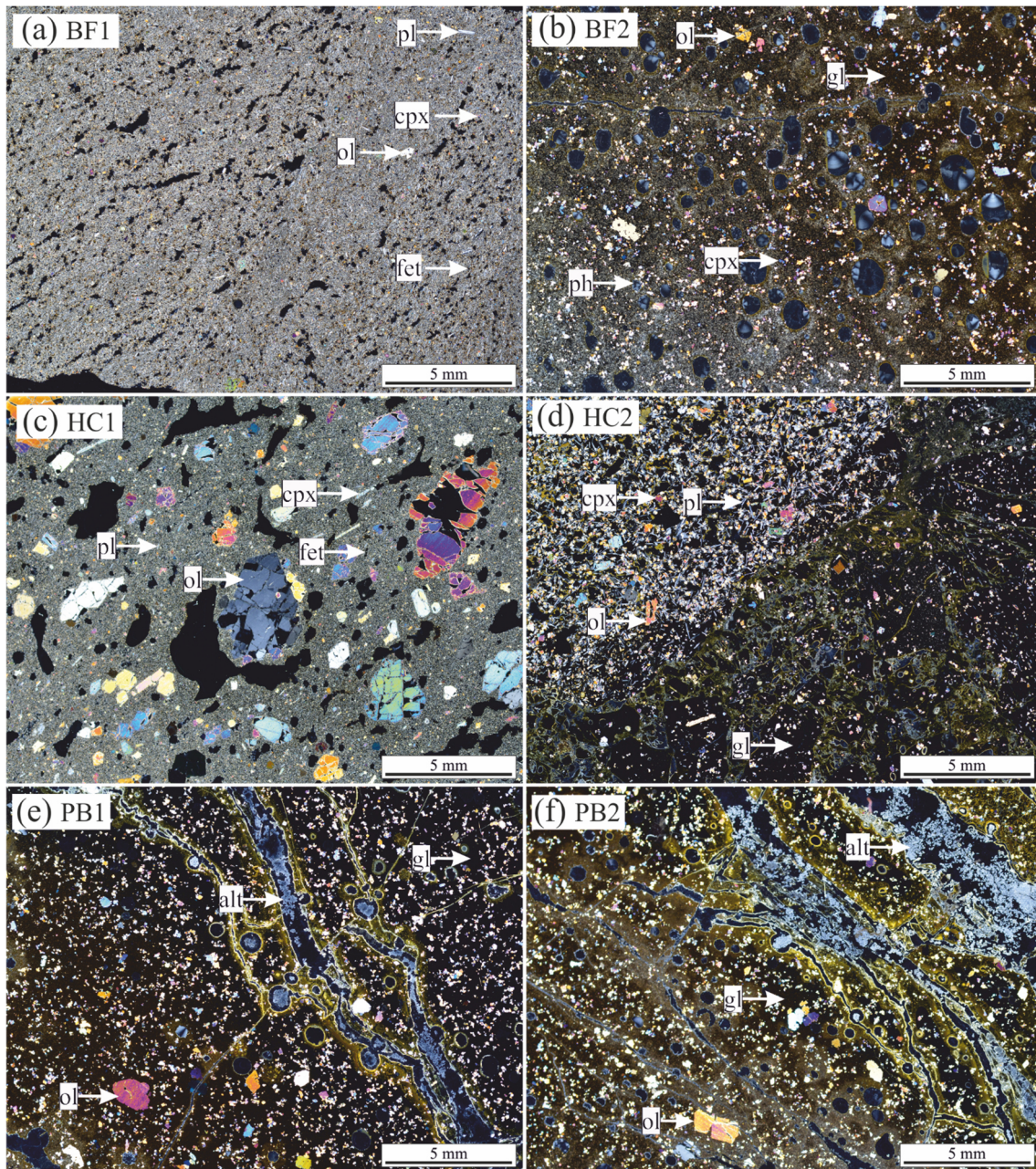
FIGURE 2-2*: Thin section photographs with cross-polarized light of HSDP2 drill core samples used for incubation experiments. **(a)**: basaltic flow (BF1) with cryptocrystalline matrix (pl (plagioclase) + ol (olivine) + cpx (clinopyroxene) + fet (Fe-Ti oxides)). **(b)**: basaltic flow (BF2) with gl (glass matrix) + ol + cpx and vesicles filled with ph (phillipsite). **(c)**: hyaloclastite (HC1) with cryptocrystalline matrix (pl + ol + cpx + fet) + ol + cpx + pl phenocrysts. **(d)**: hyaloclastite (HC2) with gl + ol + cpx + pl phenocrysts. **(e)**: pillow basalt (PB1) with gl + ol phenocrysts + alt (alteration products) in veins. **(f)**: pillow basalt (PB2) with gl + ol phenocrysts + alt in veins. The glass in all samples is partially altered to palagonite (brownish colored).*

2.2.3 Preparation of Core Samples and Synthetic Basaltic Glasses

Coarse rock fragments with relatively small contributions of fresh surfaces were used. Hence, core samples were gently crushed and sieved to separate the 1-2 mm and 0.2-1 mm fractions to minimize problems of element release from highly reactive fresh surfaces (due to sawing and breaking of samples). Fine particles were removed by washing with ultrapure H_2O in an ultrasonic bath (Sonorex RK1028, Bandelin) for 30 s. The suspension was discarded and the procedure repeated until no fine particles were observed. 350 mg of the 1-2 mm and 150 mg of the 0.2-1 mm fraction (= 0.5 g in total) were mixed and used for each experimental assay. The specific surface area (SSA) of core samples was determined using a multi-point N_2 adsorption BET method (Nova 4000e). SSAs of samples are 3.05 m^2/g (BF1), 28.89 m^2/g (BF2), 3.07 m^2/g (HC1), 33.73 m^2/g (HC2), 20.23 m^2/g (PB1) and 43.78 m^2/g (PB2). Furthermore, the amount of secondary amorphous and crystalline Fe, Al, and Si bearing phases was quantified using oxalate (17.5 g/L $C_2H_2O_4$ + 28.4 g/L $Na_2C_2O_4$) and dithionite citrate bicarbonate (70.4 g/L $Na_3C_6H_5O_7$ + 16.8 g/L $NaHCO_3$ + 0.5g $Na_2S_2O_4$) sequential extraction methods (for detailed description see [155,156]). These methods provided estimates on the proportions of different alteration phases and allowed a characterization of core samples with respect to their degree of alteration.

Natural rocks are heterogeneous concerning their mineral assemblage and degree of alteration. During submarine volcanic eruptions the basaltic melt is rapidly quenched (cooled) by its contact with seawater. The huge temperature differences between the surface (in contact with water) and the interior produces compressive stresses (interior) and tensile stresses (surface) that favor fracturing [157]. The residual stress can be released by heating the glass just below its glass transition temperature (T_g) and then slowly (< 1 K/min) cooling down to room temperature (annealing). Synthetic basaltic glasses with homogenous composition and known properties were used to investigate the influence of the Fe redox state and residual stress on microbial alteration and cell attachment. The synthetic glass was prepared from high purity powdered oxides and carbonates (SiO_2, Al_2O_3, Fe_2O_3, $CaCO_3$, $MgCO_3$, Na_2CO_3, TiO_2, K_2CO_3, $(NH_4)H_2PO_4$) and had the same major element composition than the natural glasses from HSDP2 drill core (Table 2-1; [158]). Melting was done in a platinum crucible at 1600°C for 2 h. The melt was quenched on a brass plate, crushed using a steel mortar and re-melted for an additional hour at 1600°C. A portion of the melt was then poured on a hot (550°C) steel plate, put in a chamber furnace at 550°C and slowly (< 1 °C/min) cooled down to room temperature to remove internal stresses from the glass (sample BAS1). This glass will be considered as

"stress-free" (annealed). The rest of the melt was quenched on a brass plate (sample BAS2). These two glasses were melted in air ($\log(fO_2/bar) = -0.37$) and were considered as oxidized glasses.

A portion of the quenched glass was crushed to a fine powder (< 64 µm) and put in a horizontal reduction furnace to achieve a certain Fe redox state. Here the powder was reduced below its glass transition temperature at 550°C for 24 h using Ar/H_2 gas mixture ($\log(fO_2/bar) = -21.53$). The reduced glass powder was then melted in a corundum crucible with a graphite lid on top at 1600°C for 5 min and small melt droplets were poured out and quenched on a brass plate (sample BAS3). Samples BAS2 and BAS3 were glasses with high residual stress similar to those in hyaloclastites and glassy margins of pillow basalts. The residual stress was not measured but the synthetic glasses could be seen as "endmembers" (no residual stress vs. high residual stress). The Fe redox state of the samples was determined by a wet chemistry method of Wilson [159] modified by Schuessler et al., [114]. Fe(II)/Fe$_{tot}$ ratios were 0.36 (BAS1) and 0.37 (BAS2) for glasses melted in air and 0.86 (BAS3) for the glass melted under reduced conditions (Ar/H_2).

TABLE 2-1*: Composition of the synthetic glass BAS and its natural analogue.*

Oxide	BAS [wt.%]	Garcia [158] c [wt.%]
SiO_2	54.01 ± 0.48^b	52.07 ± 0.42^d
TiO_2	2.82 ± 0.04	2.81 ± 0.42
Al_2O_3	12.70 ± 0.19	13.05 ± 0.35
FeO$_{tot}$^{a}	11.74 ± 0.44	11.80 ± 0.30
MnO	0.20 ± 0.09	0.18 ± 0.00
MgO	6.11 ± 0.12	6.26 ± 0.14
CaO	10.85 ± 0.18	10.51 ± 0.27
Na_2O	2.13 ± 0.08	2.23 ± 0.12
K_2O	0.41 ± 0.02	0.47 ± 0.05
P_2O_5	0.27 ± 0.09	0.30 ± 0.02
Total	101.26 ± 0.91	99.70 ± 0.12

^{a}all Fe expressed as FeO; ^{b} standard deviation of 90 measured points; ^{c} average chemical composition of basaltic glasses of ICDP HSDP2 drill core; ^{d} standard deviation of 14 measured glasses

2.2.4 Microorganism, Growth Medium and Culture Preparation

One of the main objectives was to investigate the microbial induced release of Fe and other major elements from core samples to solution. The growth medium should therefore entirely exclude such elements or contain them in very low concentrations to facilitate their detection when released in low concentrations. A growth medium first described in Wu et al., [150] was used for the experiments which contained only trace amounts of K, Mg, Mn, and Na and no Fe, Si, Al, Ca, and P (in the following denoted as M_{-P}). This medium was used for incubation and colonization experiments. The major constituents were: glucose (0.2 g/L), NH_4Cl (0.04 g/L), KCl (0.0005 g/L), and $MgSO_4$ (0.0005 g/L). The medium was prepared with ultrapure H_2O, the pH adjusted to 7 using ammonium hydroxide and sterilized by autoclaving at 121°C. Glucose was 0.2 μm sterile filtered and added after autoclaving. Furthermore, a second medium was prepared with the addition of NaH_2PO_4 and KH_2PO_4 0.3 g/L each (in the following denoted as M_{+P}). This medium was only used for preconditioning of the culture.

The rod-shaped Gram-negative bacterium *B. fungorum* (ATCC BAA-463) first described in Coenye et al., [160] was used. It was found in basaltic aquifers of Snake River Plain as well as Hawaiian volcanic deposits [161,162] and is known to weather rocks for nutrient acquisition [150,163]. The microorganism was obtained from the German Collection of Microorganisms and Cell Cultures (DSMZ) in Braunschweig, Germany. A microbial strain of *B. fungorum* was grown for 24 h in tryptic soy broth complete medium (17 g/L casein peptone, 2.5 g/L K_2HPO_4, 2.5 g/L glucose, 5 g/L NaCl, 3 g/L soya peptone; Sigma-Aldrich) at 30°C on a shaking table. Five milliliter were removed and centrifuged at 5000 rpm for 10 min. The supernatant was discarded, the culture washed with 5 ml M_{+P} and centrifuged. This step was repeated three times. The washed cells were again cultured for 24 h in 50 ml M_{+P} at 30°C on a shaking table. A cell density of 10^8 cells/ml was determined by counting with a hemocytometer. Five milliliter were removed, washed with M_{-P} and centrifuged. This step was repeated three times. A total of 50 μl of this culture were added to each assay in order to obtain an initial cell density of 10^5 cells/ml.

2.2.5 Incubation Experiments

Incubation experiments were performed to continuously monitor changes in solution chemistry between biotic and abiotic alteration of natural basaltic rocks from the HSDP2 drill core samples. The sample material was put in acid washed (5 M HNO_3) 100 ml glass Erlenmeyer culture flasks and sterilized in an autoclave at 105°C by a three times repeated sterilization with cooling to room temperature in between in order to kill possible spores (tyndallization). Subsequently, the sample material was washed with sterile, ultrapure H_2O to remove dissolved elements from possible mineral dissolution. The incubation experiments were conducted using 50 ml M_P medium and a fluid:rock ratio of 100:1. Three biotic and three abiotic parallels (chemical control experiments) were prepared for incubation experiments for each assay. The culture flasks were incubated on a shaking table (125 rpm) at T = 8°C and 30°C for 41 days. The two different temperatures were chosen to simulate the large temperature differences in the borehole (see section 2.2.1). Sampling was done in time intervals (after day 1, 3, 9, 28, 41) and 6.5 ml aliquots were collected each time. 6.3 ml of these aliquots were passed through a 0.2-µm nylon syringe filter for element concentration and pH measurements, 100 µl were fixed in 2% formaldehyde for total cell counting (SYBR green staining and fluorescence microscopy according to Hedrich et al., [164] and 100 µl were used for glucose measurements.

2.2.6 Colonization Experiments

Colonization experiments with synthetic basaltic glasses were performed to investigate the influence of Fe redox state and residual stress on microbial alteration and surface attachment of cells. A single melt droplet (about 1.5 g) of each sample was put in acid washed (5 M HNO_3) 100 ml glass Erlenmeyer culture flasks and processed similarly than the natural samples (see section 2.2.5). Colonization experiments were conducted using 50 ml M_P medium and a fluid:glass ratio of 50:1.5. For colonization experiments only two biotic parallels and one abiotic assay were prepared. The culture flasks were incubated on a shaking table (80 rpm) at T = 30°C for 42 days. No intermediate sampling was done for colonization experiments. After 42 days, 6.3 ml of the solution were collected and passed through a 0.2-µm nylon syringe filter for element concentration and pH measurements.

2.2.7 Chemical Analysis

Glucose consumption and pH were measured immediately after sampling on filtered solutions with glucose test strips (MQuant glucose test) and a Knick pH-Meter 766 Calimatic electrode (uncertainty of < 0.01 pH units), respectively. Glucose was measured to validate microbial growth in biotic experiments as well as absence of glucose consumption due to cell growth in abiotic controls. A total of 4.5 ml of the filtered solutions were acidified with 0.3 M HNO_3 and stored at 4°C until elemental concentration analysis. Measurement of dissolved Si, Al, Fe, Mn, Mg, Ca, Na, K, and P was done by Inductively Coupled Plasma Optical Emission Spectroscopy (ICP-OES, Varian 725-ES). Since fluid volume and element concentrations were decreasing with each sampling, the ICP-OES data were corrected as follows [150]:

$$C_{j,i}^* = \frac{C_{j,i}[V_0 - (j-1)V_s] + \sum_{h=1}^{j-1} C_{h,i}V_s}{V_0} \qquad \text{Eq. 2-1}$$

With $C_{j,i}^*$ being the corrected concentration of element i in the j sample, $C_{j,i}$ is the measured element concentration, V_0 is the initial fluid volume (0.05 L), V_s is the sampling volume (0.0065 L) and $\sum_{h=1}^{j-1} C_{h,i}V_s$ accounts for the mass of element i extracted during sampling.

2.2.8 Scanning Electron Microscopy (SEM)

The sample material from one of each parallels used in biotic incubation and colonization experiments was collected at the end of the experiments and critical point dried [165] for microscopic investigations of sample surface structures and biofilm formation. For this purpose, the cells were initially fixed with 3% glutaraldehyde in 10 mM HEPES buffer solution (pH 7) for 5 days at 4°C. Stepwise dehydration with graded series of 10, 30, 50, 70, 90, and ~100% ethanol was done for 10 min each. Following this, the samples were critical point dried to preserve cell morphologies, gold coated and stored in a desiccator until analysis. Samples were imaged on an Environmental Scanning Electron Microscope (ESEM; FEI Quanta 200) equipped with an AMETEKNew XL-30 EDX detector. A 20 kV accelerating voltage and a 10 mm working distance were used. All images were taken with a spot size 4 μm. Primary and secondary minerals as well as biofilm were identified using Energy Dispersive Spectroscopy (EDS) with a focused beam and a counting time of 100 s.

2.3 Results

2.3.1 Incubation Experiments

2.3.1.1 Glucose Consumption, Bacterial Growth and pH Shift

Glucose (200 mg/L) was added to all experimental assays (biotic and abiotic) as carbon source for microbial growth. The glucose consumption and cell densities were measured throughout the experiments in different time intervals. Fig. 2-3a,b show the glucose consumption and cell densities of *B. fungorum* grown on natural basaltic rocks at 30°C and 8°C. Bacterial growth was evidenced in all inoculated experiments by glucose consumption. Within the first 3 days glucose was no longer measurable in all 30°C experiments except for sample HC2 for which glucose was completely consumed after 28 days. The same observations were made for the 8°C experiments but more than 4-20 days delay were observed. In abiotic controls for both, 30 and 8°C, no glucose consumption was observed and concentrations remained constant at the initial concentration. At the time glucose concentrations decreased in biotic experiments, cell densities increased from initially 10^5 cells/ml to a maximum of $2 \cdot 10^8$ cells/ml (BF1 and HC1) and reached a stationary phase after 9 days in 30°C experiments. Between days 9 and 41 cell densities remained constant at $\sim 10^8$ cells/ml. For samples BF2,
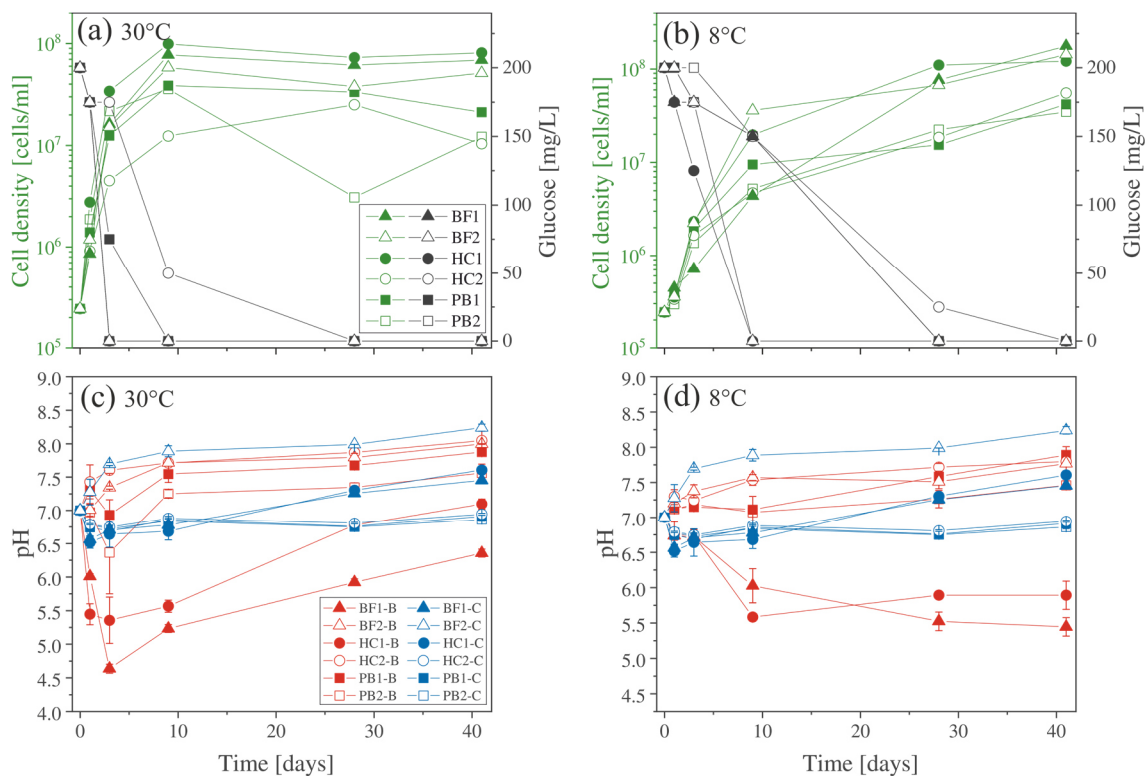

FIGURE 2-3: *Glucose consumption (black), cell growth (green) and pH evolution for biotic (red) and abiotic (blue) versus time for incubation experiments at 30°C (**a,c**) and 8°C (**b,d**). Note that cell numbers were determined for one of the three parallels only.*

HC2, PB1, and PB2 the same growth patterns were observed but with lower cell densities. In experiments at 8°C, no stationary phase was reached and cell densities increased till day 41 to more than $4 \cdot 10^8$ cells/ml. The bacteria were uniform in shape (rod-shaped) and size (1-2 μm) throughout all biotic experiments as evidenced by fluorescence microscopy. Furthermore, no cells were detected in abiotic control experiments. It is therefore concluded that abiotic controls remained sterile during the experiments.

The shift in pH of the experimental solutions for abiotic and biotic experiments is shown in Fig. 2-3c,d. For all abiotic controls pH slightly decreased during the first day by 0.5 log units and slowly approached to the initial pH 7 with time. An exception is sample BF2, where the pH increased to above 8. Considering biotic experiments at 30°C the pH for two of the samples strongly decreased in the first 3 days to 5.5 (HC1) and 4.5 (BF1) and increased with time to approach the initial pH 7. For sample HC2 and BF2 the pH rapidly increased to 7.5 and remained constant over time. For both pillow basalts (PB1 and PB2), the pH slightly decreased after day 1 followed by an increase to pH 7.5 and remained constant over time. For 8°C experiments, similar trends were observed but delayed by several days (e.g., the pH for samples BF1 and HC1 remained acidic until day 41).

2.3.1.2 Element Release

With the exception of Ca, all other elements were initially below the detection limit in the starting medium (M_P). Evaporation of the liquid during the experiments was found to be linear and in total approximately 5.5 ml over 41 days. Fig. 2-4 shows the corrected dissolved elemental concentrations vs. time for incubation experiments with natural basaltic rocks at 30°C. For samples HC2, PB1, and PB2, concentrations of dissolved Si, Mg, Ca, K, Na, P, and Mn were higher at day 1 in abiotic experiments compared to their biotic analogs. In biotic and abiotic experiments, Si and Mg concentrations steadily increased until day 41. Ca, K, Na, P, and Mn concentrations in biotic experiments increased until day 3 and reached steady-state conditions. In contrast, Ca, K, Na, P, and Mn concentrations in abiotic experiments sharply decreased after day 1 or 3 and reached steady-state conditions by day 9.

The patterns for Ca, K, Na, P, and Mn in abiotic experiments might simply reflect the precipitation of secondary phases [150]. Only the concentrations of dissolved Fe and Al were higher in biotic experiments than abiotic controls for samples HC2, PB1, and PB2. A distinct different trend was observed for samples BF1 and HC1. Here, the concentrations of dissolved Si, Mg, Ca, K, P, and Mn were lower in abiotic experiments compared to biotic analogs.
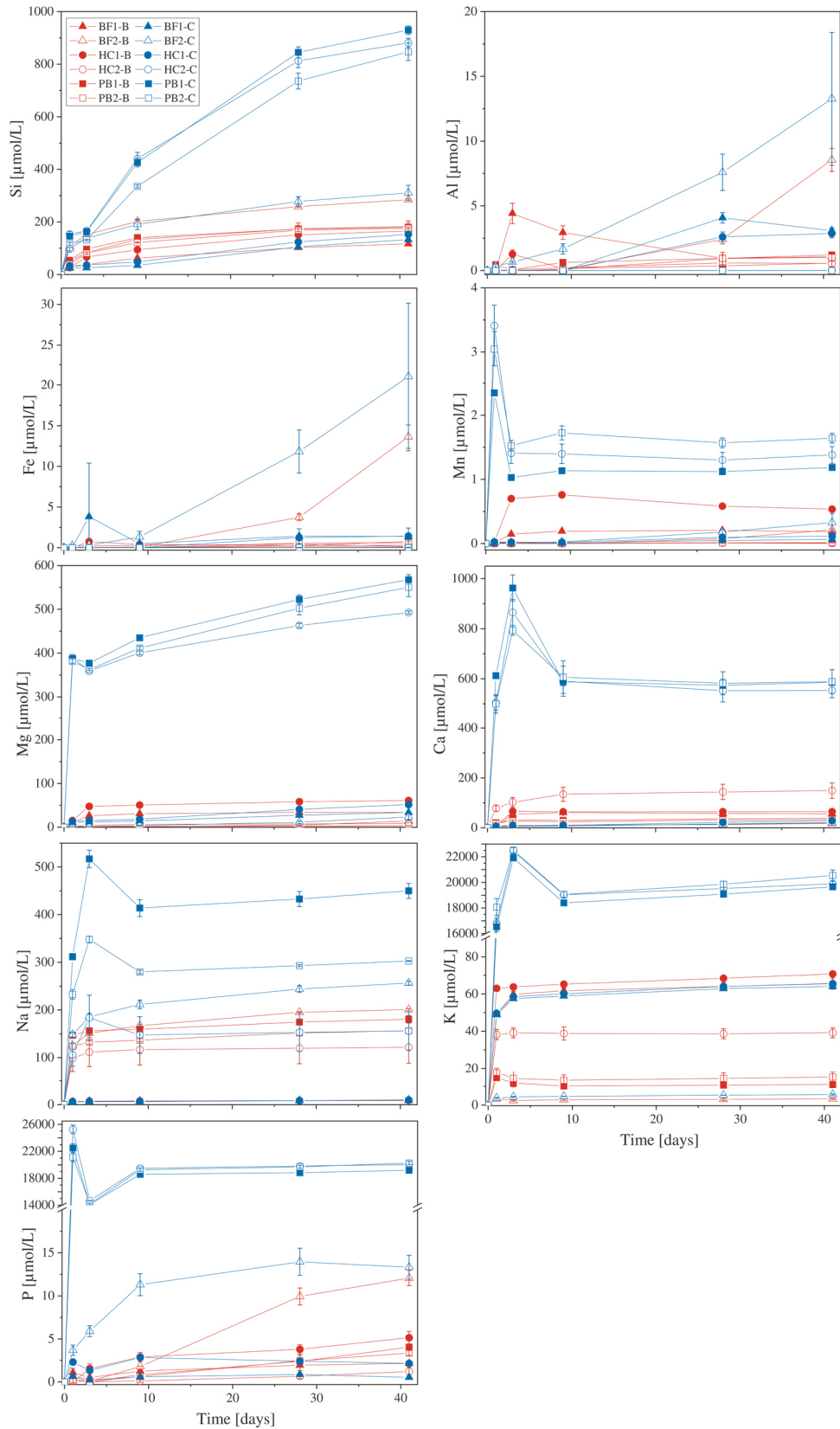
FIGURE 2-4*: Concentration versus time of dissolved major elements in biotic (red) and abiotic (blue) incubation experiments at 30°C. Error bars show the standard deviation of three parallel experiments. The sample suffixes -B and -C denote biotic and abiotic (control) experiments, respectively.*

The differences between biotic and abiotic experiments are not as pronounced as for the samples HC2, PB1, and PB2 with concentrations not more than a factor of 2 higher in biotic experiments. The concentrations of dissolved Fe and Al were higher in abiotic experiments. Dissolved Na was not measurable for samples BF1 and HC1. The concentrations of dissolved elements for sample BF2 were between those two groups (HC2, PB1, PB2 vs. HC1, BF1) described above with mostly higher concentrations in abiotic controls but nearly no dissolved K and Ca for biotic and abiotic experiments. For 8°C experiments the same trends were observed but with lower total element concentrations (for details see Supplemental Figure S2-1).

2.3.1.3 Surface Morphologies

To further investigate the attachment of microbial cells and precipitation of secondary minerals on surfaces during alteration of basaltic rocks and glasses the experimentally altered samples were analyzed using SEM. The following results are based on observations only and are not further quantified by statistical methods. Microbial cells of *B. fungorum* where found on all biotic incubated basaltic rocks in different quantities. Fig. 2-5a-f shows secondary electron images of the biotic altered natural basaltic rock samples. Attached cells of *B. fungorum* appeared in rods with 0.5-2 µm length and small nm-sized particles often adhere to the cells (Figure 2-5a; arrow). Filamentous structures connecting individual cells were common when cells were located close to each other (Figure 2-5b). Compositional analysis of the filaments was not possible due to their small size (< 0.1 µm). Glassy surfaces were in some places strongly altered and covered with precipitates. Such regions showed imprints that were well fitting in size to microbial rod-shaped cells (Figure 2-5c; arrows). Fig. 2-5d shows basaltic glass (left site) and an olivine phenocryst (right site) in direct contact. The glass surface (Figure 2-5e) was intensively covered with cells of *B. fungorum* whereas the mineral surface (Figure 2-5f) was (almost) free of cells. Although the distance on the sample between Fig. 2-5e,f was less than 100 µm, direct attachment of cells on smooth mineral surfaces was scarce and cells were often scattered.

Cells appeared to be more abundant on glassy surfaces and particularly along fractures and holes. Apart from attached microbial cells, no major differences in surface morphologies between biotic and abiotic altered basaltic rocks were observed. In Fig. 2-5g-i abiotic altered samples are shown featuring characteristics that were observed for biotic as well as abiotic altered samples. Glass surfaces were in some parts intensely altered (Figure 2-5g) and in other

parts without any signs of alteration (not shown here). Such fresh glass surfaces are probably fractured surfaces and a relic of sample preparation. Fine rock material accumulated along fractures was often covered and cemented with a mesh-like structure of secondary minerals (Figure 2-5h). In some cases, porous spherical structures located in former primary vesicles of the basaltic glass (Figure 2-5i) and round spheres adhering to the surface (not shown) were observed. Qualitative EDX analysis indicated that the porous and round spheres were most probably zeolites and carbonates, respectively.
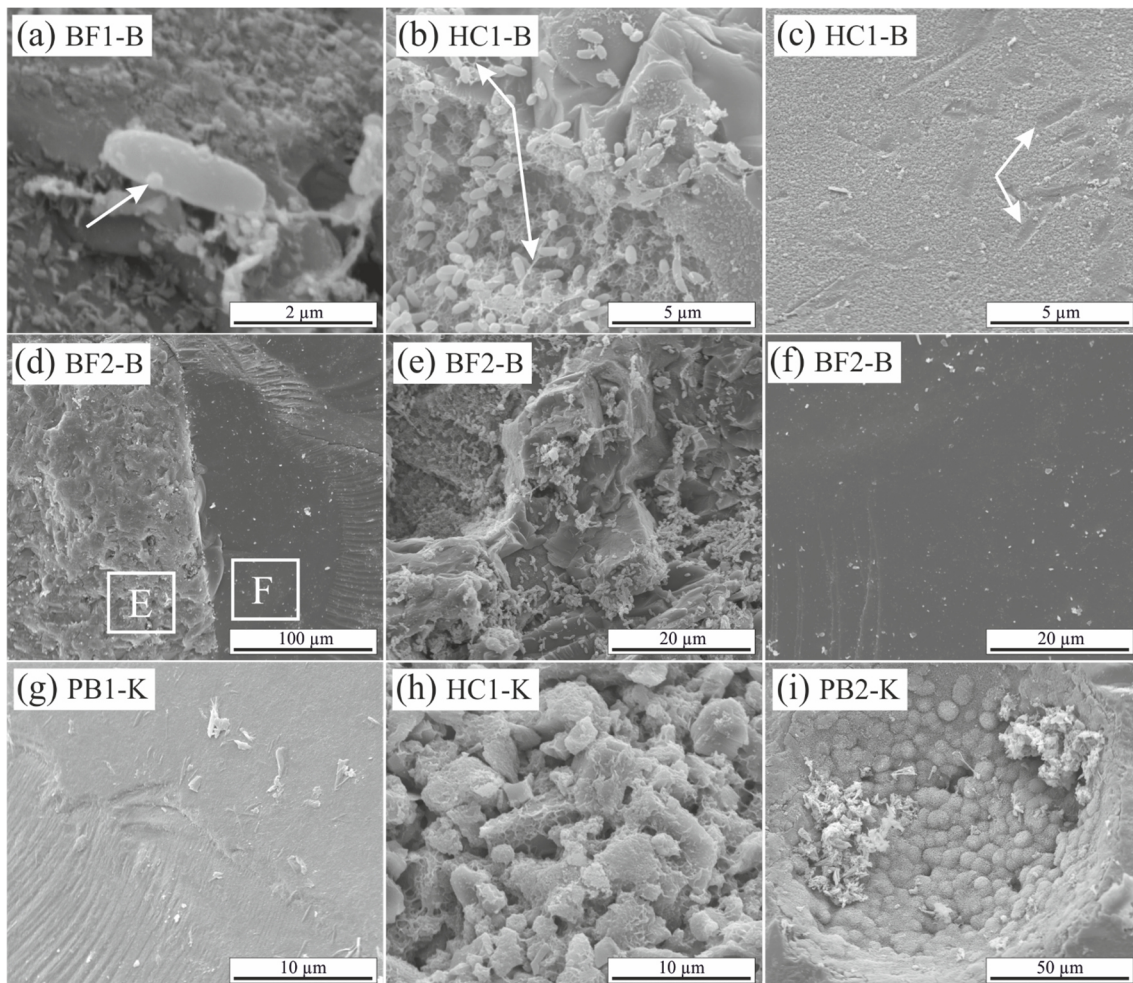
FIGURE 2-5: *Scanning electron micrographs of biotic and abiotic incubation experiments with HSDP2 core samples (**a-f**: biotic experiments; **g-i**: abiotic experiments). (**a**): single cell with small particles adhering to its surface. (**b**): clusters of cells connected by filamentous structures. (**c**): altered glass surface with possible imprints of microbial cells. (**d**): basaltic flow (BF2) showing basaltic glass (left) and olivine crystal (right). (**e**)/(**f**): enlargement of the areas indicated in image (**d**). Glass (**e**) is intensively colonized by cells of B. fungorum whereas cells are absent on olivine surfaces (**f**). (**g**): abiotic altered glass surface covered with alteration products. (**h**): small particles cemented in mesh-like alteration products. (**i**): porous spherical structures in a primary vesicle.*

2.3.2 Colonization Experiments

The colonization experiments were primarily designed only to investigate the influence of the Fe redox state and residual stress on the activity and the interaction between microorganisms and basaltic glass. For that reason, pH and concentration of dissolved elements was measured at the beginning and upon termination of the experiments.

2.3.2.1 Shift in pH

It has to be noted that information about pH variations during the experiment are not provided and, thus, the observations refer only to the start and end of the experiment. The pH of the experimental solutions in abiotic controls did not show any systematic variations with changes in residual stress or Fe(II) content and decreased from initially pH 7 to ~6.5 after 42 days (for samples BAS 1-C, BAS 2-C, BAS 3-C). Considering biotic experiments, the pH of the solution significantly decreased with increasing Fe(III) content from initially 7 to pH 6 (BAS 3-B) to pH 3.5 (BAS 1-B, BAS 2-B). No effects of residual stress on the evolution of the pH were observed (see also Supplemental Figure S2-2).

2.3.2.2 Element Release

The concentration of dissolved elements measured after 42 days is shown in Fig. 2-6. In abiotic experiments, concentrations of dissolved Ca and Mg only slightly increased with residual stress and Fe(II) content in the glass whereas for Si differences were more pronounced. Dissolved Fe and Al were below the detection limit in all abiotic experiments. K concentrations were similar for all solutions and independent of Fe redox state and residual stress. Na, Mn, and P concentrations were close to the detection limit of the ICP OES in abiotic as well as biotic experiments and, hence, not part of further investigations.

In biotic colonization experiments, concentrations of dissolved Si, Mg, Ca, Fe, and Al increased with residual stress as well as with increasing Fe(II) content in the glass. Dissolved Si concentrations increased from 7 to 15 µmol/L (BAS1→BAS2) and further to 82 µmol/L (BAS2→BAS3) with increasing Fe(II) content in the glass. Ca and Mg concentrations increased by a factor of 2 with increasing residual stress in the glasses (BAS1→BAS2) and again by more than a factor of 2 with increasing Fe(II) content (BAS2→BAS3). Dissolved Fe and Al were detected in biotic experiments only, and their concentrations strongly depended on both, residual stress (increase from 1.5 to 9 µmol/L) and

Fe redox state (further increase from 9 to 28 µmol/L). K concentrations were found to be independent from residual stress and Fe(II) similar to abiotic experiments.
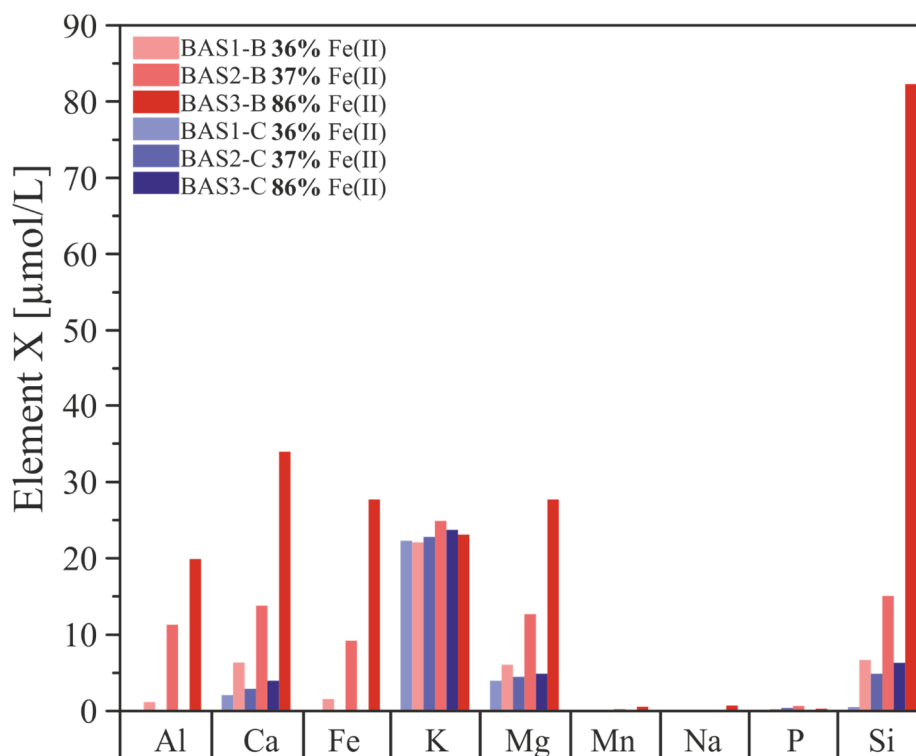
FIGURE 2-6: *Concentration of dissolved major elements in biotic (red) and abiotic (blue) colonization experiments after 42 days. Note that concentrations have been measured in one of the parallels only and these data represent absolute values. The sample suffix -B and -C denotes biotic and abiotic (control) experiments, respectively. BAS1: annealed (no residual stress), low Fe(II) content. BAS2: quenched (residual stress), low Fe(II) content. BAS3: quenched (residual stress), high Fe(II) content.*

2.3.2.3 Colonization Experiments

The influence of single parameters such as Fe redox state and residual stress on microbial alteration as well as the attachment of cells on surfaces were investigated in detail in colonization experiments with synthetic basaltic glasses. The following results are based on observations only and were not further quantified by statistical methods. Nevertheless, the images are representative for the entire sample and no strong variations were observed (see Supplemental Figure S2-3). Compared to the incubation experiments with natural samples, cells adhering to the surface and biofilm formation on it were more pronounced (Figure 2-7). The abundance of cells and the extent of the biofilm on the glass surface seemed to depend on the residual stress and only to a minor extent on the Fe(II) content of the glass. Considering the

residual stress, glass BAS1 (annealed = no residual stress) was sparsely colonized with cells and biofilm that were scattered over the glass surface (Figure 2-7a).

With increasing residual stress, the abundance of cells and the extent of biofilm formation seemed to increase for sample BAS2 (Figure 2-7b). The morphology of the cells was not as uniform as observed in incubation experiments and could be distinguished by two different forms: Cells similar in shape and size to those described previously and cells encapsulated in biofilm. Those encapsulated cells were round shaped, up to 10 μm in diameter and grouped together to form colonies (Figure 2-7c; white arrow). With the presence of two types of cells, two types of filamentous structures were observed. The first was comparable to those observed
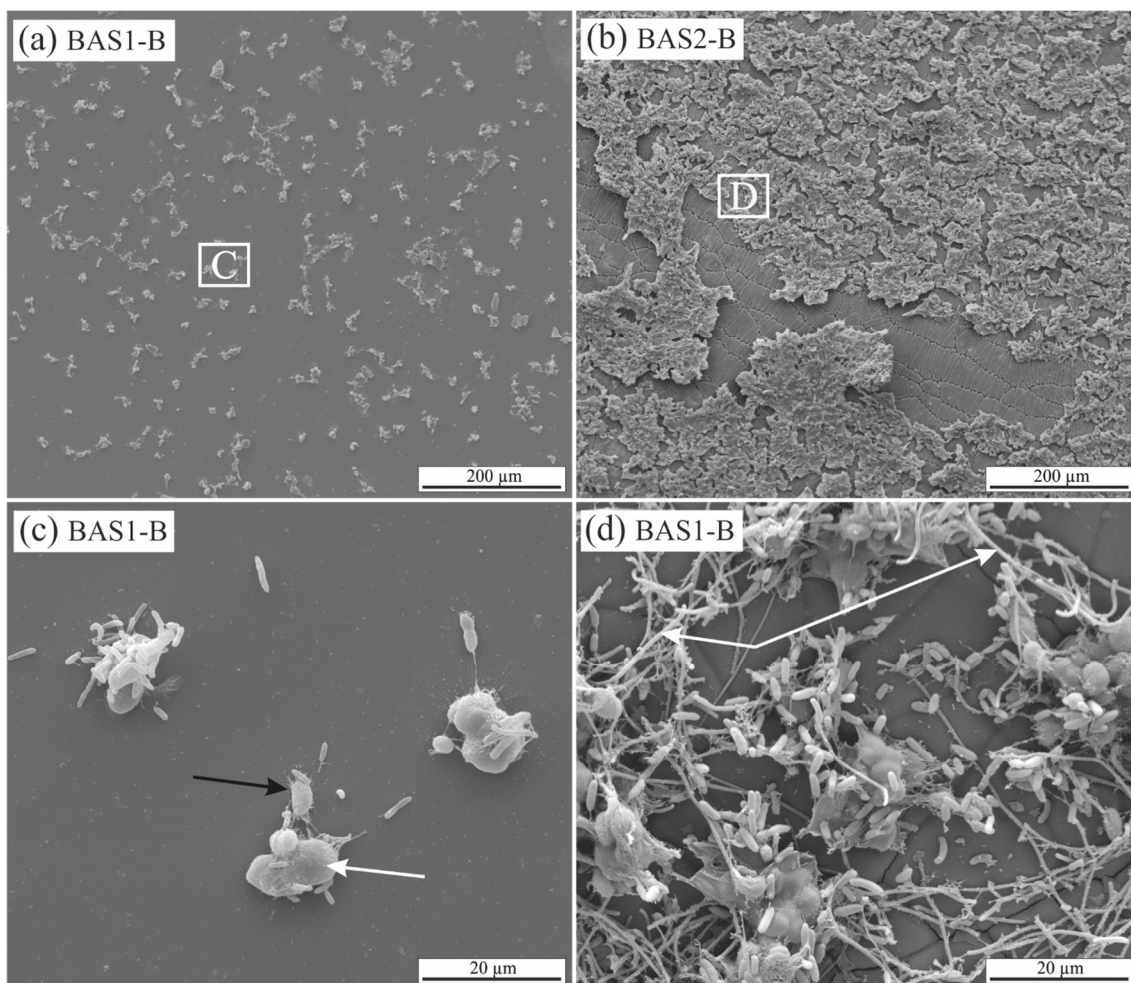
FIGURE 2-7: *Scanning electron micrographs of biotic colonization experiments with synthetic basaltic glasses.* **(a)**: *BAS1 (no residual stress; low Fe(II) content) with clustered cells scattered on the surface.* **(b)**: *BAS2 (residual stress; low Fe(II) content) showing intense colonization and biofilm formation on the surface. Note also the network of cracks that became altered during the experiment.* **(c)**: *enlargement of the area indicated in image* **(a)**. *Two cell types were observed: cells comparable in shape and size to those observed in incubation experiments and large (up to 10 μm), round shaped cells forming colonies (white arrow). Filamentous structures (nm sized) seem to facilitate cell-surface attachment (black arrow).* **(d)**: *enlargement of the area indicated in image* **(b)**. *A second type of filamentous structures (μm sized) was observed connecting the colonies (white arrow).*

56

in incubation experiments. The filaments were a few nm thin, associated with individual cells and seemed to facilitate direct attachment of cells to the glass surface (Figure 2-7c; black arrow). The second type of filaments was much thicker (up to 1 µm) and connected the previously described colonies (Figure 2-7d; arrow). The biofilm did not entirely cover the glass and seemed to be partly disrupted. It is assumed that this had happened during sample preparation for SEM since the critical point drying process involves several steps that could damage the biofilm.

Comparison of the unaltered and altered glass surfaces by laser scanning microscopy showed considerable differences in surface alteration between biotic and abiotic experiments (Figure 2-8). The quenched glasses (BAS2 and BAS3) exhibited a fine network of cracks at the surface related to thermal contraction at the interface between the melt and air during cooling (Figure 2-8a). Analysis of images from laser scanning microscopy showed that such cracks were closed before the experiments (Figure 2-8a; profile). In abiotic experiments, the cracks were partially altered and deepened after 42 days (Figure 2-8b; profile). The surface did not show any signs of dissolution or mineral precipitation. In biotic experiments, however, alteration of the surface was much stronger pronounced. All cracks were intensively altered and deepened up to 2 µm (Figure 2-8c; profile). The glass surface had become rough, possibly by precipitation of secondary phases. No signs of individual etch pits were observed. The intensity of the glass surface alteration was found to be mainly related to residual stress and only to a minor extent to the Fe(II) content.
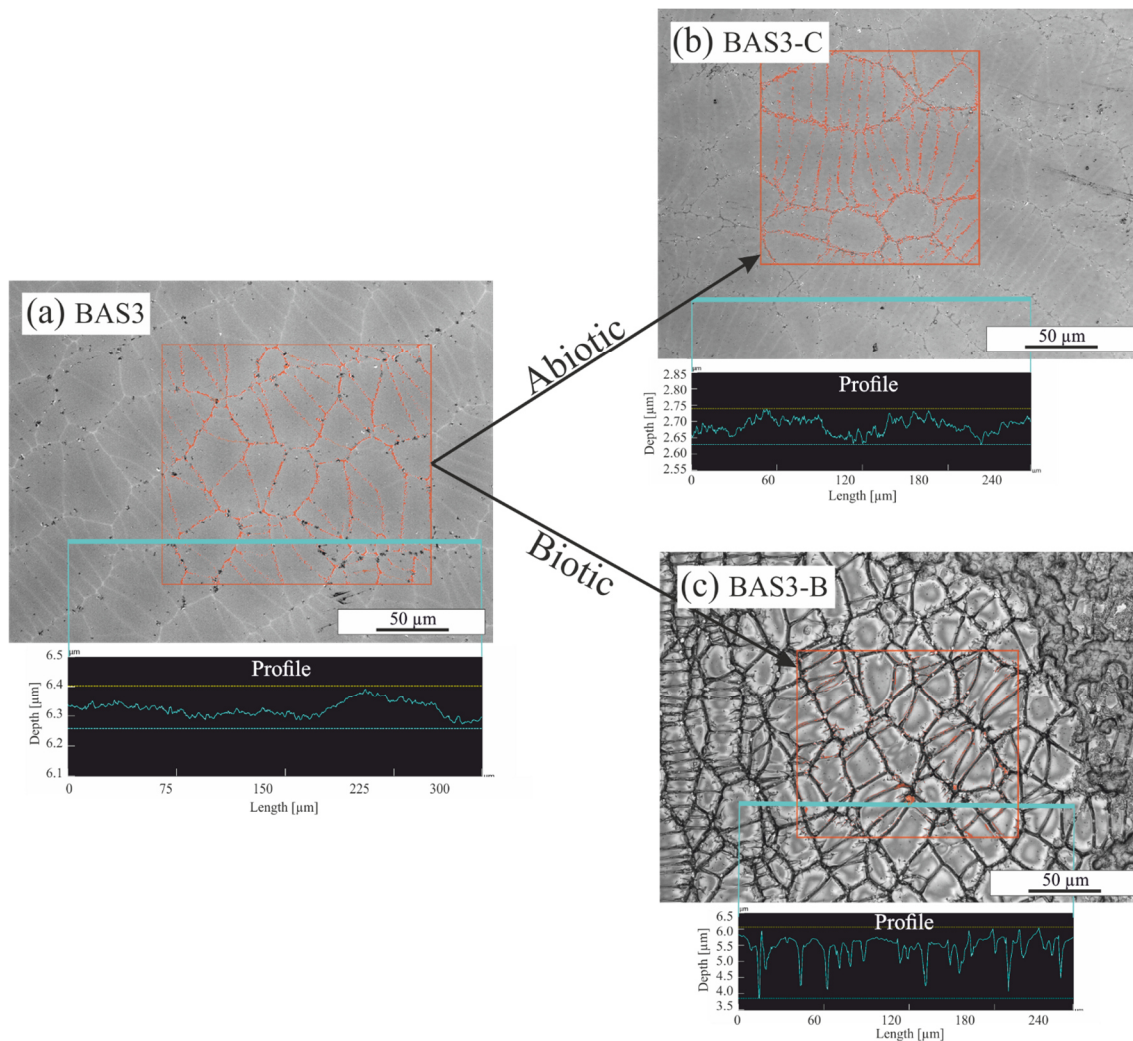
FIGURE 2-8*: Laser scanning microscopy images of glass BAS3 surfaces before and after biotic and abiotic experiments. **(a)** Glass surface prior to the experiments. A fine network of stress-induced cracks is visible. **(b)** Glass surface after abiotic colonization experiment. Some of the cracks are slightly altered but changes are negligible. **(c)** Glass surface after biotic colonization experiments. The entirety of the cracks is intensively altered and the surface is covered with biofilm (upper right corner). The measured profiles indicate that cracks are not deepened prior to and after abiotic experiments (see **(a,b)**) but are up to 2 µm deep after biotic alteration (see **(c)**). Note the different scales on the y-axis for the profiles.*

2.4 Discussion

2.4.1 Microbial Growth with Basaltic Rocks as a Nutrient Source

Microbial life is ubiquitous in the oceanic crust and contributes a substantial part to geochemical element cycling [65,166–168]. It is well known that microorganisms are capable of producing organic acids and metal specific organic ligands to sequester essential nutrients [79,81,169]. Some metal-oxidizing bacteria are also able to biological catalyze Fe(II) or Mn(II) oxidation for energy gain [74,75,77,147,148]. However, there is still uncertainty whether microorganisms actively scavenge elements from the rock or simply incorporate elements that are released by abiotic weathering processes [143,151,167,170–173].

In the incubation experiments with natural basaltic rocks a marked uptake of elements by *B. fungorum* from solution was observed. Considering Fig. 2-4 the uptake of elements from solution by *B. fungorum* in biotic incubation experiments was high for samples HC2, PB1, and PB2, e.g., concentration of dissolved Ca in abiotic controls was > 500 µmol/L compared to < 200 µmol/L in biotic experiments. These samples were characterized by high SSAs (> 30 m^2/g). Deviations from the aforementioned behavior included samples BF1 and HC1 with low SSAs of 3.05 and 3.07 m^2/g, respectively. Here, the concentration of released elements was lower in abiotic controls compared to the biotic experiments, e.g., concentration of dissolved Ca in chemical controls was < 30 µmol/L compared to > 50 µmol/L in biotic experiments. These distinct trends were observed for all major elements except Fe and Al. Concentrations of dissolved Fe were low for most samples in both, biotic and abiotic experiments. However, only from these observations it cannot be deduced that basaltic rocks from HSDP2 drill core are a nutrient source and facilitate growth of *B. fungorum*.

As a consequence of autoclaving at 105°C large amounts of elements were released into solution possibly by dissolution of secondary minerals. Removal of such elements by washing with sterile H$_2$O was not sufficient enough and relics of secondary minerals may be rapidly dissolved at the beginning of the experiments resulting in high initial concentrations of Mn, Mg, Ca, Na, K, and P in the solution (see Figure 2-4). Considering a marked release of elements during autoclaving, one would expect such elements being released in all assays (biotic and abiotic) in about the same quantity. Although a portion of the elements released during autoclaving in biotic assays were most probably scavenged by *B. fungorum* no clear indication was obtained that the bacteria actively participated in dissolution of the basaltic rocks in incubation experiments.

By contrast, the results of colonization experiments with synthetic basaltic glasses clearly showed that *B. fungorum* was capable of obtaining nutrients directly from the glass instead of passively scavenging dissolved elements as stated above. First, the release of major elements during sterilization (autoclaving) of synthetic basaltic glasses was lower compared to the natural basaltic rocks of HSDP2 drill core. Hence, the environment in colonization experiments was supposed to be nutrient depleted in the initial stages of the experiments. Second, the presence of *B. fungorum* strongly enhanced the basaltic glass dissolution and the release of major elements to solution relative to abiotic controls (see Figure 2-6). This is most pronounced for dissolved Fe and Al which were detected in biotic experiments only. The basaltic glass in colonization experiments was the only source for the microbes to obtain essential nutrients such as Fe and P. It is therefore most likely that *B. fungorum* was forced to actively scavenge nutrients for microbial growth and metabolism in colonization experiments from the basaltic glasses (in contrast to a nutrient rich environment in incubation experiments).

The low concentrations of dissolved Fe in biotic incubation experiments are in contrast to what was observed in biotic colonization experiments with synthetic basaltic glasses. Due to the relatively high concentrations of dissolved P in incubation experiments (up to 18 mmol/L for samples HC2, PB1, and PB2) it is possible that the Fe had been precipitated as Fe-phosphate. However, no Fe-phosphate precipitates at the surface of the natural samples during SEM analysis were observed. Wu et al., [150] also investigated the interaction of *B. fungorum* with basaltic rocks and found relatively high (up to 15 µmol/L) concentrations of Fe but no P in their biotic experiments. They assigned the release of Fe in the experiments to microbially produced chelators. Besides from experiments with a minimal growth medium (M-$_P$; see 2.2.4) they also performed experiments with a P-rich medium (2.5 mmol/L P) and here, no dissolved Fe was detected in biotic experiments.

Comparing the observations of Wu et al., [150] and those of this study, it seems likely that P was a limiting factor for the growth of *B. fungorum*. In case the solution was depleted in P, the release of Fe from the glass/rock was higher than its uptake by the microbes and the concentration of Fe in the solution increased. If the solution was enriched in P, all the dissolved Fe was either used by *B. fungorum* or precipitated as secondary Fe-phosphates. This would mean that P was preferentially dissolved from the glass which also contained Fe in appreciable amounts. This assumption is also supported by colonization experiments. Here the concentration of dissolved P in biotic experiments was close to the detection limit for all glasses (see Figure 2-6). Dissolved Fe, on the other hand, was detected in all biotic experiments in

appreciable amounts. The need of some microorganisms for P was also evidenced by Bailey et al., [147] in laboratory experiments. Microbial growth on basaltic glasses was enhanced on those doped with apatite as P source. From this observations it seems to be likely that in case *B. fungorum* was not able to obtain nutrients from solution only, the organism started to attack the rock/glass possibly by lowering the pH (as observed for samples HC1/BF1 and BAS1/BAS2) to acquire essential nutrients and thus increasing the overall dissolution rate.

2.4.2 Factors Influencing the Intensity of Microbial Alteration

The SSA is an important parameter as it determines the reactive surface susceptible to chemical exchange with the environment and might also have an influence on microbial behavior during alteration. A high release of Si, Mn, Mg, Ca, Na, K, and P to solution for samples with high SSA was observed. As previously mentioned this release is ascribed to be an artifact resulting from autoclaving. For instance, the results from the sequential extractions (see section 2.2.3) provide evidence that for samples with a high SSA (BF2 = 28.89 m^2/g, HC2 = 33.73 m^2/g, PB1 = 20.23 m^2/g, PB2 = 43.78 m^2/g) the amount of amorphous secondary Fe, Al, and Si phases are five times higher (Ø 484 µmol/g) compared to samples with a low SSA (BF1 = 3.05 m^2/g, HC1 = 3.07 m^2/g) (Ø 85 µmol/g). Dissolution of these amorphous secondary phases during autoclaving is favored as an explanation for unusual high initial dissolved element concentrations. It is therefore difficult to ascribe specific observation in the experiments to the SSA. Nielsen and Fisk [27] measured SSA's of different extrusive volcanic rocks of the oceanic crust and inferred that the SSA is not a limiting parameter for biomass production and cell attachment. From the observation it seems likely that SSA contribute only to a minor part to the microbial alteration rate and is a parameter mainly controlling elemental release rates during abiotic alteration.

The Fe redox state of basaltic rocks from the ICDP drill core is a mixture of different Fe sources from primary minerals (e.g., Fe(II) from olivine), glass (Fe(II) and Fe(III)), and secondary minerals (mainly Fe(III)). Thus, the Fe redox state was quite heterogeneous and varied in the same sample making predictions about its contribution to microbial alteration difficult. For this reason, chemically homogeneous synthetic basaltic glasses with well-known Fe redox state were used as an analog for natural glasses. It was observed that the concentration of dissolved Fe and other major elements in biotic colonization experiments increased with increasing Fe(II) content (see Figure 2-6). In abiotic colonization experiments the concentration of dissolved elements (except Fe and Al) increased with increasing Fe(II) content as well but

less pronounced compared to biotic experiments. Within this study, it was not the goal to point out the mechanisms by which *B. fungorum* participated in the basalt dissolution. However, in the following possible mechanisms that seem reasonable to us are discussed. A variety of marine Fe oxidizing microorganisms (FeOB) such as the neutrophilic, chemolithotrophic bacterium *Mariprofundus ferrooxydans* are able to grow on basaltic glasses and are capable of using Fe(II) as an energy source [75]. However, abiotic oxidation and hydration of Fe(II) at circumneutral pH and oxygenated conditions are fast [174]. Microorganisms circumvent this problem by living in an acid or microaerophilic environment where Fe(II) is more stable [74]. Both of the aforementioned situations are not applicable to the experiments of this study. Changes in the solution pH were not restricted to the silicate-biofilm interface [175] but affected the whole solution. Moreover, pH variations were not uniform among the samples and for some the pH became basic with time, thus, it seems unlikely that *B. fungorum* used Fe(II) as an energy source.

The chemical durability of silicate glasses is mostly controlled by their composition. Network formers such as Si and Al increase the chemical durability by polymerizing the glass structure whereas network modifiers such as Na and Ca weaken the glass structure [31]. Fe(III) has been shown to act as a network former similar to Al(III) increasing the chemical durability of glasses [176]. Fe(II) on the other hand was found to be a network modifier depolymerizing the glass network and decreasing its chemical durability [177]. The pH changes observed in colonization experiments for high Fe(III) glasses (BAS1/BAS2) can therefore be considered as a reaction of *B. fungorum* to release nutrients from the chemically more durable glass possibly by production of organic acids. This assumption is also promoted by observations from incubation experiments. As mentioned before, crystalline basaltic rocks are chemically more resistant than basaltic glasses. The solution in experiments with crystalline samples and low SSA (BF1/HC1) became acidified whereas an increase to slightly basic pH was observed for those rocks with high amounts of glass and high SSA (see Figure 2-3b). Finally, microbial cells were absent on olivine crystals containing solely Fe(II) but abundant on glassy parts with at least 10% of its total Fe being Fe(III).

Considering Fig. 2-6, dissolved Fe and Al were only measured in biotic colonization experiments. Moreover, the concentrations of dissolved Fe and Al increased in the same manner. The redox state of the dissolved Fe is unknown but based on the experimental conditions it is likely that all dissolved Fe was present as Fe(III). Perez et al., [81] have shown that during interaction of *Pseudomonas aeruginosa* with basaltic glasses of various Fe redox

states siderophore production increases with decreasing Fe(III) in the glass. In a previous study, trivalent metal chelators were found to interact with both, Fe(III) and Al(III), enhancing the overall glass dissolution [81]. Simultaneous microbial dissolution of Fe(III) and Al(III) and an increased overall glass dissolution was also observed in colonization experiments during this study indicating the presence of microbial produced chelators. In another study *Pseudomonas stutzeri VS-10* exhibited elevated growth in the presence of basaltic glass in Fe-limited heterotrophic media [148]. It is not clear if *B. fungorum* is capable of producing such metal specific chelators even if some authors suggest it.

An alternative hypothesis would be that the release of Fe and Al was induced by pH lowering. In silicate glasses, large amounts of Fe and Al can be extracted at acidic $pH \leq 3$ [176]. However, in the range from pH 4 to 9, Fe and Al are stable and their dissolution rates are low. Considering colonization experiments, the release of Fe and Al were highest at near neutral pH (glass BAS3; pH 6). There is the possibility that the pH dropped during the initial stage of this experiment similar to samples BAS1 and BAS2, and approached to near neutral conditions with time possibly by proton consumption. In this case the solution at the time at which the pH was acidic simply wouldn't have been sampled.

During the colonization experiments, basaltic glasses with residual stress were less chemically resistant than without under abiotic as well as biotic influences. However, whereas the concentration of dissolved elements in abiotic controls increased slightly with increasing residual stress, the effect was more pronounced in biotic experiments where concentrations were twice as high. Furthermore, cells of *B. fungorum* seemed to attach in greater numbers on glasses with residual stress compared to stress-free (annealed) glasses. A network of fine cracks beneath the surface of the quenched glasses (BAS2; BAS3) was observed, that was intensively altered in biotic experiments (see Figure 2-8). Dissolution was strongest along these weaker zones leaving the central parts relatively unaltered. It is quite clear that this alteration was solely caused by *B. fungorum*. Unfortunately, little is known about the effect of residual stress on microbial alteration so far. Dissolution of silicate minerals and glasses is not uniform and preferred in places with microfractures and dislocations [138]. Residual stress in quenched glasses favors fracturing which results in an increase in the SSA exposed to solution and, hence, increasing dissolution rates. Rosso et al., [178] have shown that the bacterium *Shewanella putrefaciens* dissolves the surface of hematite crystals at locations that are energetically favorable and distinct from its point of attachment. Considering that volcanic islands as well as

the oceanic crust hold large amounts of volcanic glass, residual stress can be a significant factor controlling the extent of alteration.

2.4.3 Cell Attachment and Biofilm Formation

Biofilm formation is widespread among continental and oceanic volcanic rocks but significantly more distinct in aqueous, nutrient rich environments [77,148,179–181]. Microorganisms associated with seafloor basalts can have various morphological appearances from individual or clustered cells to extensive biofilm formation adhering to surfaces [171,182]. Whether microbes attach to mineral surfaces depends on the availability of nutrients necessary for metabolic processes and microbial growth [79,147]. The circumstances that promote surface attachment of microorganisms are diverse but it is ambiguous if direct attachment to mineral and glass surfaces is common or if it is a microbial reaction of changing environmental influences. The experimental findings indicate that cell attachment on surfaces is complex and influenced by several specific parameters. Observations from the incubation experiments with natural rock samples indicate that in a nutrient rich environment (as for samples HC2, PB1, and PB2) cells are occasionally found on surfaces. Under nutrient limited conditions (as for samples BF1 and HC1), attachment of microbial cells to glass surfaces appeared to be more pronounced. Based on nutritional conditions, McEldowney and Fletcher [183] also reported a strong influence of the nutrient availability on the affinity of some freshwater microorganisms to attach on solid surfaces with greater attachment under nutrient-limiting conditions. Another interesting observation was the preference of *B. fungorum* for attachment on glass surfaces rather than mineral surfaces (e.g., olivine; see Figure 2-5e,f). It is supposed that *B. fungorum* specifically attacked the basaltic glass to acquire P and Fe.

This idea is in line with the results from the colonization experiments and findings of Rogers and Bennett, [79]. Also, the fact that apatite was not observed in the natural samples supports this assumption as basaltic glass is the only P source for *B. fungorum* in incubation experiments. Indication that a nutrient depleted environment favors surface attachment was also obtained from colonization experiments. Furthermore, the abundance of attached cells seemed to be positively correlated with residual stress in the order BAS1 < BAS2/BAS3. The cell and biofilm morphologies in colonization experiments were more diverse than in incubation experiments. The nm sized filamentous structures seemed to facilitate either connection of cells among each other or to the glass surface. The larger filaments only observed in colonization experiments seemed to connect solely the larger cells. The use of such structures linking

individual cells is still not completely understood but assumed to play a role in electron transport between bacteria [148,184]. The observations from incubation and colonization experiments of this study indicate that surface attachment of microorganisms might be favored in nutrient depleted environments and can possibly be an adapted strategy under extreme conditions.

2.5 Conclusions

Understanding microbe-mineral interactions is of importance for geochemical element cycles and in particular the release of limiting nutrients (e.g., Fe and P) from rocks to the environment. It was shown that *B. fungorum* is capable of obtaining essential nutrients by itself via dissolution of basaltic glasses. This study provides new insights about how rock properties, such as Fe redox state and residual stress, can affect microbial rock colonization and weathering. With increasing residual stress or high Fe(II) content, the synthetic basaltic glasses became more susceptible for microbial alteration. Furthermore, a correlation between nutrient-limiting conditions and surface attachment of microorganisms was emphasized. Cells of *B. fungorum* preferentially attached on glass surfaces of natural basaltic rocks that contained beneficial nutrients. It was also shown that biotic alteration could significantly contribute to the release of major elements in a nutrient depleted environment when microorganisms are forced to actively scavenge nutrients from rocks. The need of *B. fungorum* to acquire P for microbial growth was found to enhance the release of Fe and other elements from synthetic basaltic glasses to solution and is in agreement with previous studies [150]. However, the amount of elements released in biotic experiments might be an underestimation and elements such as Fe and P, that are nutrients for microorganisms, were located and fixed (possibly unavailable for liquid phase analysis) in the biomass.

There are some limitations when transferring the findings of this work to the larger environment. The experiments were performed with a single bacterial species whereas natural rocks comprise diverse microbial communities that interact with each other. Furthermore, microbial growth was enhanced by adding glucose as a carbon source. The growth medium was prepared with a minimum concentration of salts (comparable to ground waters) to be able to measure even small amounts of elements released from the rocks and glasses. The experiments are therefore not directly applicable to seawater conditions. Despite these limitations, the findings of this study are of great importance for the element release during weathering of volcanic islands and all leaching systems with highly permeable rocks. Within the highly porous rocks that are ubiquitous on the island of Hawaii, marked shares of soluble chemical weathering products are immediately transported away leaving a nutrient depleted environment behind that can favor microbial alteration.

Chapter III

Far from Equilibrium Basaltic Glass Alteration: The Influence of Fe Redox State and Thermal History on Dissolution Rates.

Marius Stranghoener[1], Stefan Dultz[2], Harald Behrens[1] and Axel Schippers[3]

[1] *Institute of Mineralogy, Leibniz Universität Hannover, Hanover, Germany*
[2] *Institute of Soil Science, Leibniz Universität Hannover, Hanover,Germany*
[3] *Geomicrobiology, Federal Institute for Geosciences and Natural Resources, Hanover, Germany*

Abstract

Long term basaltic glass dissolution rates at far from equilibrium conditions as a function of the Fe redox state ($Fe(II)/Fe_{tot}$ = 0.35 and 0.80) and thermal history (quenched↔annealed) were measured at 25°C, and in the presence and absence of oxalic acid at pH 2 and 5. A flow-through column setup was used to ensure that basaltic glass and the solution are in disequilibrium at all time during the experiments. In the initial stage basaltic glasses dissolution was incongruent but progressively changed to congruent dissolution with time. Calculated long term basaltic glass dissolution rates at pH 5 were ~1.46±0.22 · 10^{-10} [mol/m²/s] and independent of the Fe redox state and thermal history. With decreasing pH from 5 to 2 the long term dissolution rates increased and varied as a function of the Fe redox state with 5.18±0.10 · 10^{-10} and 3.51±0.20 · 10^{-10} [mol/m²/s] for Fe(III)-rich and Fe(II)-rich glasses, respectively. Indication was obtained that the long term release of Fe(II) and Fe(III) at pH 2 is closely related to the stoichiometric proportions of Fe(II) and Fe(III) in the original basaltic glass. At pH 2 and in the presence of 1 mM oxalic acid a strong dependence of basaltic glass dissolution on the thermal history was observed, i.e. annealed basaltic glasses showed decreased long term dissolution rates. Moreover, oxalate accelerated the mobilization of major elements from quenched glasses by 17 to 20% and the bulk glass dissolution by 0.3% relative to annealed glasses. The findings suggest that the Fe redox state and thermal history of silicate glasses are important parameters that needs to be considered for the prediction of glass dissolution rates.

3.1 Introduction

Volcanic glasses, formed by rapid cooling of lava, are widespread among the earth surface and occur in a variety of geological settings. The extent of alteration of these silicate glasses is mainly controlled by their composition, structure, and environmental influences [28,29,37,185]. Because of its widespread occurrence, natural basaltic glass plays an important role for different (bio)geochemical element and global carbon cycles [16,17,186], subsurface CO_2 storage [7,8], and were recently considered as a natural analogue for vitrification of high-level nuclear waste [9,187].

The durability of silicate glasses mainly depends on their SiO_2 content and the abundance of other metal cations that either act as network formers (e.g., Al) or network modifiers (e.g., Na, Ca) [29]. Here, Fe plays an important role as it is ubiquitous in natural silicate glasses with FeO_{tot} up to 13 wt.% in basaltic glasses and acting as both, network former (Fe(III)) and modifier (Fe(II)) depending on its redox state [188,189]. Among the network modifying cations, alkali metals (K, Na) are preferred for charge balancing TO_4^- tetrahedra (T = Al, Fe(III)) and hereby increasing polymerization of the glass network [190].

Dissolution of silicate glasses is a complex multi-step process affected not only by solution chemistry but also microorganisms [29,92,191–193]. Subsequent to the fast removal of mono- and divalent cations from the glass surface dissolution proceeds by protonation and breaking of T-O-Si bonds (T = Al(III), Fe(III)) and opening of the network due to formation of non-bridging Si-OH bonds [46]. Furthermore, metal-organic surface complexes formed with organic ligands such as oxalate weaken the metal-oxygen bond and the detachment of surface metal species is facilitated [194]. The rate limiting step for silicate glass dissolution is, however, the complete destruction of the slowest breaking bonds which, for basaltic glasses, are Si-O-Si bonds [102]. Thus, basaltic glass dissolution can be described using long term Si release rates determined by the point at which steady-state (= time independent) Si release is attained.

Besides of compositional effects including chemistry and oxidation state of compounds, the durability of silicate glasses is supposed to be affected by the thermal history (quenching↔annealing) [33,39]. During quenching of natural basaltic glasses the huge temperature differences between the surface (in contact with water or air) and the interior produces compressive (interior) and tensile stresses (surface) that favor fracturing of the glass [157]. The quench rate of a glass determines the point at which the glass structure is frozen in and termed the fictive temperature (T_f) [31]. Structural relaxation (e.g., by annealing) is

expressed by a decrease in T_f which can be measured by differential scanning calorimetry (DTA) and used to make an assumption on the thermal history of the glass [35,195].

The dissolution of silicate minerals and glasses is not uniform and preferred in places with microfractures and dislocations [138]. Whereas the effect of thermal history is poorly determined for basaltic glasses, some recent studies exist for technical glasses. For soda-lime and borosilicate glasses increased hydrogen diffusion and leached layer formation and significantly increased dissolution was observed for rapidly quenched samples [37–39]. Crazing of the basaltic glass surface after acid leaching suggests preferential dissolution along zones of high residual stress [102,185]. It is furthermore suspected that the thermal history of the glass affects also microbial colonization by providing reactive sites that are energetically favorable for dissolution and nutrient acquisition [92,178,196]. It was shown in a previous work that dissolution of quenched and reduced basaltic glasses is enhanced in the presence of microorganisms possibly by acidification and the presence of organic ligands [92].

Despite the large number of studies investigating basaltic glass dissolution little is known about the impact of Fe redox state and thermal history on the dissolution rate. Within this study, far from equilibrium dissolution experiments with synthetic basaltic glasses were performed, in which the Fe redox state and thermal history were systematically varied. A flow-through column setup was used to investigate the influence of these two factors on the dissolution rate of synthetic basaltic glasses at low ionic strength and two different pH values. The effect of organic ligands on the dissolution rate in this system was considered as well. The advantage of percolation experiments using flow-through columns over batch experiments was a continuous renewal of the solution during the experiments. Thus, the basaltic glass and the solution were in disequilibrium at all time during the experiment. Furthermore, dissolved elements were transported with the fluid and effects of the dissolving glass on the solution pH were negligible. This allowed for tracing glass alteration at far from equilibrium conditions and determination of long term release rates after three constant consecutive release rates were obtained.

3.2 Material and Methods

3.2.1 Preparation of Synthetic Basaltic Glasses

The synthetic basaltic glass was prepared from high purity powdered oxides and carbonates (SiO_2, Al_2O_3, Fe_2O_3, $CaCO_3$, $MgCO_3$, Na_2CO_3, TiO_2, K_2CO_3, $(NH_4)H_2PO_4$)) based on the composition of natural Hawaiian basalts (Table 3-1). Melting was done in a platinum crucible at 1600°C for 2 h. The melt was quenched on a brass plate, crushed using a steel mortar and re-melted for an additional hour at 1600°C. A portion of the melt was then poured on a hot (550°C) steel plate, transferred to a chamber furnace at 550°C and slowly (< 1 K/min) cooled down to room temperature to remove internal stresses from the glass (denoted as B-OA in Table 3-2). This glass was considered as "stress-free" (annealed). The rest of the melt was quenched on a brass plate (B-OQ). These two glasses were melted in air ($\log(fO_2/bar) = -0.37$) and considered as oxidized glasses with $Fe(II)/Fe_{tot}$ ratios of 0.35 (B-OQ) and 0.39 (B-OA) measured by a colorimetric wet-chemistry method (see chapter 3.2.3). A portion of the quenched glass was crushed to a fine powder (< 50 µm) and put in a horizontal reduction

TABLE 3-1: *Chemical composition of the synthetic oxidized and reduced basaltic glass samples used in this study in comparison with the natural analogue.*

| Oxide | Synthetic basaltic glasses | | Natural analogue |
| | oxidized | reduced | |
	B-O[a] [wt.%]	B-R [wt.%]	Garcia [158]c [wt.%]
SiO_2	53.21 ± 0.36[b]	53.21 ± 0.36	52.07 ± 0.42[d]
TiO_2	2.79 ± 0.02	2.79 ± 0.02	2.81 ± 0.42
Al_2O_3	12.86 ± 0.21	12.86 ± 0.21	13.05 ± 0.35
Fe_2O_3	8.22 ± 0.22	2.61 ± 0.12	-
FeO	4.34 ± 0.17	9.39 ± 0.27	11.80 ± 0.30[e]
MnO	0.19 ± 0.07	0.19 ± 0.07	0.18 ± 0.00
MgO	6.10 ± 0.12	6.10 ± 0.12	6.26 ± 0.14
CaO	10.63 ± 0.14	10.63 ± 0.14	10.51 ± 0.27
Na_2O	2.15 ± 0.07	2.15 ± 0.07	2.23 ± 0.12
K_2O	0.44 ± 0.02	0.44 ± 0.02	0.47 ± 0.05
P_2O_5	0.26 ± 0.09	0.26 ± 0.09	0.30 ± 0.02
Total	101.19 ± 0.63	100.63 ± 0.63	99.70 ± 0.12

[a] For both Fe redox states, quenched (B-OQ; B-RQ) and annealed (B-OA; B-RA) glasses were prepared;
[b] Standard deviation; n = 100; [c] average chemical composition of basaltic glasses of ICDP HSDP2 drill core;
[d] Standard deviation; n = 14; [e] Total Fe as FeO

furnace (Nabertherm) to achieve a certain Fe redox state. Here the powder was reduced ~100°C below its glass transition temperature (T_g = ~655°C determined by DTA analysis [197]) at 560°C for 24 h using Ar/H_2 gas mixture (log(fO_2/bar) = -20.02).

About 2.5 g of the reduced glass powder was then filled in $Au_{80}Pd_{20}$ capsules and welded shut. The capsules were placed in a chamber furnace at 1200°C for 1 h and subsequently quenched in water (B-RQ) or annealed (B-RA) at 563°C under reducing atmosphere (Ar/H_2) and slowly cooled (< 5 K) to room temperature. These two glasses are considered as reduced glasses with Fe(II)/Fe_{tot} ratios of 0.78 (B-RQ) and 0.80 (B-RA). Samples B-OQ and B-RQ are glasses with high residual stress similar to those in hyaloclastites and glassy margins of pillow basalts. The thermal history of the glasses was characterized by DTA analysis (Setaram Setsys Evolution 1750) regarding the fictive temperature (T_f). Oxidized basaltic glasses were measured with a heating/cooling rate of 5 °C/min in a flowing He atmosphere (20 ml/min). A ΔT_f = 6°C was observed between quenched (T_f = 658°C) and annealed (T_f = 652°C) basaltic glasses (Figure 3-1a). Furthermore, fragmentation of the quenched glass without extraneous influences was observed upon cooling whereas the annealed glass remained unimpaired. Hence, the quenched and annealed glasses are considered as "endmembers" with ideally largest differences: no residual stress and high residual stress.
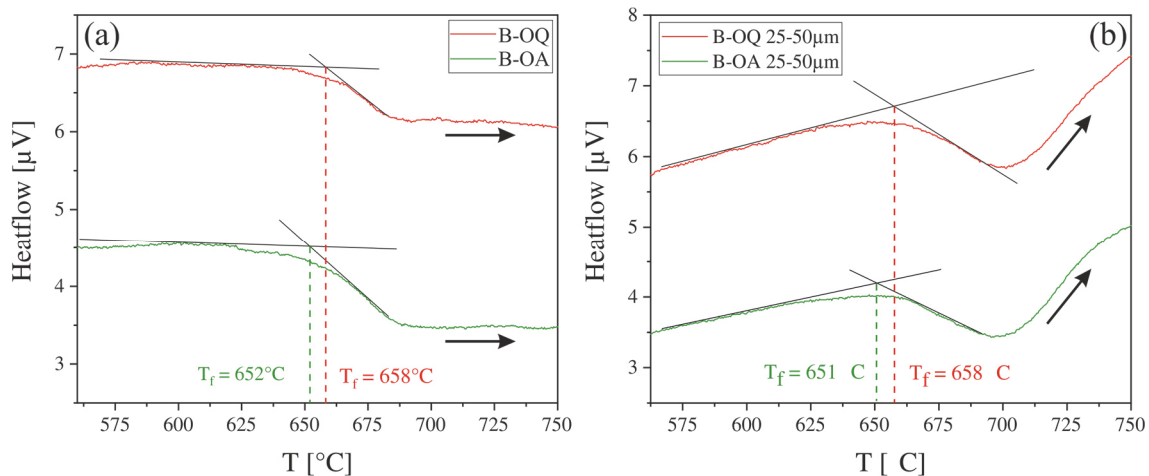
FIGURE 3-1: Heatflow for DTA upscans of whole basaltic glass pieces (a) and 25-50 μm ground basaltic glass powder (b) of oxidized quenched and annealed glasses and determination of the fictive temperature (T_f) using the tangential method. Black arrows indicate the direction of measurement.

For the percolation experiments, the glasses were ground using an agate mortar and sieved in the dry state to obtain a grain size between 25 and 50 μm. T_f of ground quenched and annealed glasses was 658°C and 651°C, respectively, and provided evidence that residual stresses were not released during sample processing (Figure 3-1b). The SSA_{GEO} (geometric surface area) was

shown to yield more consistent results with respect to glass dissolution rates [193,198] and was calculated according to Wolff-Boenisch et al., [29].

3.2.2 Percolation Experiments

All percolation experiments were performed in 5 ml syringes using 16 channel peristaltic pumps (Type 205s and 202u; Watson Marlow). The syringes were prepared as follows (Figure 3-2): a 3 µm glass-fibre prefilter (Sartorius) and above a 15 µm black ribbon ash-less filter (Schleicher & Schuell) were put on the outlet site of the syringe to retain the sample material. About 1 g of acid washed 0.5 to 1 mm sized quartz sand was added followed by 0.2 g basaltic glass sample material and another layer of 1 g acid washed quartz sand on top. This layer packing was established to ensure that the basaltic glass sample was water saturated during the percolation experiment. The pump tubing of which the solution driped on the upper layer of glass sand was inserted from the top of the syringe. The pumps were used with a flow rate of 0.44±0.01 ml/h (≙ 10.56±0.24 ml/day). Experiments were run in triplicates at 25°C for a total duration of 504 h. The percolated solution was sampled in time intervals (after 24, 48, 72, 96, 144, 192, 240, 288, 360, 432, 504 h), and the pH controlled in the percolate. The flow rate was calculated for each assay by weighting the amount of percolated solution. A control experiment containing no sample material was simultaneously run to control dissolved Si stemming from the quartz sand.
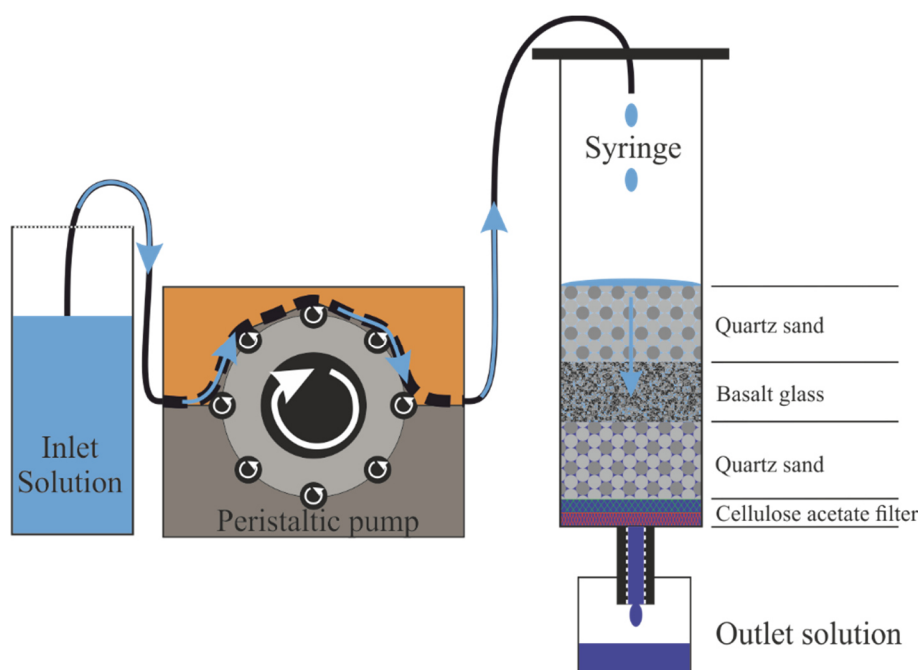

FIGURE 3-2: Schematic overview of the experimental setup of the percolation experiment.

For experimental solutions, either Ultrapure water (UPW; electrical resistivity 18.2 MΩ) or 1 mM oxalic acid ($C_2H_2O_4$; reagent grade; Alfa Aesar) were used. The concentration of oxalate was close to that in natural environments and close to the minimum concentration at which a dissolution enhancing effect was observed [199]. The UPW and OA were adjusted to pH 5 by dropwise addition of 0.1 M HCl and NaOH, respectively. The solutions were allowed equilibrating with air during the experiment. Furthermore, no pH buffer was used to avoid impact on mineral and glass dissolution [53]. For microscopic analysis after the last sampling, the filling of one of the three parallel columns was washed in ethanol and the basaltic glass fragments were separated from the quartz sand by sieving.

The two remaining parallels of each assay were used in a follow-up percolation experiment. First, the columns were flushed with UPW for 24 h for complete removal of the solution from the previous experiment. The columns percolated with UPW (pH 5) in the first experiment were then percolated using UPW adjusted to pH 2 with HCl. The other columns, percolated with UPW + 1 mM oxalic acid at pH 5, were then percolated with UPW + 1 mM oxalic acid adjusted to pH 2. Both solutions were not buffered and allowed to equilibrate with air at all time during the experiments. Experiments were run in duplicates at 25°C for a total duration of 385 h. The percolated solution was sampled in time intervals (after 7, 24, 48, 71, 97, 169, 241, 313 and 385 h), and the pH controlled in the percolate. The fluid flowrate was calculated as mentioned above. Again, for microscopic analysis after the last sampling, the column filling was washed in ethanol and separated from quartz sand by sieving.

The micromorphology of fresh and altered basaltic glass fragments was determined with an Environmental Scanning Electron Microscope (ESEM; FEI Quanta 200). EDX analyses of the composition of the surface layer and secondary phases were done with an SEM (JEOL JSM-7610FPlus Energy Dispersive Spectroscopy (EDS)) with a 20 kV accelerating voltage and a working distance of 15 mm. Point analysis were made using a focused beam and a counting time of 30 s.

3.2.3 Chemical Analysis

The Fe redox state of the basaltic glass samples was determined by a wet chemistry method of Wilson, [159] modified by Schuessler et al., [114]. Furthermore, solutions from pH 2 experiments were analyzed for the redox state of the dissolved Fe using this method. The pH of all percolates was measured at 25°C immediately after sampling using a VWR SM-123 pH gel electrode (uncertainty of < 0.01 pH units). For quantification of Si, Al, Fe, Mn, Mg, Ca, Na, K, and P by Inductively Coupled Plasma Optical Emission Spectroscopy (ICP-OES; Varian 725-ES) 0.3 M HNO_3 was added to the remaining solution. The measured concentrations were used to calculate elemental release rates ($r_{i,j}$) using the following equation according to [103]:

$$r_{i,j} = \frac{c_i FR}{SSA_j m_j} \qquad \text{Eq. 3-1}$$

with c_i = measured concentration of the *i*-th element in the outlet fluid; FR = fluid flow rate; SSA_j = geometric (GEO) surface area of the basaltic glass; m_j = mass of the basaltic glass used.

The calculated long term release rates of Si and Al provide evidence of how fast or slow a glass reacts over long timescales. However, it does not allow for comparison of the total amount of mobilized elements between the different basaltic glasses over the total experimental duration. It is therefore necessary to calculate the cumulative element concentration in solution for a given glass and element by the sum of elemental concentrations measured during each sampling.

3.3 Results

3.3.1 pH and Proton Buffering Reaction

The experiments were not exactly started with pH 2 (pH 2 and 2.1) and 5 (pH 5.5 and 5.2). In the following, however, the experiments will be simply denoted as pH 2 and pH 5 experiments. In the experiments at pH 2 a pH increase by ~0.2 units within the first 7 h for both experimental series was apparent (Figure 3-3a,b). Between 7 h and 24 h the pH rapidly decreased and approached to the initial pH 2 (Figure 3-3a) and pH 2.1 (Figure 3-3b). The control experiment showed only a weak increase by 0.05 units and followed the trend of the assays containing basalt glass samples. At pH 2 with the addition of oxalate (Figure 3-3b), the control experiment showed the same trend as the assays containing basaltic glass.

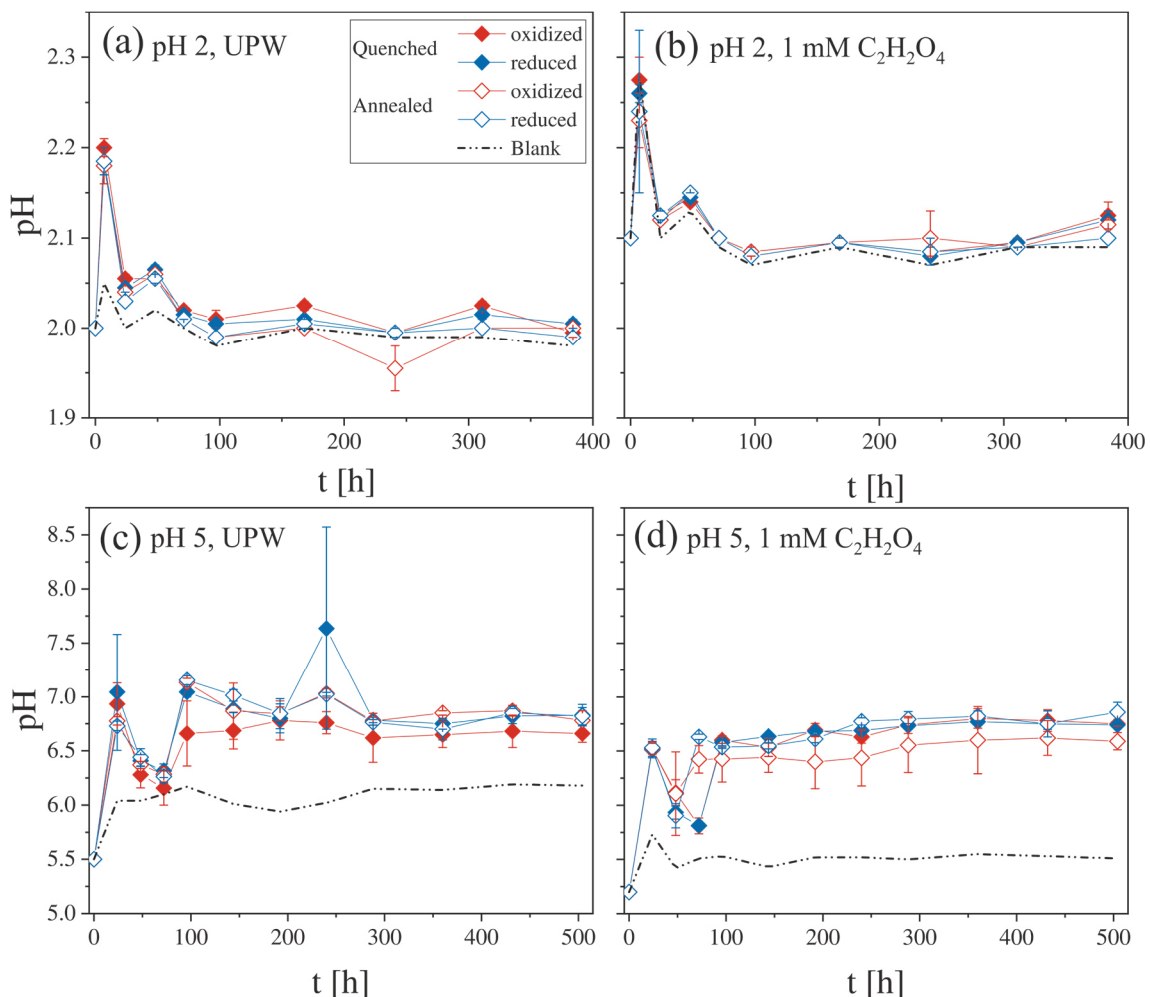FIGURE 3-3: *Course of pH during the runtime of the percolation experiments at pH 2 without (**a**) and with (**b**) 1 mM oxalate and pH 5 without (**c**) and with (**d**) 1 mM oxalate. Experiments were started at pH 2.0 (**a**), 2.1 (**b**), 5.5 (**c**) and 5.2 (**d**). The evolution of the control experiment (quartz sand without basaltic glass sample) is shown for comparison. Solid lines are only for guidance of the eye.*

A similar course of pH values over time was observed in percolation experiments at pH 5 (Figure 3-3c,d). During the first 24 h, the pH increased by ~1.5 and ~1.2 units to pH ~7 (c) and ~6.5 (d). Between 24 h and 72 h the pH in all experimental assays decreased to pH ~6.2 (Figure 3-3c) and ~5.7 (Figure 3-3d). Subsequently an increase to pH ~7 and ~6.5 occurred, and the pH remained constant at ~6.7 (Figure 3-3c,d). The pH of the control experiments for both experimental series without and with oxalate did not increase by more than 0.5 units from the initial value and remained constant at pH ~6.2 (Figure 3-3c) and ~5.5 (Figure 3-3d).

Whereas in the percolation experiment at pH 5 Si, Ca, Mg, and Na were clearly detectable in the percolates during the whole runtime, K was close to the ICP-OES detection limit in the period following the initial stage of dissolution of ~72 h. Al and Fe mobilized at pH 5 were only measurable in solution during the first sampling after 24 h. However, all elements showed high release at pH 2 throughout the experiments. In the following, the focus will therefore lie on pH 2 experiments.

3.3.2 Long Term Si and Al Release Rates

Dissolved Si was measurable at pH 2 but dropped below the concentration of the control experiment in experiments with 1 mM oxalic acid. The reason for this is not clear and deviates from observations of other studies (e.g., [185]). However, to facilitate the comparison between oxalate-free and oxalate containing solutions at pH 2 Al was used to calculate basaltic glass dissolution rates. At pH 2 and oxalate-free solutions initial Al dissolution rates were the same for all glasses and dropped within the first 48 h by 1.2 log units (Figure 3-4a). At this point Al release rates for oxidized and reduced glasses started to deviate and oxidized glasses showed ~0.2 log units higher long term Al release rates (Figure 3-4a; grey area). In the presence of 1 mM oxalic acid at pH 2 similar initial Al dissolution rates were observed (Figure 3-4b). After 48 h Al release rates of annealed glasses decreased faster than their quenched analogues. Compared to quenched glasses, long term Al release rates of oxidized and reduced annealed glasses were 0.1 and 0.2 log units lower, respectively.

In pH 5 experiments (Figure 3-4c,d), glasses of different Fe redox states and thermal histories showed similar Si release rates and no major differences were observed. In the presence of 1 mM oxalic acid all glasses showed a slight increase in the long term Si dissolution rates by 0.1 to 0.15 log units (Figure 3-4d; grey area).
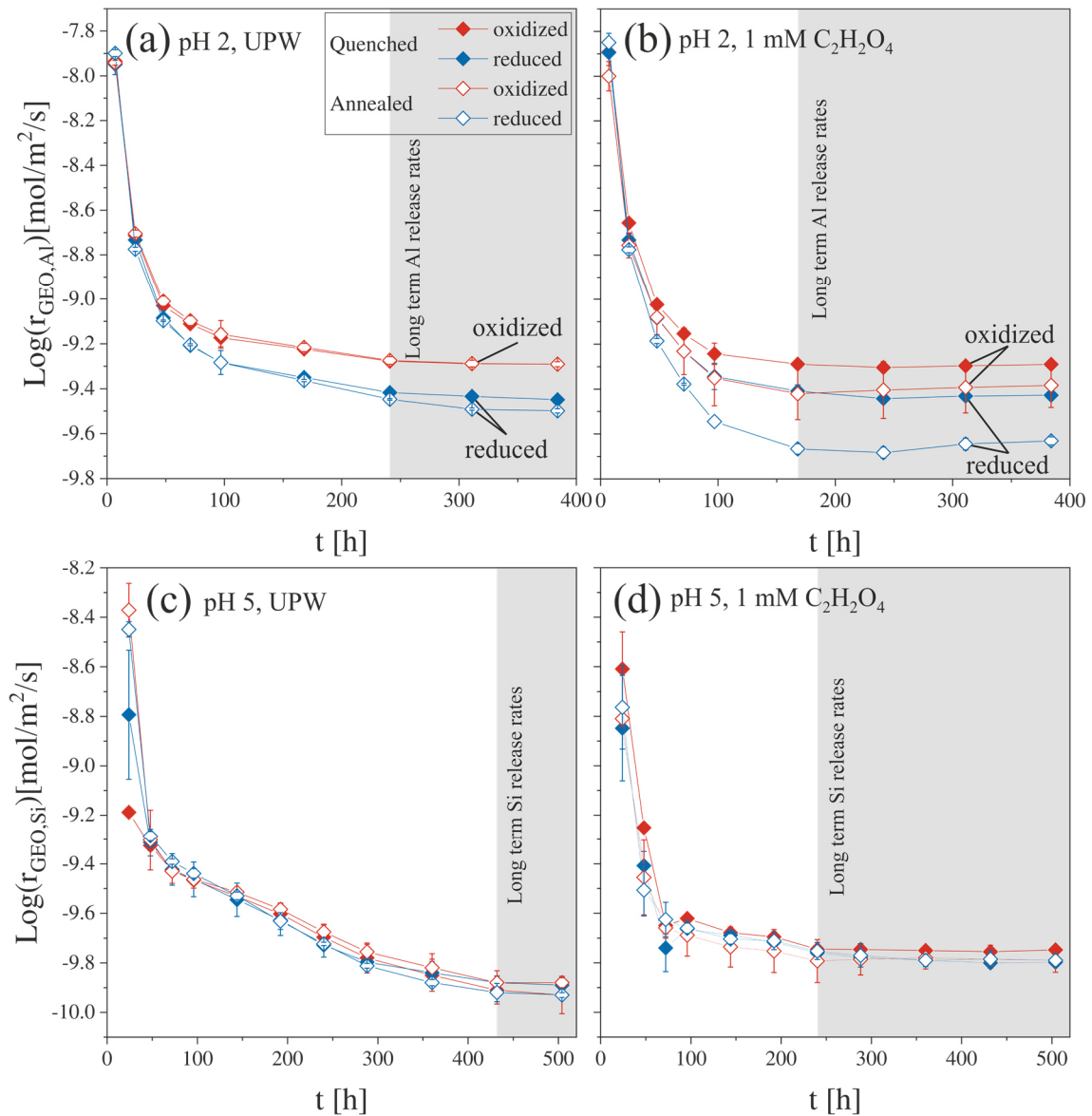
FIGURE 3-4: *Blank corrected, initial and long term Al and Si release rates from basaltic glass samples at pH 2 and 5, respectively measured in UPW (**a,c**) and 1 mM oxalic acid (**b,d**). Solid lines are only for guidance of the eye.*

The point at which long term Si and Al release rates were achieved depended strongly on the pH and the presence of organic ligands (Figure 3-4a-d; grey areas). In oxalate-free solutions long term Si and Al release rates at pH 2 and pH 5 were observed after 240 h and 432 h, respectively (Figure 3-4a,c; Table 3-2). The time period for which long term Si and Al release rates were achieved was dramatically decreased in the presence of 1 mM oxalic acid. At pH 2 long term Al release rates were attained after 168 h whereas 240 h were sufficient to reach long term Si release rates at pH 5 (Figure 3-4b,d; Table 3-2).

TABLE 3-2: Long term Si and Al release rates measured form percolation experiments at pH 5 and 2. Sample names indicate their Fe redox state (O = oxidized; R = reduced), their thermal history (Q = quenched; A = annealed) and the experimental conditions (5 = pH 5; 2 = pH 2; Ox = 1 mM oxalic acid).

Sample	SSA_{GEO} (m²/g)	$Fe(II)/Fe_{tot}$	Solution	Initial pH	Flow rate [ml/h]	Long term Al and Si release rates	
						Log $r_{Al,GEO}$ [mol/m²/s]	Log $r_{Si, GEO}$ [mol/m²/s]
B-OQ-1	0.06	0.35±0.02	UPW[c]	2.0	1.29	-9.28	-9.50
B-RQ-1	0.06	0.78±0.02	UPW	2.0	1.26	-9.43	-9.66
B-OA-1	0.06	0.39±0.02	UPW	2.0	1.33	-9.28	-9.48
B-RA-1	0.06	0.80±0.02	UPW	2.0	1.37	-9.48	-9.68
B-OQ-2	0.06	0.35±0.02	UPW+OA[d]	2.1	1.20	-9.30	-
B-RQ-2	0.06	0.78±0.02	UPW+OA	2.1	1.27	-9.43	-
B-OA-2	0.06	0.39±0.02	UPW+OA	2.1	1.23	-9.39	-
B-RA-2	0.06	0.80±0.02	UPW+OA	2.1	1.14	-9.65	-
B-OQ-3	0.06	0.35±0.02	UPW	5.5	0.69	-	-9.92
B-RQ-3	0.06	0.78±0.02	UPW	5.5	0.66	-	-9.89
B-OA-3	0.06	0.39±0.02	UPW	5.5	0.69	-	-9.88
B-RA-3	0.06	0.80±0.02	UPW	5.5	0.71	-	-9.92
B-OQ-4	0.06	0.35±0.02	UPW+OA	5.3	0.68	-9.95	-9.75
B-RQ-4	0.06	0.78±0.02	UPW+OA	5.3	0.68	-9.98	-9.80
B-OA-4	0.06	0.39±0.02	UPW+OA	5.3	0.70	-10.01	-9.78
B-RA-4	0.06	0.80±0.02	UPW+OA	5.3	0.63	-10.02	-9.78

[a] ultra pure water (18 MΩ)
[b] 1 mM oxalic acid

3.3.3 Cumulative Element Release

Fig. 3-5 shows the total amount of mobilized elements normalized to its bulk concentration in the solid glass. Differences for the cumulative amount of mobilized major elements at pH 5 were minor between the four different glasses introduced (Figure 3-5a). None of the major elements was mobilized to more than 1% relative to its total content in the glass. In absolute terms the element mobilization generally decreased in the order K > Ca > Mn > P > Si≈Mg≈Na > Fe > Al. A slight trend for higher mobilization of all elements from annealed glasses was observed. With the addition of 1 mM oxalic acid, the mobilization of di- and trivalent cations slightly increased (Figure 3-5b). This is strongest pronounced for quenched glasses with Mn concentrations of more than twice as high. The amount of mobilized elements generally decreased in the order Mn > K > Ca≈Mg≈Fe > Al≈Na≈P≈Si. Furthermore, the observed trend

for oxalate-free solutions seemed to be reversed and quenched glass showed a higher mobilization of all measured elements.
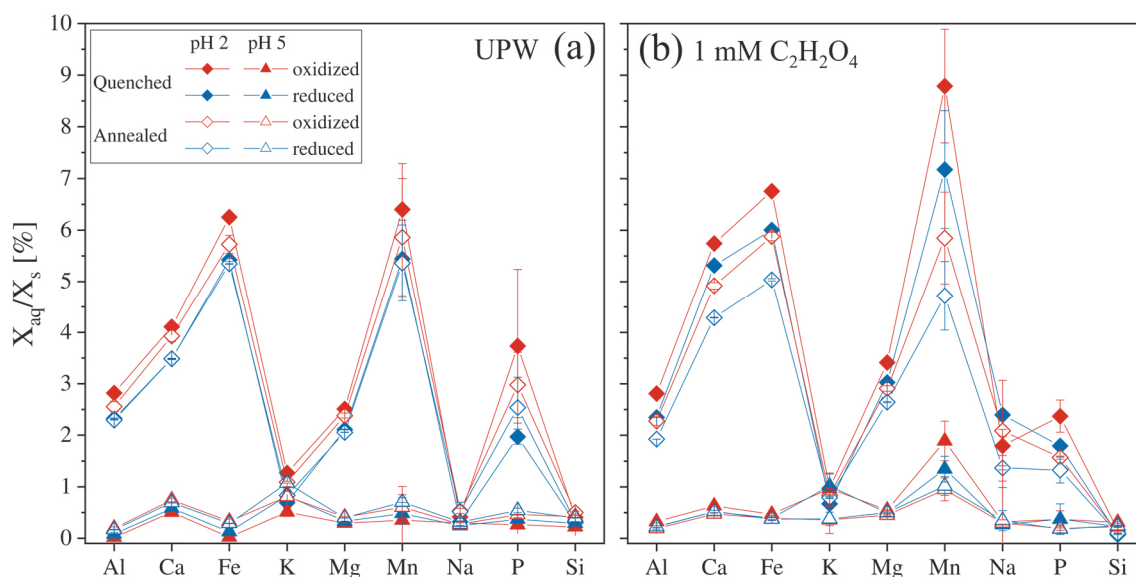

FIGURE 3-5*: Cumulative mobilization of major oxides from basaltic glasses normalized to their content in the original glass at pH 5 and 2 in UPW **(a)** and with addition of oxalic acid **(b)**. Solid lines are only for guidance of the eye.*

At pH 2, however, the mobilization of all di- and trivalent cations and P increased at least five times compared to pH 5 (Figure 3-5a). This is strongest pronounced for Fe and Mn for which the concentrations increased 15 and 10 times, respectively. Glasses high in Fe(III) showed a higher mobilization of all di- and trivalent cations compared to glasses high in Fe(II). The amount of mobilized elements generally decreased in the order Fe≈Mn > Ca > Al≈P > Mg > K > Na≈Si. With the addition of 1 mM oxalic acid the mobilization of Ca, Mn, and Na increased compared to oxalate-free conditions whereas P slightly decreased (Figure 3-5b). The amount of mobilized elements generally decreased in the order Mn≈Fe≈Ca > Al≈Mg > Na≈P > K > Si. Furthermore, quenched glasses showed a higher mobilization of elements when oxalic acid was present similar to quenched glasses at pH 5 (Figure 3-5b).

3.3.4 Reactions at the Glass Surface: SEM

Investigations by SEM showed significant differences in the particle size distribution between the unaltered starting material and the experimental products formed at pH 5 and pH 2 (Figure 3-6a-c). The starting material was heterogeneous with most of the particles being in the range of 25-50 μm (Figure 3-6a). However, a considerable amount of very fine particles (< 3 μm) was observed which was nearly absent after reaction for 504 h at pH 5 (Figure 3-6b).

The fine particles (< 3 μm) were washed out of the syringes during the initial stages of the experiment and observed in the percolated solution of the first sampling step. It appeared that the particle sizes of the sample material altered for 388 h at pH 2 were similar to the starting material with a substantial amount of fine particles (< 10 μm) (Figure 3-6c). It is assumed that these particles originated from the detachment of a leached layer on the surface of glass grains due to the washing and sieving procedure after the pH 2 experiments. This is supported by remnants of a nm thick leached layer observed on some glass surfaces as well as conglomerates of smaller particles enriched in SiO_2 adhering to surfaces of larger grains (see Supplemental Figure S3-1).
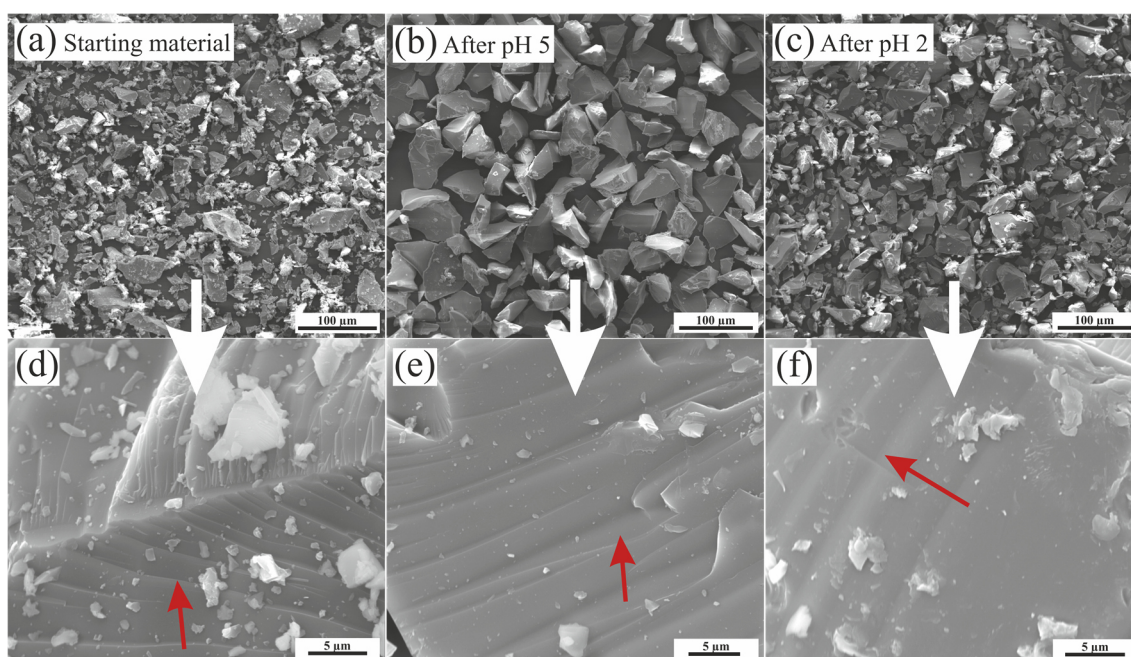
FIGURE 3-6: *Scanning electron micrographs of percolation experiments with synthetic basaltic glasses. (a) Unaltered basalt glass B-OQ. Ultra-fine particles originated during grinding adhere to the surface of larger grains. (b) basalt glass B-OQ-5 altered at pH 5 for 504 h. Note that ultra-fine particles are nearly absent. (c) basalt glass B-OQ-2 percolated at pH 2 for 388 h. Besides of large particles (> 20 μm) also finer particles (< 5 μm) are present. (d) Fresh basalt glass B-RQ. Besides of ultra-fine particles adhering to the surface, steps are visible at the surface (red arrow). (e) basalt glass B-RQ-5 altered at pH 5 for 504 h. Sharp edges of the steps of unaltered glass (d) became rounded (red arrow). (f) basalt glass altered at pH 2 for 388 h. The smoothened steps observed at pH 5 (e) are nearly completed dissolved (red arrow).*

A closer look on the surfaces of unaltered (Figure 3-6d) and altered (Figure 3-6e,f) glasses revealed some notable differences. Surfaces of glass grains, regardless of their Fe redox state and thermal history, showed conchoidal fractures with sharp edges that are typical for amorphous materials (Figure 3-6d; red arrow). With time, the edges of these conchoidal fractures became rounded during alteration at pH 5 and appeared somehow deepened (Figure 3-6e; red arrow). With the progress of time and decreasing pH from 5 to 2, the steps of the fractures became flat and almost disappeared (Figure 3-6f).

3.4 Discussion

3.4.1 Release of Fe(II) and Fe(III) from the Dissolving Glass

Fe in basaltic glasses was present as either Fe(II) or Fe(III), and the Fe(II)/Fe$_{tot}$ ratio was controlled by the oxygen fugacity during glass synthesis. Fe(II) and Fe(III) have different structural roles in silicate glasses, with Fe(II) being a network modifier similar to other divalent cations (e.g., Ca and Mg) and Fe(III) assumed to act as a network former at a low Fe(II)/Fe$_{tot}$ ratio similar to Al in silicate glasses [189,200]. Based on an ideal glass structure it seems reasonable to assume that Fe(II) and Fe(III) are mobilized in different quantities from the glass. Dissolved Fe in the percolated solution was only detectable at pH 2. The redox state of dissolved Fe in pH 2 solutions as well as the total Fe content in solution were measured spectrophotometrically by complexation with 2,2'-bipyridine. According to the spectrochemical series of ligands, 2,2'-bipyridine is a stronger ligand than oxalate and, thus, oxalate that forms a complex with Fe is supposed to be replaced by 2,2'-bipyridin. This assumption is in good agreement with the spectrophotometrically measured total Fe content and the one measured by ICP-OES (see Supplemental Figure S3-2).

Under oxalate-free conditions, the initial Fe(II)/Fe$_{tot}$ ratio in solutions containing reduced glasses was ~0.6 and lower compared to that of the fresh basaltic glass (Fe(II)/Fe$_{tot}$ ~0.8) (Figure 3-7a). Solutions containing oxidized glasses showed the same trend (Fe(II)/Fe$_{tot}$ ~0.25) but with less differences to the initial Fe redox state of the solid basaltic glass (Fe(II)/Fe$_{tot}$ ~0.4). The Fe(II)/Fe$_{tot}$ ratio of the solutions slowly increased and reached that of the original basaltic glass after ~300 h and ~250 h for reduced and oxidized glasses, respectively. In the presence of oxalic acid, the Fe(II)/Fe$_{tot}$ ratio of solutions dropped for reduced and oxidized glasses from initially ~0.55 and ~0.35, respectively, to ~0.10 within the first 250 h. Ratios increased again over time but didn´t reach the Fe(II)/Fe$_{tot}$ ratio of the solid basaltic glass till the end of the experiments. Quenched and annealed basaltic glasses showed a similar trend and values varied within their errors.

Indirect evidence was obtained that the lower initial Fe(II)Fe$_{tot}$ ratio of solutions is an artefact caused by dissolution of Fe (oxyhydr)oxides that formed during pH 5 experiments: (i) dissolved Fe concentrations were close to the detection limit of the ICP-OES in pH 5 experiments, (ii) possible precipitation of leached Fe as Fe (oxyhydr)oxides according to the simplified reaction

$$Fe^{3+} + 2H_2O \rightarrow FeOOH + 3H^+ \qquad \text{Eq. 3-2}$$
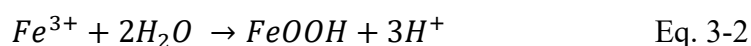
was evidenced by a decrease in pH at the onset of pH 5 experiments (Figure 3-3c;d) and (iii) a sharp pH increase at the beginning of pH 2 experiments due to proton buffering by the dissolving Fe (oxyhydr)oxides that formed at pH 5 after Eq. 3-2. The dominant fraction of this Fe is suspected to be Fe(III) and assumed to be responsible for the lower $Fe(II)/Fe_{tot}$ ratio observed during the first 250 to 300 h of the experiments. However, the long term Fe mobilization > 250 h was not affected and can be used for the interpretation of the data. From the observations it appears that in the long term (> 250 h) Fe(II) and Fe(III) were mobilized in proportions close to their stoichiometry in the original basaltic glass.
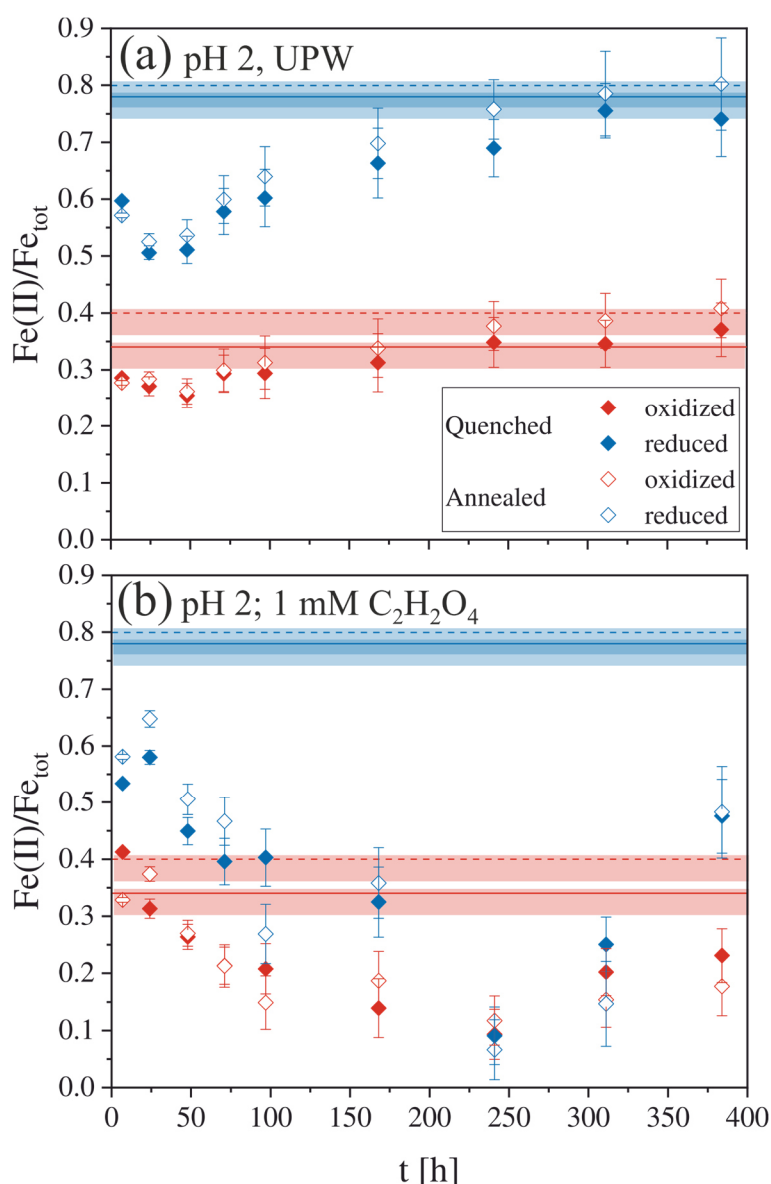

FIGURE 3-7: *Redox state of mobilized Fe at pH 2 without (a) and with oxalate (b) measured spectrophotometrically. Solid and dashed lines show the $Fe(II)/Fe_{tot}$ of the quenched (B-OQ; B-RQ) and annealed (B-OA; B-RA) basaltic glass, respectively. Semitransparent blue and red areas indicate the standard deviation.*

With the addition of 1 mM oxalic acid, the concentration of Fe(III) in solution increased steadily and comprised ~90% to the total dissolved Fe after ~250 h (Figure 3-7b). From that point, the Fe(II)/Fe$_{tot}$ ratio increased but didn´t reach the ratio of the solid basaltic glass till the end of the experiments. Oxalate binds to both, di- and trivalent cations but its affinity for trivalent cations was observed to be much higher [201]. This trend could reflect the depletion of Fe(III) in the surface layer due to strong leaching during the first 250 h of reaction. As the surface became depleted in Fe(III), either the free oxalate anions started to form complexes with Fe(II), or Fe(II) was mobilized to maintain the proposed Fe(II)/Fe$_{tot}$ equilibrium in the solution.

Based on Fig. 3-7a it is assumed that in oxalate-free solutions at pH 2 no preferential dissolution of a certain Fe species from the glass occurred in the long term glass dissolution (> 250 h). This also explains that no difference in the bulk Fe(II)/Fe$_{tot}$ ratio between fresh and altered glasses was observed (measured according to the method in chapter 3.2.3).

3.4.2 Influence of Fe(II) and Fe(III) on Basaltic Glass Dissolution

Based on the discussion of the oxidation state of dissolved Fe in the previous chapter it is likely that neither Fe(II) nor Fe(III) were preferentially mobilized from the glass samples in the dissolution experiments. It was shown that the proportions to which both were mobilized from the glass strongly depended on the Fe redox ratio of the basaltic glass and the presence of chelating agents (Figure 3-7). Considering the different structural roles of Fe(II) and Fe(III) in silicate glasses an effect of the Fe redox state on the dissolution behavior of the other major cations in the glasses such as Na, K, Mg, Ca, and Al is assumed. Fig. 3-8 compares the cumulative mobilization of major elements (denoted as X in Figure 3-8) of quenched (X_{B-OQ}/X_{B-RQ}) and annealed (X_{B-OA}/X_{B-RA}) glasses high in Fe(III) and Fe(II) over time at pH 2 in UPW. Values greater than 1 indicate a higher mobilization of alkaline, alkaline earth elements and Al from Fe(III)-rich glasses. The mobilization of K and P did not show a trend but large scatter and is not shown in Fig. 3-8 for reasons of clarity. The comparison of dissolution of quenched and annealed glasses can be divided in two parts:

(i) the initial (or short term) element mobilization that might be superimposed by artefacts stemming from the previous pH 5 experiments. Here, di- and trivalent cations (±Al) were preferentially mobilized from Fe(II)-rich glasses during the initial stage of dissolution (0-50 h (a) and 0-100 h (b)). By contrast, Si and Na were mobilized in higher quantities from Fe(III)-rich glasses.

(ii)   the steady state (or long term) element mobilization that is considered to be no longer affected by the artefacts. In the long term (> 100 h (a) and 275 h (b)) all major elements were mobilized in greater quantities from quenched and annealed, Fe(III)-rich glasses than could be expected from stoichiometric composition. The mobilization of Si and Na from Fe(III)-rich quenched glasses steadily increased over the course of the experiment, but for Na in annealed glasses, the difference was diminished after 100 h and Na was mobilized in the same proportion regardless of the Fe redox state.

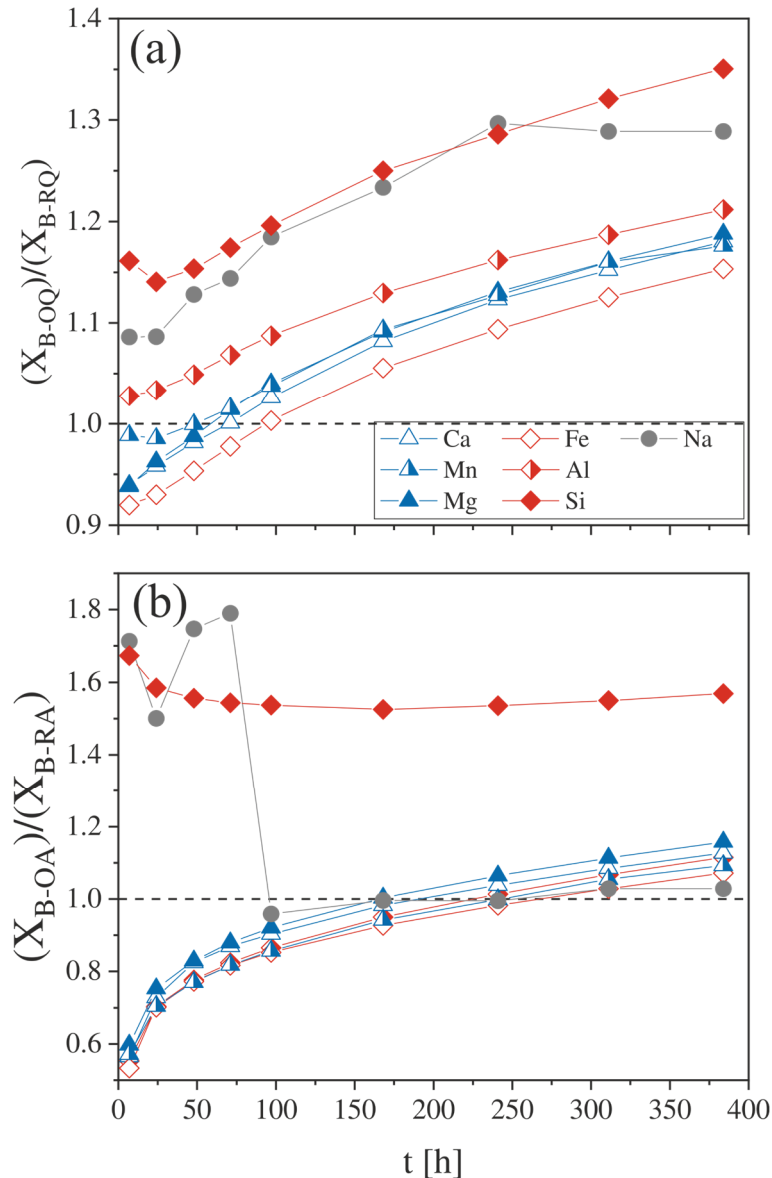**FIGURE 3-8**: *Ratios of mobilized Si, Al, Fe, Ca, Mn, Mg and Na from oxidized and reduced glasses at pH 2. (a) Quenched glasses. (b) annealed glasses. B-OQ = Oxidized-Quenched; B-RQ = Reduced-Quenched; B-OA = Oxidized-Annealed; B-RA = Reduced-Annealed. The dotted line corresponds to mobilization independent of the Fe redox state. Solid lines are only for guidance of the eye.*

The point at which the element mobilization from annealed Fe(III)-rich glasses exceeded that of Fe(II)-rich glasses was delayed by ~175 h compared to quenched glasses. This delay is probably related to structural differences between quenched and annealed glasses. On an atomic basis, the structure of annealed glasses is more ordered and dense compared to quenched glasses which is also evidenced by lower T_f values (Figure 3-1). This implies that short initial reaction rates are slower and it takes more time until the effect of the Fe redox state becomes apparent.

The observation that Fe(III) dominated glasses showed a higher mobilization of all major cations over timescales > 300 h is surprising and cannot be easily explained. A fact to be considered is the similarity of the structural role of Fe(III) and Al(III). In silicate glasses Fe(III) is predominantly in tetrahedral coordinated TO_4^- sites and supposed to fulfill a similar role as Al, linking SiO_4 tetrahedra by the formation of T-O-Si bonds (T = Al, Fe(III)) [188]. Both, Fe(III) and Al(III) on tetrahedral sites require a charge compensating cation and for doing so they prefer alkali over alkaline earth elements due to their lower ionic field strength and higher complex stability [202]. Hence Fe(III) and Al(III) compete for alkali metals when (Na+K) < (Fe(III)+Al(III)). FeO_4^- sites are preferentially charge compensated by alkali metals whereas AlO_4^- sites are complexed by excess alkali metals followed by alkaline earth [190]. Considering glasses used within this study, oxidized glasses did not contain sufficient alkali metals (K+Na) to even charge compensate FeO_4^- sites alone. Consequently, at high Fe(III) contents alkali metals first charge compensate FeO_4^- sites and the number of weaker Ca-O-Al and Mg-O-Al bonds increases. The higher abundance of weaker Al-O bonds lead to a depolymerization of the glass structure which is also reflected by decreasing melt viscosities [190]. For Fe(II)-rich glasses, on the other hand, an excess of (K+Na) is present that is available to charge compensate AlO_4^- units and, thus, stabilizes the network and increases the durability.

This hypothesis is supported by Hamilton et al., [30] who showed that the durability of aluminosilicate glasses at acidic and basic pH decreases with increasing Al/Si from albite to jadeite to nepheline glasses due to an increasing abundance of Al-O-Si linkages per SiO_4 tetrahedron and lengthening of this bond. Protonation of T-O-Si bonds (T = Al, Fe(III)) is faster than for Si-O-Si bonds and the removal of adjoining TO_4^- tetrahedra from the glass leads to the formation of Si-OH bonds and, thus, partly liberation of SiO_4 tetrahedra [46]. The reactivity of these partially liberated SiO_4 tetrahedral units increases with further detachment of TO_4^- units [203]. With respect to the glass system of this study this would imply that the glass network becomes increasingly vulnerable with increasing Fe(III) contents: The more FeO_4^-

units are present, the higher is the number of Fe(III)-O-Si linkages per SiO_4 tetrahedra and the faster is the glass dissolution. Furthermore, this reaction is more effective at high concentrations of H^+ (e.g., pH 2). The higher long term Fe mobilization at pH 2 from Fe(III) dominated compared to Fe(II) dominated glasses with $\sim 3.5 \cdot 10^{-11}$ [mol/m²/s] and $\sim 2.3 \cdot 10^{-11}$ [mol/m²/s], respectively, support this assumption.

In conclusion, it is suggested that the higher dissolution rates of Fe(III)-rich glasses are due to a coupled effect of a greater number Al-O bonds charge compensated by alkaline earth elements and a higher abundance of weaker Fe(III)-O-Si bonds replacing strong Si-O-Si bonds.

3.4.3 Influence of Oxalate on Thermal History and Basaltic Glass Dissolution

The effect of oxalate on the overall glass dissolution in dependence of the thermal history is shown in Fig. 3-9. Basaltic glasses altered at pH 5 for 504 h have lost in total ~ 0.24 to 0.4% of their cations (Figure 3-9a). The effect of 1 mM oxalic acid at pH 5 on the glass dissolution rate was negligible for annealed glasses whereas quenched glasses showed slightly enhanced glass dissolution in the presence of oxalate with the oxidized glass being stronger affected. As the pH decreased to pH 2, glass dissolution increased more than 4 times and dissolution of oxidized glasses was faster compared to reduced glasses with absolute values of $\sim 1.83 \pm 0.06\%$ and $1.55 \pm 0.08\%$, respectively (Figure 3-9b). Upon addition of 1 mM oxalic acid dissolution of quenched glasses was stronger enhanced compared to their annealed analogues, e.g., loss of cations increased for Fe(III)-rich annealed glasses from $\sim 1.80 \pm 0.04\%$ to $2.01 \pm 0.06\%$ compared to an increase from $\sim 1.86 \pm 0.08\%$ to $2.32 \pm 0.07\%$ for Fe(III)-rich quenched glasses. This corresponds to a 0.3% (Δ_{Q-A}) higher bulk glass dissolution of quenched glasses. When directly compared, the total mobilized elements from quenched glasses in the presence of 1 mM oxalic acid was 17 to 20% higher compared to annealed glasses.

Dissolution of crystals and glasses occurs preferentially on surface sites with abundant defects (kinks/steps) or edges that are more reactive for protonation and especially adsorption of organic complexes [204–206]. Adsorption of organic complexes on reactive surfaces sites is involved in weakening and breaking of M-O framework bonds [207]. Surfaces of basaltic glasses used within this study showed conchoidal fractures regardless of their thermal history (Figure 3-6d). Assuming that quenched glasses comprise higher surface fracture densities [208], it is suggested that even in the absence of oxalate, protonation of these reactive surface sites

and therefore dissolution rates should be faster for quenched than for annealed glasses. It was observed that dissolution rates of quenched and annealed glasses at pH 2 in oxalate-free solutions were the same and conclude that the higher bulk glass dissolution in the presence of oxalate cannot be caused by a higher abundance of surface sites alone.
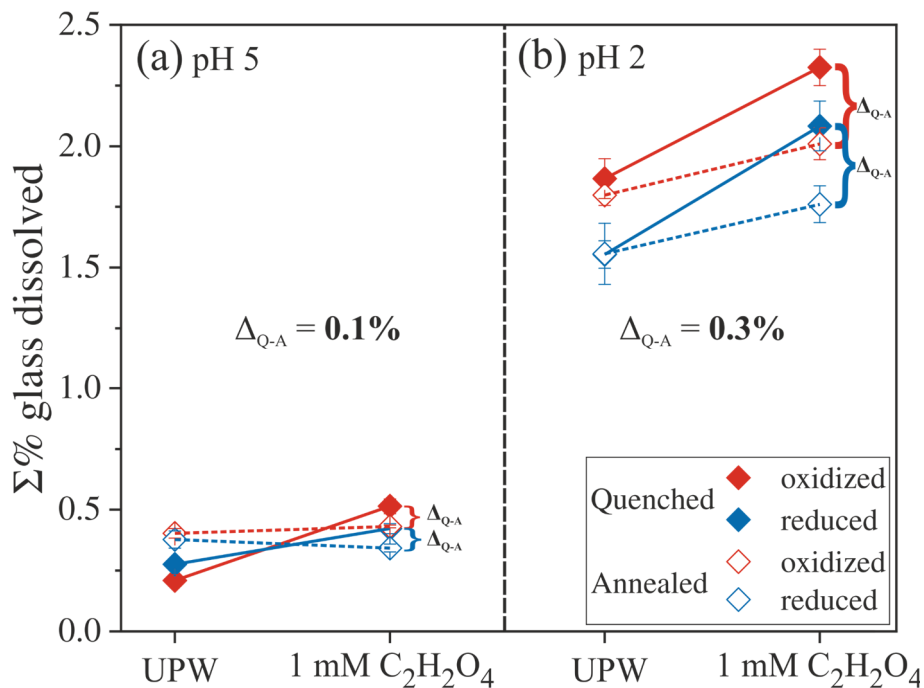
FIGURE 3-9: *Coupled influence of oxalate and thermal history on bulk basaltic glass dissolution at pH 5 **(a)** and pH 2 **(b)**. Solid and dashed lines are only for guidance of the eye. For pH 5 error bars are within the symbol. Δ_{Q-A} is the difference (Δ) in the bulk glass dissolution between quenched (Q) and annealed (A) glass in the presence of 1mM oxalic acid.*

It is assumed that the mechanism by which oxalate enhanced the bulk dissolution of quenched glasses is related to the glass structure itself as observed by higher fictive temperatures (e.g., more open glass structure of quenched glasses). This is also supported by faster reaction rates of quenched glasses observed in Fig. 3-8 and discussed in chapter 3.4.2. Whether the higher mobilization of divalent cations from quenched glasses is caused by strained bonds as suggested by some authors [33,205] is not clear and needs further investigations.

3.4.4 Possible Leached Layer Formation and Dissolution Mechanism at pH 2

In percolation experiments at pH 2 dissolution of all basaltic glasses was incongruent during the whole runtime and all elements were preferentially mobilized with respect to Si that was retained in the leached glass surface. This was expected since the solubility of Si decreases with decreasing pH and formation of a Si-rich leached layer at pH 2 is preferred. However, no extensive leached layer formation was observed by SEM but edges and conchoidal fractures at the surface appeared rounded (Figure 3-6f). It is nevertheless most likely that the fine particles observed after pH 2 experiments originally constituted a leached surfaces layer. This is further evidenced by the presence of conglomerates of fine, Si-rich particles observed by SEM. Gislason and Oelkers, [102] observed grazing and partial detachment of an altered layer from the surface of glassy ash particles after leaching at pH < 3. Here it was suggested that this could be an artifact of grain drying. Similar observations were also made on surfaces of synthetic basaltic glasses [185].

Further evidence for leached layer formation at pH 2 can be obtained comparing dissolved elements and their concentration in the glass (X_{aq}/X_s) relative to Al (Al_{aq}/Al_s) (Figure 3-10). Monovalent cations (Na, K) and P showed large scatter and are excluded for reasons of clarity. For all considered elements a strong correlation with Al was obvious at pH 2 (Figure 3-10a). During the initial stage of the experiments, dissolution was incongruent with Mn and Fe preferentially mobilized from the glass and Mg, Ca, and Si retained relative to Al. With time, however, the dissolution became nearly congruent with respect to Al except for Si. This observation is consistent with other studies of dissolution of basaltic glasses [46,191,209]. The higher (Fe, Mn) and lower (Si, Ca, Mg) mobilization of some elements relative to Al at the beginning of pH 2 experiments is probably related to the previous leaching of the glasses at pH 5. Here, elements such as Al and Fe (and possibly Mn) are weakly soluble at pH 5 and bound in alteration phases. Thus, with the change to pH 2, a higher mobilization of Al, Fe, and Mn is expected during the initial stage of dissolution.

From the slopes of the linear regressions in Fig. 3-10 it can be deduced that the mobilization of divalent cations (Ca, Mg, Mn) as well as Fe increased relative to Al at pH 2 in the presence of oxalate compared to oxalate-free conditions (Figure 3-10b). Long term Al release rates from quenched glasses were not affected by oxalate with $\Delta\log r_{Al,GEO}$ [mol/m²/s] = 0.00 to 0.02 between oxalate-free conditions and in the presence of

oxalate (Figure 3-4a-b; Table 3-2). Annealed glasses, on the other hand, showed a decrease in the long term Al release rates with $\Delta \log r_{Al,GEO}$ [mol/m²/s] = 0.11 to 0.17 upon addition of oxalate (Figure 3-4a-b; Table 3-2). So far, the inhibition of Al release from annealed glasses in the presence of oxalate at pH 2 cannot be reasonably explained but formation of insoluble Al oxalate is not expected due to their high solubility at this pH [210].
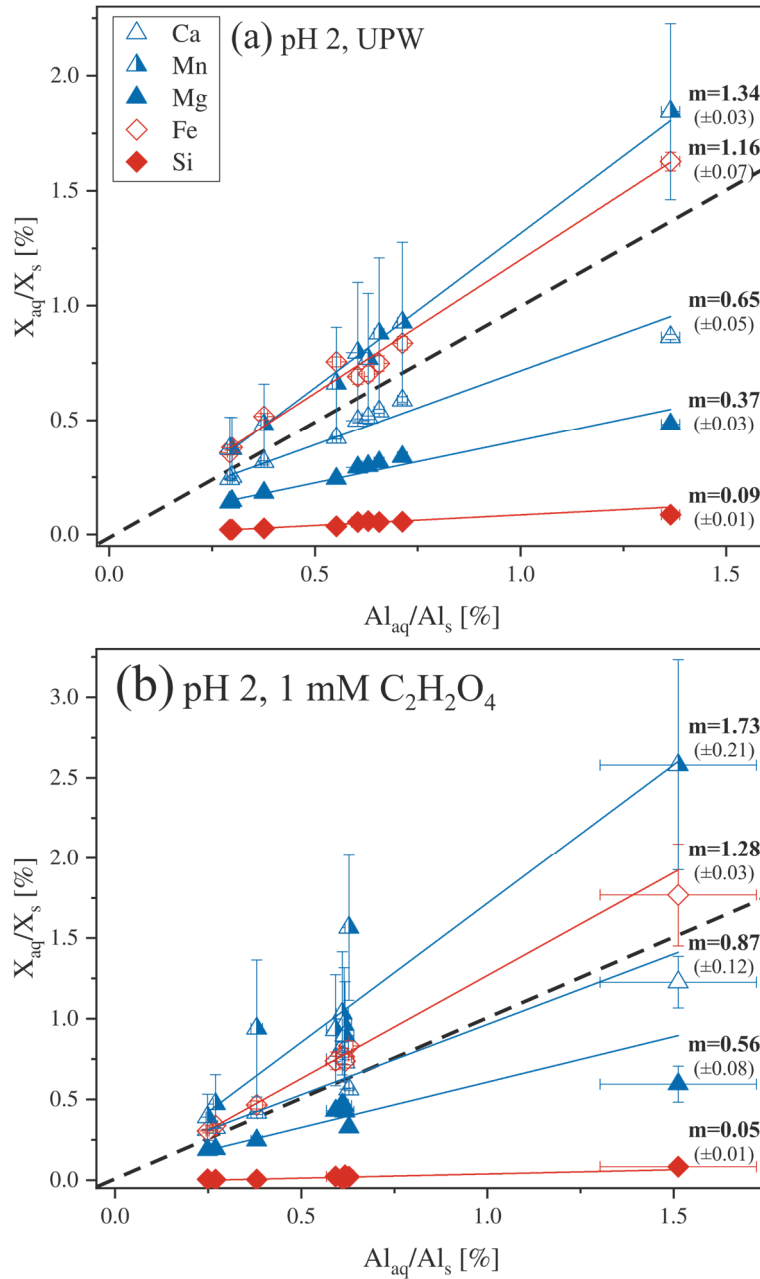

FIGURE 3-10: *Comparison of enrichment or depletion of Mg, Ca, Mn, Fe and Si in the quenched and oxidized basaltic glass relative to Al at pH 2 **(a)** and at pH 2 and 1 mM oxalic acid **(b)**. Dashed line corresponds to the Al/X ratio of the dissolving basaltic glass. m is the slope of the linear regression with the corresponding error in brackets.*

It was shown by some authors that organic anions inhibit mineral dissolution by blocking of active surface sites thereby hindering other dissolution enhancing species (e.g., H^+) to interact with these sites [63,95]. Considering oxalate, its dissolution promoting effect on quenched basaltic glasses is well studied and accepted [7,46,82,191,201]. However, it is assumed that the inhibition of Al release slowed down the mobility of other elements (e.g., Ca, Mg) and is responsible for the observed lower overall dissolution of annealed compared to quenched glasses (compare Figure 3-9).

It is thought that the overall influence of the Fe redox state and thermal history affects basaltic glass dissolution at pH 2 and far from equilibrium conditions assuming that

(i)   Fe(III) is a network former similar to Al

(ii)   Oxalate directly interacts with Al and Fe surface sites at basaltic glass surfaces

as follows:

Mobilization of divalent and trivalent cations from the basaltic glass is incongruent with respect to Al during the initial stage of dissolution regardless of the Fe redox state, thermal history or the presence of oxalate (Figure 3-10). For glasses with varying Fe redox states, strong Si-O-Si bonds are replaced with increasing Fe(III) content from reduced to oxidized basaltic glasses by weaker T-O-Si bonds (T = Fe(III)). Due to the higher abundance of T-O-Si bonds, protonation and dissolution of oxidized glasses proceeds faster compared to reduced glasses. This mechanism becomes stronger pronounced at low pH where the concentration of H^+ in solution is high and, with that, protonation of surface sites. With faster protonation of the glass network of oxidized glasses, the mobilization of other elements is increased (Figure 3-8). Whether Fe(III) or Fe(II) were preferentially mobilized during the initial stage of dissolution cannot be deduced from the data. In the long term, however, dissolved Fe(III) and Fe(II) approach the stoichiometric proportions in the original glass (Figure 3-7).

Basaltic glasses of the same Fe redox state but different thermal histories showed no differences in their dissolution behavior at pH 2. It is therefore suggested that the abundance of surface sites in quenched and annealed glasses does not significantly impact on the observed different dissolution rates, at least in the absence of organic ligands. During fast cooling of quenched glasses reordering of the network structure is suppressed which possibly weakens the critical T-O bonds (T = Al, Fe(III)) and increase their reactivity towards adsorption and complexation by oxalate.

3.5 Conclusions

Basaltic glasses with variable $Fe(II)/Fe_{tot}$ and thermal histories were synthesized and dissolved at far from equilibrium conditions to investigate their dissolution kinetics in dependence of the pH and the presence of oxalate. It was found that basaltic glass dissolution is strongly affected by the Fe redox state and thermal history in the presence of oxalate at pH 2 with the highest dissolution rates for Fe(III)-rich quenched glasses. Long term Al release rates increased by 0.15 to 0.2 log units with an increase from 20 to 65% Fe(III) in the glasses. This is attributed to the progressive replacement of strong Si-O-Si with weaker Fe(III)-O-Si. There is no preferential mobilization of either Fe(II) or Fe(III) from the glasses and in the long term, both are mobilized close to their stoichiometric proportions in the original basaltic glass.

The stronger effect of oxalate on dissolution of quenched glasses cannot be fully explained but a relation to the glass network structure and the nature of network bonds in quenched glasses is suggested. Dissolution of basaltic glass surfaces took place on reactive sites (e.g., edges, steps) that appeared to be preferentially dissolved. Despite the fact that a direct proof for leached surface layer formation in pH 2 experiments is missing there is evidence by (i) the incongruent glass dissolution indicating Si enrichment in the glass surface and (ii) the abundance of fine, Si-rich particle observed by SEM that supports this assumption. These alteration products could have been a sink also for other elements (e.g., Fe, Mn).

The experimental results of this study demonstrate that basaltic glass dissolution is affected by the Fe redox state and the thermal history at pH < 3 and even low concentrations of oxalic acid (~ 1 mM). Both, the Fe redox state and thermal history, are suggested to be considered for the prediction of the long term stability of basaltic glasses. Moreover, the thermal history might be a parameter of great importance also in microbial alteration experiments as observed in a previous study [92].

General Conclusions

Within this PhD project the main goals were to characterize differentially altered subsurface basaltic rocks with respect to Fe containing phases and to study the potential biotic and abiotic Fe mobilization from these rocks and basaltic glasses. Moreover, it was tried to elucidate the effects of Fe(II)/Fe(III) and thermal history on basaltic glass dissolution. The findings of this study demonstrate the significance of volcanic islands for geochemical element cycles between lithosphere and hydrosphere and provide a better understanding of microbial mediated alteration and the relationship between compositional and structural properties of basaltic glasses and their dissolution behavior.

A sequential extraction was applied to differentially altered subsurface basaltic rocks to determine the type of chemical bonding of Fe that is a prerequisite for its release from the rocks. It was shown that amorphous to weakly crystalline secondary phases (based on Fe_o/Fe_d ratios) dominate. Their abundance was strongly related to the depositional environment with highest contents in seawater influenced rocks. Here, altered pillow basalts and hyaloclastites have to be emphasized from which a high release of limiting nutrients and especially Fe is expected. However, circulation of groundwater is fast within the highly porous rocks of volcanic islands and leached elements are transported away from their source and discharged into the ocean. Evidence was provided from microbial alteration experiments that the microorganisms acquired essential nutrients by direct microbe-surface interactions which is supposed to be an adapted strategy under nutrient limiting conditions. Due to the high groundwater flow within volcanic islands and mid-ocean ridges these locations may provide conditions were microbe-surface interactions and microbial alteration are supported.

Moreover, microbial alteration experiments indicated that the Fe-redox state and thermal history of basaltic glasses have a direct influence on the microbial activity. Dissolution was accelerated by microbial activity and increased in the order annealed Fe(III)-rich < quenched Fe(III)-rich < quenched Fe(II)-rich basaltic glass. Furthermore, the abundance of microbial cells attached to glass surfaces was directly correlated with the thermal history and increased from annealed to quenched glasses. Within the percolation experiments dissolution of quenched basaltic glasses at pH 2 was enhanced in the presence of an organic ligand (oxalate) relative to annealed glasses of the same composition. This allows to conclude that in the microbial alteration experiments the microorganisms have most likely produced an organic ligand that enhanced the dissolution of quenched relative to annealed glasses similar to what was observed

in the percolation experiments. The exact mechanisms by which organic ligands accelerated the dissolution of quenched basaltic glasses is yet not clear and needs further and more detailed investigations.

Finally, it was demonstrated in percolation experiments that the long term durability of basaltic glasses is affected by the Fe redox state and decreases with increasing Fe(III) content. This observation was surprising since a higher chemical durability with increasing network former content and, thus, for Fe(III)-rich glasses was expected. For aluminosilicate glasses it is well documented that dissolution increases as the number of Al atoms per Si tetrahedral increases from albite to jadeite to nepheline glasses [30]. A similar influence of Fe(III) in basaltic glasses is assumed but more systematic studies are needed.

Open Questions and Future Research

High concentrations of dissolved Fe in ocean surface waters were not only observed in the vicinity of Hawaii but also at other volcanic islands [23,24]. The potential for the release of soluble Fe from volcanic islands was investigated based on a case study on subsurface basaltic rocks of Hawaii. The question remains whether Hawaii is a unique example or applicable also to other volcanic setting where large amounts of fresh basaltic rocks are in direct contact with seawater. Other parameters such as rock composition, temperature, porosity, and dissolved species need to be considered that potentially impact on aging of secondary phases. However, the temperature and abundance of dissolved species can hardly be determined for naturally altered rocks as they were observed to vary even on small scales. It is therefore necessary to perform alteration experiments with fresh and altered basaltic rocks under well-known temperature conditions and solution compositions to investigate (i) the secondary phases that form from fresh basaltic rocks and (ii) the change in the crystallinity of preexisting secondary phases. A better understanding of the processes that influence aging of secondary phases is of great importance also for other research fields such as the long term behavior of nuclear glasses which is strongly controlled by secondary phase formation [9].

A question that remains still unclear from Chapter II is the mechanism by which the microbes enhanced the liberation of elements from quenched basaltic glass over that of their annealed analogues. Even though a part of this question was answered in Chapter III where it was shown that dissolution of quenched glasses is accelerated in the presence of a single organic ligand, it is still unknown if *B. fungorum* is capable of producing organic ligands and, if it does, of what kind they are and how they interact with the basalt surface.

Most of the work done so far investigated the alteration of basaltic glasses with respect to the chemistry of the glasses and environmental influences. These studies, however, do seldom consider the effects of varying Fe redox state and thermal history. It appears from the study that Fe(III) decreases the durability of basaltic glasses whereas the thermal history affects basaltic glass dissolution in the presence of organic ligands. More systematic studies are needed to reveal the exact mechanisms. Basaltic glass "endmembers" with $Fe(II)/Fe_{tot}$ close to 0 and 1 would be a useful tool to determine the individual effects of Fe(II) and Fe(III). However, the synthesis of such glasses is problematic. A precise control on the oxygen fugacity during the experiments is needed to avoid unwanted effects such as precipitation of Fe^0 below the IW (Iron-Wüstite) buffer. Furthermore, homogenization of the melt with respect to

Fe(II)/Fe(III) is difficult. It was shown in Chapter III that reduction of a very fine (< 50 μm) basaltic glass powder below its T_g is sufficient to achieve a homogenous reduction of the Fe in the glass.

References

(1) Sutton, J. N., André, L., Cardinal, D., Conley, D. J., Souza, G. F. De, Dean, J., Dodd, J., Ehlert, C., Ellwood, M. J., Frings, P. J., Grasse, P., Hendry, K., Leng, M. J., Michalopoloulos, P., Panizzo, V. N. & Swann, G. E. A. A review of the stable isotope bio-geochemistry of the global silicon cycle and its associated trace elements. *Front. Earth Sci.* **5**, (2018).

(2) Walton, A. W., Schiffman, P. & MacPherson, G. L. Alteration of hyaloclastites in the HSDP 2 Phase 1 Drill core: 2. Mass balance of the conversion of sideromelane to palagonite and chabazite. *Geochemistry, Geophys. Geosystems* **6**, (2005).

(3) Oelkers, E. H., Jones, M. T., Pearce, C. R., Jeandel, C., Salome, E. & Gislason, S. R. Riverine particulate material dissolution in seawater and its implications for the global cycles of the elements. *Comptes Rendus - Geosci. - Geosci.* **344**, 646–651 (2012).

(4) Staudigel, H., Furnes, H., McLoughlin, N., Banerjee, N. R., Connell, L. B. & Templeton, A. 3.5 billion years of glass bioalteration: Volcanic rocks as a basis for microbial life? *Earth-Science Rev.* **89**, 156–176 (2008).

(5) Dessert, C., Dupré, B., Gaillardet, J., François, L. M. & Allègre, C. J. Basalt weathering laws and the impact of basalt weathering on the global carbon cycle. *Chem. Geol.* **202**, 257–273 (2003).

(6) Wilson, M. J. Weathering of the primary rock-forming minerals: processes, products and rates. *Clay Miner.* **39**, 233–266 (2004).

(7) Wolff-Boenisch, D., Wenau, S., Gislason, S. R. & Oelkers, E. H. Dissolution of basalts and peridotite in seawater, in the presence of ligands, and CO2: Implications for mineral sequestration of carbon dioxide. *Geochim. Cosmochim. Acta* **75**, 5510–5525 (2011).

(8) Gysi, A. P. & Stefánsson, A. CO2-water-basalt interaction. Low temperature experiments and implications for CO2 sequestration into basalts. *Geochim. Cosmochim. Acta* **81**, 129–152 (2012).

(9) Ducasse, T., Gourgiotis, A., Pringle, E., Moynier, F., Frugier, P., Jollivet, P. & Gin, S. Alteration of synthetic basaltic glass in silica saturated conditions : Analogy with nuclear glass. *Appl. Geochemistry* **97**, 19–31 (2018).

(10) Crovisier, J., Advocat, T. & Dussossoy, J.-L. Nature and role of natural alteration gels formed on the surface of ancient volcanic glasses (Natural analogs of waste containment glasses). *J. Nucl. Mater.* **321**, 91–109 (2003).

(11) Coale, K. H. *et al.* A massive phytoplankton bloom induced by an ecosystem-scale iron fertilization experiment in the equatorial Pacific Ocean. *Nature* **383**, 495–501 (1996).

(12) Morgan, N. A. & Spera, F. J. Glass transition, structural relaxation, and theories of viscosity: A molecular dynamics study of amorphous CaAl2Si2O8. *Geochim. Cosmochim. Acta* **65**, 4019–4041 (2001).

(13) Nakamura, K. Preliminary estimate of global volcanic production rate. in *The Utilization of Volcano Energy* (eds. Colp, J. S. & Furumoto, A. S.) 273–285 (N.M. Sandia Laboratories, 1974).

(14) Peterson, D. W. & Moore, R. b. Geologic History and Evolution of Geologic concepts: Island of Hawaii. in *Volcanism in Hawaii* (eds. Decker, R. W., Wright, T. L. & Stauffer, P. H.) 149–186 (U.S. Geological Survey Professional Paper, 1987).

(15) Depaolo, D. J. & Stolper, E. M. Models of Hawaiian volcano growth and plume structure: Implications of results from the Hawaii Scientific Drilling Project. *J. Geophys. Res.* **101**, 11643–11654 (1996).

(16) Boyd, P. W. & Ellwood, M. J. The biogeochemical cycle of iron in the ocean. *Nat. Geosci.* **3**, 675–682 (2010).

(17)   Van Der Merwe, P., Bowie, A. R., Quéroue, F., Armand, L., Blain, S., Chever, F., Davies, D., Dehairs, F., Planchon, F., Sarthou, G., Townsend, A. T. & Trull, T. W. Sourcing the iron in the naturally fertilised bloom around the Kerguelen Plateau: Particulate trace metal dynamics. *Biogeosciences* **12**, 739–755 (2015).

(18)   Windom, H. L., Moore, W. S., Niencheski, L. F. H. & Jahnke, R. A. Submarine groundwater discharge: A large, previously unrecognized source of dissolved iron to the South Atlantic Ocean. *Mar. Chem.* **102**, 252–266 (2006).

(19)   Langmann, B. Volcanic Ash versus Mineral Dust: Atmospheric Processing and Environmental and Climate Impacts. *ISRN Atmos. Sci.* 1–17 (2013). doi:10.1155/2013/245076

(20)   Wu, J., Wells, M. L. & Rember, R. Dissolved iron anomaly in the deep tropical-subtropical Pacific: Evidence for long-range transport of hydrothermal iron. *Geochim. Cosmochim. Acta* **75**, 460–468 (2011).

(21)   Sullivan, C. W., Arrigo, K. R., Moclain, C. R., Comiso, J. C. & Firestone, J. Distributions of Phytoplankton Blooms in the Southern Ocean. *Science (80-.).* **262**, 1832–1837 (1993).

(22)   Brown, M. T., Landing, W. M. & Measures, C. I. Dissolved and particulate Fe in the western and central North Pacific: Results from the 2002 IOC cruise. *Geochemistry, Geophys. Geosystems* **6**, (2005).

(23)   Pollard, R., Sanders, R., Lucas, M. & Statham, P. The Crozet Natural Iron Bloom and Export Experiment (CROZEX). *Deep. Res. II* **54**, 1905–1914 (2007).

(24)   Chever, F., Sarthou, G., Bucciarelli, E., Blain, S. & Bowie, A. R. An iron budget during the natural iron fertilisation experiment KEOPS (Kerguelen Islands, Southern Ocean). *Biogeosciences* **7**, 455–468 (2010).

(25)   Rad, S. D., Allègre, C. J. & Louvat, P. Hidden erosion on volcanic islands. *Earth Planet. Sci. Lett.* **262**, 109–124 (2007).

(26)   Schopka, H. H. & Derry, L. A. Chemical weathering fluxes from volcanic islands and the importance of groundwater: The Hawaiian example. *Earth Planet. Sci. Lett.* **339–340**, 67–78 (2012).

(27)   Nielsen, M. E. & Fisk, M. R. Surface area measurements of marine basalts: Implications for the subseafloor microbial biomass. *Geophys. Res. Lett.* **37**, 1–5 (2010).

(28)   Staudigel, H. & Hart, S. R. Alteration of basaltic glass: Mechanisms and significance for the oceanic crust-seawater budget. *Geochim. Cosmochim. Acta* **47**, 337–350 (1983).

(29)   Wolff-Boenisch, D., Gislason, S. R., Oelkers, E. H. & Putnis, C. V. The dissolution rates of natural glasses as a function of their composition at pH 4 and 10.6, and temperatures from 25 to 74°C. *Geochim. Cosmochim. Acta* **68**, 4843–4858 (2004).

(30)   Hamilton, J. P., Brantley, S. L., Pantano, C. G., Criscenti, L. J. & Kubicki, J. D. Dissolution of nepheline , jadeite and albite glasses : Toward better models for aluminosilicate dissolution. *Geochim. Cosmochim. Acta* **65**, 3683–3702 (2001).

(31)   Scholze, H. *Glass Nature, Structure, Properties*. **1**, (Springer Verlag, 1991).

(32)   Angeli, F., Villain, O., Schuller, S., Charpentier, T., Ligny, D. De, Bressel, L. & Wondraczek, L. Effect of temperature and thermal history on borosilicate glass structure. *Phys. Rev. B* **85**, 1–15 (2012).

(33)   Pantano, C. G. *What do we know about glass surfaces? Chapter 12 in A Collection of Papers Presented at the 61st Conference on Glass Problems: Ceramic Engineering and Science Proceedings 22* (The American Ceramic Society, 2001). doi:10.1002/9780470294659

(34)   Gottsmann, J., Harris, A. J. L. & Dingwell, D. B. Thermal history of Hawaiian pahoehoe lava crusts at the glass transition : implications for flow rheology and emplacement. *Earth Planet. Sci. Lett.* **228**, 343–353 (2004).

(35) Nichols, A. R. L., Potuzak, M. & Dingwell, D. B. Cooling rates of basaltic hyaloclastites and pillow lava glasses from the HSDP2 drill core. *Geochim. Cosmochim. Acta* **73**, 1052–1066 (2009).

(36) Potuzak, M., Nichols, A. R. L., Dingwell, D. B. & Clague, D. A. Hyperquenched volcanic glass from Loihi Seamount , Hawaii. *Earth Planet. Sci. Lett.* **270**, 54–62 (2008).

(37) Amma, S., Luo, J., Kim, S. H. & Pantano, C. G. Effects of fi ctive temperature on the leaching of soda lime silica glass surfaces. 1424–1431 (2017). doi:10.1111/jace.14754

(38) Stone-Weiss, N., Pierce, E. M., Youngman, R. E., Gulbiten, O., Smith, N. J., Du, J. & Goel, A. Understanding the structural drivers governing glass – water interactions in borosilicate based model bioactive glasses. *Acta Biomater.* **65**, 436–449 (2018).

(39) Angeli, F., Charpentier, T., Jollivet, P., de Ligny, D., Bergler, M., Veber, A., Gin, S. & Li, H. Effect of thermally induced structural disorder on the chemical durability of International Simple Glass. *Mater. Degrad.* **31**, 1–11 (2018).

(40) Christie, D. M., Carmichael, I. S. E. & Langmuir, C. H. Oxidation states of mid-ocean ridge basalt glasses. *Earth Planet. Sci. Lett.* **79**, 397–411 (1986).

(41) Taylor, K. G. & Konhauser, K. O. Iron in Earth Surface Systems: A Major Player in Chemical and Biological Processes. *Elements* **7**, 83–88 (2011).

(42) Rue, E. L. & Bruland, K. W. Complexation of iron (III) by natural organic ligands in the Central North Pacific as determined by a new competitive ligand equilibration / adsorptive cathodic stripping voltammetric method. *Mar. Chem.* **50**, 117–138 (1995).

(43) Gledhill, M. & Buck, K. N. The organic complexation of iron in the marine environment: A review. *Front. Microbiol.* **3**, 1–17 (2012).

(44) Cornell, R. M. & Schwertmann, U. Soils. in *The Iron Oxides: Structure, Properties, Reactions, Occurences and Uses* (eds. Cornell, R. M. & Schwertmann, U.) 433–474 (Wiley-VCH Verlag GmbH & Co. KGaA, 2003).

(45) Gislason, S. & Eugster, H. P. Meteoric water-basalt interactions. II: A field study in N.E. Iceland. *Geochim. Cosmochim. Acta* **51**, 2841–2855 (1987).

(46) Oelkers, E. H. General kinetic description of multioxide silicate mineral and glass dissolution. *Geochim. Cosmochim. Acta* **65**, 3703–3719 (2001).

(47) Techer, I., Advocat, T., Lancelot, J. & Liotard, J. Dissolution kinetics of basaltic glasses : control by solution chemistry and protective effect of the alteration film. *Chem. Geol.* **176**, 235–263 (2001).

(48) Gin, S., Jollivet, P., Fournier, M., Angeli, F., Frugier, P. & Charpentier, T. Origin and consequences of silicate glass passivation by surface layers. *Nat. Commun.* **6**, (2015).

(49) Stefánsson, A. & Gíslason, S. R. Chemical weathering of basalts, southwest Iceland: Effect of rock crystallinity and secondary minerals on chemical fluxes to the ocean. *Am. J. Sci.* **301**, 513–556 (2001).

(50) Colombier, M., Wadsworth, F. B., Gurioli, L., Scheu, B., Kueppers, U., Di Muro, A. & Dingwell, D. B. The evolution of pore connectivity in volcanic rocks. *Earth Planet. Sci. Lett.* **462**, 99–109 (2017).

(51) Dultz, S., Simonyan, A. V., Pastrana, J., Behrens, H., Plötze, M. & Rath, T. Implications of pore space characteristics on diffusive transport in basalts and granites. *Environ. Earth Sci.* **69**, 969–985 (2013).

(52) Navarre-Sitchler, A., Steefel, C. I., Yang, L., Tomutsa, L. & Brantley, S. L. Evolution of porosity and diffusivity associated with chemical weathering of a basalt clast. *J. Geophys. Res. Earth Surf.* **114**, 1–14 (2009).

(53) Hausrath, E. M., Neaman, A. & Brantley, S. L. Elemental release rates from dissolving basalt and granite with and without organic ligands. *Am. J. Sci.* **309**, 633–660 (2009).

(54) Declercq, J., Diedrich, T., Perrot, M., Gislason, S. R. & Oelkers, E. H. Experimental determination of rhyolitic glass dissolution rates at 40 – 200 ° C and 2 < pH < 10.1. *Geochim. Cosmochim. Acta* **100**, 251–263 (2013).

(55) Michelin, A., Burger, E., Rebiscoul, D., Bruguier, F., Drouet, E., Dillmann, P. & Gin, S. Silicate Glass Alteration Enhanced by Iron: Origin and Long-Term Implications. *Environ. Sci. Technol.* **47**, 750–756 (2013).

(56) Pichler, T., Ridley, W. I. & Nelson, E. Low-temperature alteration of dredged volcanics from the Southern Chile Ridge: Additional information about early stages of seafloor weathering. *Mar. Geol.* **159**, 155–177 (1999).

(57) Arena, H., Rébiscoul, D., Podor, R., Garcés, E., Cabie, M., Mestre, J. & Godon, N. Impact of Fe , Mg and Ca elements on glass alteration : Interconnected processes. *Geochim. Cosmochim. Acta* **239**, 420–445 (2018).

(58) Walton, A. W. & Schiffman, P. Alteration of hyaloclastites in the HSDP 2 phase 1 drill core1. Description and paragenesis. *Geochemistry, Geophys. Geosystems* **4**, (2003).

(59) Giorgetti, G., Marescotti, P., Cabella, R. & Lucchetti, G. Clay mineral mixtures as alteration products in pillow basalts from the eastern flank of Juan de Fuca Ridge: a TEM-AEM study. *Clay Miner.* **36**, 75–91 (2001).

(60) Yang, K., Park, H., Baik, H., Kogure, T. & Kim, J. The formation of Fe-bearing secondary phase minerals from the basalt-sediment interface, South Pacific gyre: IODP expedition 329. *Clays Clay Miner.* **66**, 1–8 (2018).

(61) Stroncik, N. A. & Schmincke, H. U. Palagonite - A review. *Int. J. Earth Sci.* **91**, 680–697 (2002).

(62) Ostwald, W. Studien über die Bildung und Umwandlung fester Körper. 1. Abhandlung: Übersättigung und Überkältung. *Zeitschrift fur Phys. Chemie* **22**, 289–330 (1897).

(63) Johnson, S. B., Yoon, T. H. & Brown, G. E. Adsorption of organic matter at mineral/water interfaces: 5. Effects of adsorbed natural organic matter analogues on mineral dissolution. *Langmuir* **21**, 2811–2821 (2005).

(64) Brady, K., Bigham, J., Jaynes, W. & Logan, T. Influence of sulfate on Fe-oxide formation: comparisons with a stream receiving acid mine drainage. *Clays Clay Miner.* **34**, 266–274 (1986).

(65) Furnes, H. & Staudigel, H. Biological mediation in ocean crust alteration: How deep is the deep biosphere? *Earth Planet. Sci. Lett.* **166**, 97–103 (1999).

(66) Furnes, H., Staudigel, H., Thorseth, I. H., Torsvik, T., Muehlenbachs, K. & Tumyr, O. Bioalteration of basaltic glass in the oceanic crust. *Geochemistry, Geophys. Geosystems* **2**, 2000GC000150 (2001).

(67) Fisk, M. R., Popa, R. & Wacey, D. Tunnel Formation in Basalt Glass. *Astrobiology* **19**, 1–13 (2019).

(68) Mccollom, T. M. & Donaldson, C. Experimental Constraints on Abiotic Formation of Tubules and Other Proposed Biological Structures in Subsurface Volcanic Glass. *Astrobiology* **19**, 53–63 (2019).

(69) Furnes, H., Muehlenbachs, K., Tumyr, O., Torsvik, T. & Thorseth, I. H. Depth of active bio-alteration in the ocean crust: Costa Rica Rift (Hole 504B). *Terra Nov.* **11**, 228–233 (1999).

(70) Walton, A. W. Microtubules in basalt glass from Hawaii Scientific Driling Project #2 phase 1 core and Hilina slope, Hawaii: Evidence of the occurrence and behavior of endolithic microorganisms. *Geobiology* **6**, 351–364 (2008).

(71) Byloos, B., Maan, H., Houdt, R. Van, Boon, N. & Leys, N. The Ability of Basalt to Leach Nutrients and Support Growth of Cupriavidus metallidurans CH34 Depends on Basalt Composition and Element Release. *Geomicrobiol. J.* **35**, 438–446 (2018).

(72) Roden, E. E. & Zachara, J. M. Microbial Reduction of Crystalline Iron (III) Oxides: Influence of Oxide Surface Area and Potential for Cell Growth. *Environ. Sci. Technol.* **30**, 1618–1628 (1996).

(73) Clarke, A. The thermal limits to life on Earth. *Int. J. Astrobiol.* **13**, 141–154 (2014).

(74) Emerson, D., Fleming, E. J. & McBeth, J. M. Iron-Oxidizing Bacteria: An Environmental and Genomic Perspective. *Annu. Rev. Microbiol.* **64**, 561–583 (2010).

(75) Henri, P. A., Rommevaux-Jestin, C., Lesongeur, F., Mumford, A., Emerson, D., Godfroy, A. & Ménez, B. Structural iron (II) of basaltic glass as an energy source for zetaproteobacteria in an abyssal plain environment, off the mid atlantic ridge. *Front. Microbiol.* **6**, 1–18 (2016).

(76) Konhauser, K. O., Kappler, A. & Roden, E. E. Iron in microbial metabolisms. *Elements* **7**, 89–93 (2011).

(77) Templeton, A. S., Staudigel, H. & Tebo, B. M. Diverse Mn(II)-oxidizing bacteria isolated from submarine basalts at Loihi seamount. *Geomicrobiol. J.* **22**, 127–139 (2005).

(78) Uroz, S., Calvaruso, C., Turpault, M. P. & Frey-Klett, P. Mineral weathering by bacteria: ecology, actors and mechanisms. *Trends Microbiol.* **17**, 378–387 (2009).

(79) Rogers, J. R. & Bennett, P. C. Mineral stimulation of subsurface microorganisms: Release of limiting nutrients from silicates. *Chem. Geol.* **203**, 91–108 (2004).

(80) Ahmed, E. & Holmström, S. J. M. Microbe-mineral interactions: The impact of surface attachment on mineral weathering and element selectivity by microorganisms. *Chem. Geol.* **403**, 13–23 (2015).

(81) Perez, A., Rossano, S., Trcera, N., Huguenot, D., Fourdrin, C., Verney-Carron, A., van Hullebusch, E. D. & Guyot, F. Bioalteration of synthetic Fe(III)-, Fe(II)-bearing basaltic glasses and Fe-free glass in the presence of the heterotrophic bacteria strain Pseudomonas aeruginosa: Impact of siderophores. *Geochim. Cosmochim. Acta* **188**, 147–162 (2016).

(82) Eick, M. J., Grossl, P. R., Golden, D. C., Sparks, D. L. & Ming, D. W. Dissolution of a lunar basalt simulant as affected by pH and organic anions. *Geoderma* **74**, 139–160 (1996).

(83) Santelli, C. M., Orcutt, B. N., Banning, E., Bach, W., Moyer, C. L., Sogin, M. L., Staudigel, H. & Edwards, K. J. Abundance and diversity of microbial life in ocean crust. *Nature* **453**, 653–657 (2008).

(84) Kruber, C., Thorseth, I. H. & Pedersen, R. B. Seafloor alteration of basaltic glass: Textures, geochemistry, and endolithic microorganisms. *Geochemistry, Geophys. Geosystems* **9**, 1–18 (2008).

(85) Dold, B., Aguilera, a, Cisternas, M. E., Bucchi, F. & Amils, R. Sources for Iron Cycling in the Southern Ocean. *Environ. Sci. Technol.* **47**, 6129–6136 (2013).

(86) Zakharova, E. A., Pokrovsky, O. S., Dupré, B., Gaillardet, J. & Efimova, L. E. Chemical weathering of silicate rocks in Karelia region and Kola peninsula, NW Russia: Assessing the effect of rock composition, wetlands and vegetation. *Chem. Geol.* **242**, 255–277 (2007).

(87) Simonyan, A. V., Dultz, S. & Behrens, H. Diffusive transport of water in porous fresh to altered mid-ocean ridge basalts. *Chem. Geol.* **306**–**307**, 63–77 (2012).

(88) Navarrete, J. U., Cappelle, I. J., Schnittker, K. & Borrok, D. M. Bioleaching of ilmenite and basalt in the presence of iron-oxidizing and iron-scavenging bacteria. *Int. J. Astrobiol.* **12**, 123–134 (2013).

(89) Beckingham, L. E., Steefel, C. I., Swift, A. M., Voltolini, M., Yang, L., Anovitz, L. M., Sheets, J. M., Cole, D. R., Kneafsey, T. J., Mitnick, E. H., Zhang, S., Landrot, G., Ajo-Franklin, J. B., DePaolo, D. J., Mito, S. & Xue, Z. Evaluation of accessible mineral surface areas for improved prediction of mineral reaction rates in porous media. *Geochim. Cosmochim. Acta* **205**, 31–49 (2017).

(90) Seyfried, W. E. & Bischoff, J. L. Low temperature basalt alteration by sea water: an experimental study at 70°C and 150°C. *Geochim. Cosmochim. Acta* **43**, 1937–1947 (1979).

(91) Maher, K. The dependence of chemical weathering rates on fluid residence time. *Earth Planet. Sci. Lett.* **294**, 101–110 (2010).

(92) Stranghöner, M., Schippers, A., Dultz, S. & Behrens, H. Experimental microbial alteration and Fe mobilization from basaltic rocks of the ICDP HSDP2 drill core, Hilo, Hawaii. *Front. Microbiol.* **9**, 1252 (2018).

(93) Schwertmann, U. & Taylor, R. M. Iron oxides. in *Minerals in Soil Environments* (eds. Dixon, J. B. & Weed, S. B.) 379–438 (SSSA Book Ser., vol. 1, SSSA, Madison, WI, 1989).

(94) Steefel, C. I. & Van Cappellen, P. A new kinetic approach to modeling water-rock interaction: The role of nucleation, precursors, and Ostwald ripening. *Geochim. Cosmochim. Acta* **54**, 2657–2677 (1990).

(95) Johnson, S. B., Yoon, T. H., Kocar, B. D. & Brown, G. E. Adsorption of organic matter at mineral/water interfaces. 2. Outer-sphere adsorption of maleate and implications for dissolution processes. *Langmuir* **20**, 4996–5006 (2004).

(96) Schwertmann, U. & Latham, M. Properties of iron oxides in some new Caledonian oxisols. *Geoderma* **39**, 105–123 (1986).

(97) Jones, A. M., Collins, R. N., Rose, J. & Waite, T. D. The effect of silica and natural organic matter on the Fe(II)-catalysed transformation and reactivity of Fe(III) minerals. *Geochim. Cosmochim. Acta* **73**, 4409–4422 (2009).

(98) Tomaszewski, E. J., Cronk, S. S., Gorski, C. A. & Ginder-Vogel, M. The role of dissolved Fe(II) concentration in the mineralogical evolution of Fe (hydr)oxides during redox cycling. *Chem. Geol.* **438**, 163–170 (2016).

(99) Thompson, A., Rancourt, D. G., Chadwick, O. A. & Chorover, J. Iron solid-phase differentiation along a redox gradient in basaltic soils. *Geochim. Cosmochim. Acta* **75**, 119–133 (2011).

(100) Canfield, E. Reactive iron in marine sediments. *Geochim. Cosmochim. Acta* **53**, 619–632 (1989).

(101) Filgueiras, A. V., Lavilla, I. & Bendicho, C. Chemical sequential extraction for metal partitioning in environmental solid samples. *J. Environ. Monit.* **4**, 823–857 (2002).

(102) Gislason, S. R. & Oelkers, E. H. Mechanism, rates, and consequences of basaltic glass dissolution: II. An experimental study of the dissolution rates of basaltic glass as a function of pH and temperature. *Geochim. Cosmochim. Acta* **67**, 3817–3832 (2003).

(103) Gudbrandsson, S., Wolff-Boenisch, D., Gislason, S. R. & Oelkers, E. H. An experimental study of crystalline basalt dissolution from 2 < = pH < = 11 and temperatures from 5 to 75°C. *Geochim. Cosmochim. Acta* **75**, 5496–5509 (2011).

(104) Révillon, S., Teagle, D. A. H., Boulvais, P., Shafer, J. & Neal, C. R. Geochemical fluxes related to alteration of a subaerially exposed seamount: Nintoku seamount, ODP Leg 197, Site 1205. *Geochemistry, Geophys. Geosystems* **8**, 1–26 (2007).

(105) Garcia, M. O., Haskins, E. H., Stolper, E. M. & Baker, M. Stratigraphy of the Hawai'i Scientific Drilling Project core (HSDP2): Anatomy of a Hawaiian shield volcano. *Geochemistry, Geophys. Geosystems* **8**, (2007).

(106) Sharp, W. D. & Renne, P. R. The 40Ar/39Ar dating of core recovered by the Hawaii Scientific Drilling Project (phase 2), Hilo, Hawaii. *Geochemistry, Geophys. Geosystems* **6**, (2005).

(107) Stolper, E. M., DePaolo, D. J. & Thomas, D. M. Deep Drilling into a Mantle Plume Volcano: The Hawaii Scientific Drilling Project. *Scientific Drilling* **7**, 4–14 (2009).

(108) Büttner, G. & Huenges, E. The heat transfer in the region of the Mauna Kea (Hawaii) - constraints from borehole temperature measurements and coupled thermo-hydraulic modeling. *Tectonophysics* **371**, 23–40 (2003).

(109) Thomas, D. M. & Conrad, M. E. Hydrogeology of the Hawaii Scientific Drilling Project borehole KP-1 2. Groundwater geochemistry and regional flow patterns. *J. Geophys. Res.* **101**, 11683–11694 (1996).

(110) Rhodes, J. M. & Vollinger, M. J. Composition of basaltic lavas sampled by phase-2 of the Hawaii Scientific Drilling Project: Geochemical stratigraphy and magma types. *Geochemistry, Geophys. Geosystems* **5**, (2004).

(111) Quane, S. L., Garcia, M. O., Guillou, H. & Hulsebosch, T. P. Magmatic history of the East Rift Zone of Kilauea Volcano, Hawaii based on drill core from SOH 1. *J. Volcanol. Geotherm. Res.* **102**, 319–338 (2000).

(112) Fisk, M. R., Storrie-Lombardi, M. C., Douglas, S., Popa, R., McDonald, G. & Di Meo-Savoie, C. Evidence of biological activity in Hawaiian subsurface basalts. *Geochemistry, Geophys. Geosystems* **4**, (2003).

(113) Poulton, S. W. & Canfield, D. E. Development of a sequential extraction procedure for iron: Implications for iron partitioning in continentally derived particulates. *Chem. Geol.* **214**, 209–221 (2005).

(114) Schuessler, J. A., Botcharnikov, R. E., Behrens, H., Misiti, V. & Freda, C. Oxidation state of iron in hydrous phono-tephritic melts. *Am. Mineral.* **93**, 1493–1504 (2008).

(115) Dultz, S., Behrens, H., Simonyan, A., Kahr, G. & Rath, T. Determination of porosity and pore connectivity in feldspars from soils of granite and saprolite. *Soil Sci.* **171**, 675–694 (2006).

(116) Henkel, S., Kasten, S., Poulton, S. W. & Staubwasser, M. Determination of the stable iron isotopic composition of sequentially leached iron phases in marine sediments. *Chem. Geol.* **421**, 93–102 (2016).

(117) Roebbert, Y., Rabe, K., Lazarov, M., Schuth, S., Schippers, A., Dold, B. & Weyer, S. Fractionation of Fe and Cu isotopes in acid mine tailings: Modification and application of a sequential extraction method. *Chem. Geol.* **493**, 67–79 (2018).

(118) Moussallam, Y., Edmonds, M., Scaillet, B., Peters, N., Gennaro, E., Sides, I. & Oppenheimer, C. The impact of degassing on the oxidation state of basaltic magmas: A case study of Kīlauea volcano. *Earth Planet. Sci. Lett.* **450**, 317–325 (2016).

(119) Stolper, E., Sherman, S., Garcia, M., Baker, M. & Seaman, C. Glass in the submarine section of the HSDP2 drill core, Hilo, Hawaii. *Geochemistry, Geophys. Geosystems* **5**, (2004).

(120) Drief, A. & Schiffman, P. Very low-temperature alteration of sideromelane in hyaloclastites and hyalotuffs from Kilauea and Mauna Kea volcanoes: Implications for the mechanism of palagonite formation. *Clays Clay Miner.* **52**, 622–634 (2004).

(121) Frey, F. A., Wise, W. S., Garcia, M. O., West, H. & Kennedy, A. Evolution of Mauna Kea Volcano, Hawaii: Petrologic and geochemical constraints on postshield volcanism. *J. Geophys. Res.* **95**, 1271–1300 (1990).

(122) Rhodes, J. M. Geochemical stratigraphy of lava flows sampled by the Hawaii Scientific Drilling Project. *J. Geophys. Res.* **101**, 11,729-11,746 (1996).

(123) Navarre-Sitchler, A., Steefel, C. I., Sak, P. B. & Brantley, S. L. A reactive-transport model for weathering rind formation on basalt. *Geochim. Cosmochim. Acta* **75**, 7644–7667 (2011).

(124) Schiffman, P., Watters, R. J., Thompson, N. & Walton, A. W. Hyaloclastites and the slope stability of Hawaiian volcanoes: Insights from the Hawaiian Scientific Drilling Project's 3-km drill core. *J. Volcanol. Geotherm. Res.* **151**, 217–228 (2006).

(125) Moore, J. G. Density of basalt core from Hilo drill hole, Hawaii. *J. Volcanol. Geotherm. Res.* **112**, 221–230 (2001).

(126) Raiswell, R., Canfield, D. E. & Berner, R. A. A comparison of iron extraction methods for the determination of degree of pyritisation and the recognition of iron-limited pyrite formation. *Chem. Geol.* **111**, 101–110 (1994).

(127) Rózański, S., Bartkowiak, A. & Jaworska, H. Forms of iron as an indicator of pedogenesis in profiles of selected soil types of the northern area of Kujawsko-Pomorskie province, Poland. *Soil Sci. Annu.* **64**, 98–105 (2013).

(128) Vazquez, M., Bauluz, B., Nieto, F. & Morata, D. Illitization sequence controlled by temperature in volcanic geothermal systems: The Tinguiririca geothermal field, Andean Cordillera, Central Chile. *Appl. Clay Sci.* **134**, 221–234 (2016).

(129) Hu, Y., Lee, B., Bell, C. & Jun, Y. S. Environmentally abundant anions influence the nucleation, growth, ostwald ripening, and aggregation of hydrous Fe(III) oxides. *Langmuir* **28**, 7737–7746 (2012).

(130) Kühnel, R. A., Roorda, H. J. & Steensma, J. J. The crystallinity of minerals-A new variable in pedogenetic processes: A study of goethite and associated silicates in laterites. *Clays Clay Miner.* **23**, 349–354 (1975).

(131) Mayer, T. D. & Jarrell, W. M. Formation and stability of iron(II) oxidation products under natural concentrations of dissolved silica. *Water Res.* **30**, 1208–1214 (1996).

(132) Pokrovski, G. S., Schott, J., Farges, F. & Hazemann, J.-L. Iron (III)-silica interactions in aqueous solution: insights from X-ray absorption fine structure spectroscopy. *Geochim. Cosmochim. Acta* **67**, 3559–3573 (2003).

(133) Thien, B. M. J., Kosakowski, G. & Kulik, D. A. Differential alteration of basaltic lava flows and hyaloclastites in Icelandic hydrothermal systems. *Geotherm. Energy* **3**, 1–32 (2015).

(134) Walsch, J. & Dultz, S. Effects of pH, Ca- and SO4-concentration on surface charge and colloidal stability of goethite and hematite – consequences for the adsorption of anionic organic substances. *Clay Miner.* **45**, 1–13 (2010).

(135) Chen, C., Kukkadapu, R. & Sparks, D. L. Influence of coprecipitated organic matter on Fe2+(aq)-catalyzed transformation of ferrihydrite: implications for carbon dynamics. *Environ. Sci. Technol.* **49**, 10927–10936 (2015).

(136) Vempati, R. K. & Loeppert, R. H. Influence of Structural and Adsorbed Si on the Transformation of Synthetic Ferrihydrite. *Clays Clay Miner.* **37**, 273–279 (1989).

(137) Parfitt, R. L., Van Der Gaast, S. J. & Childs, C. W. A structural model for natural siliceous ferrihydrite. *Clays Clay Miner.* **40**, 675–681 (1992).

(138) Stumm, W. *Chemistry of the Solid-Water Interface: Processes at the Mineral-Water and Particle-Water Interface in Natural Systems. New York* (John Wiley & Sons, 1992).

(139) Dultz, S., Boy, J., Dupont, C., Halisch, M., Behrens, H., Welsch, A.-M., Erdmann, M., Cramm, S., Helsch, G. & Deubener, J. Alteration of a Submarine Basaltic Glass under Environmental Conditions Conducive for Microorganisms: Growth Patterns of the Microbial Community and Mechanism of Palagonite Formation. *Geomicrobiol. J.* **31**, 813–834 (2014).

(140) Furnes, H. Experimental palagonitization of basaltic glasses of varied composition. *Contrib. to Mineral. Petrol.* **50**, 105–113 (1975).

(141) Franke, W. A. The durability of rocks - Developing a test of rock resistance to chemical weathering. *Am. J. Sci.* **309**, 711–730 (2009).

(142) Dultz, S., Behrens, H., Helsch, G. & Deubener, J. Electrolyte effects on surface chemistry of basaltic glass in the initial stages of dissolution. *Chem. Geol.* **426**, 71–84 (2016).

(143) Thorseth, I. H., Furnes, H. & Heldal, M. The importance of microbiological activity in the alteration of natural basaltic glass. *Geochim. Cosmochim. Acta* **56**, 845–850 (1992).

(144) Torsvik, T., Furnes, H., Muehlenbachs, K., Thorseth, I. H. & Tumyr, O. Evidence for microbial activity at the glass-alteration interface in oceanic basalts. *Earth Planet. Sci. Lett.* **162**, 165–176 (1998).

(145) Alt, J. C. & Mata, P. On the role of microbes in the alteration of submarine basaltic glass: A TEM study. *Earth Planet. Sci. Lett.* **181**, 301–313 (2000).

(146) Daughney, C., Rioux, J.-P., Fortin, D. & Pichler, T. Laboratory Investigation of the Role of Bacteria in the Weathering of Basalt Near Deep Sea Hydrothermal Vents. *Geomicrobiol. J.* **21**, 21–31 (2004).

(147) Bailey, B., Templeton, A., Staudigel, H. & Tebo, B. M. Utilization of substrate components during basaltic glass colonization by Pseudomonas and Shewanella Isolates. *Geomicrobiol. J.* **26**, 648–656 (2009).

(148) Sudek, L. A., Wanger, G., Templeton, A. S., Staudigel, H. & Tebo, B. M. Submarine basaltic glass colonization by the heterotrophic Fe(II)-oxidizing and siderophore-producing deep-sea bacterium Pseudomonas stutzeri VS-10: The potential role of basalt in enhancing growth. *Front. Microbiol.* **8**, 1–12 (2017).

(149) Edwards, K. J., Bach, W., McCollom, T. M. & Rogers, D. R. Neutrophilic iron-oxidizing bacteria in the ocean: Their habitats, diversity, and roles in mineral deposition, rock alteration, and biomass production in the deep-sea. *Geomicrobiol. J.* **21**, 393–404 (2004).

(150) Wu, L., Jacobson, A. D., Chen, H.-C. & Hausner, M. Characterization of elemental release during microbe–basalt interactions at T=28°C. *Geochim. Cosmochim. Acta* **71**, 2224–2239 (2007).

(151) Stockmann, G. J., Shirokova, L. S., Pokrovsky, O. S., Bénézeth, P., Bovet, N., Gislason, S. R. & Oelkers, E. H. Does the presence of heterotrophic bacterium Pseudomonas reactans affect basaltic glass dissolution rates? *Chem. Geol.* **296–297**, 1–18 (2012).

(152) Santelli, C. M., Edgcomb, V. P., Bach, W. & Edwards, K. J. The diversity and abundance of bacteria inhabiting seafloor lavas positively correlate with rock alteration. *Environ. Microbiol.* **11**, 86–98 (2009).

(153) Knowles, E., Staudigel, H. & Templeton, A. Geochemical characterization of tubular alteration features in subseafloor basalt glass. *Earth Planet. Sci. Lett.* **374**, 239–250 (2013).

(154) Blöthe, M., Wegorzewski, A., Müller, C., Simon, F., Kuhn, T. & Schippers, A. Manganese-Cycling Microbial Communities Inside Deep-Sea Manganese Nodules. *Environ. Sci. Technol.* **49**, 7692–7700 (2015).

(155) Mehra, O. P. & Jackson, M. L. Iron Oxide Removal from Soils and Clays by a Dithionite-Citrate System Buffered with Sodium Bicarbonate. *Clays Clay Miner.* **7**, 317–327 (1960).

(156) Schwertmann, U. Differenzierung der Eisenoxide des Bodens durch Extraktion mit Ammoniumoxalat-Lösung. *Zeitschrift für Pflanzenernährung, Düngung, Bodenkd.* **105**, 194–202 (1964).

(157) Narayanaswamy, O. S. & Gardon, R. Calculation of Residual Stresses in Glass. *J. Am. Ceram. Soc.* **52**, 554–558 (1969).

(158) Garcia, M. O. Petrography and olivine and glass chemistry of lavas from the Hawaii Scientific Drilling Project. *J. Geophys. Res.* **101**, 11701–11713 (1996).

(159) Wilson, A. D. The Micro-determination of Ferrous Iron in Silicate Minerals by a Volumetric and a Colorimetric Method. *Analyst* **85**, 823–827 (1960).

(160) Coenye, T., Laevens, S., Willems, A., Ohle, M., Hannant, W., Govan, J. R. W., Gillis, M., Falsen, E., Ccug, T. & Differential, T. Burkholderia caledonica sp . nov ., two new species isolated from the environment , animals and human clinical samples. *Int. J. Syst. Evol. Microbiol.* **51**, 1099–1107 (2001).

(161) Sebat, J. L., Colwell, F. S., Ronald, L. & Crawford, R. L. Metagenomic Profiling : Microarray Analysis of an Environmental Genomic Library. *Appl. Environ. Microbiol.* **69**, 4927–4934 (2003).

(162) Dunfield, K. E. & King, G. M. Analysis of the distribution and diversity in recent Hawaiian volcanic deposits of a putative carbon monoxide dehydrogenase large subunit gene. *Environ. Microbiol.* **7**, 1405–1412 (2005).

(163) Mailloux, B. J., Alexandrova, E., Keimowitz, A. R., Wovkulich, K., Freyer, G. A., Herron, M., Stolz, J. F., Kenna, T. C., Pichler, T., Polizzotto, M. L., Dong, H., Bishop, M. & Knappett, P. S. K. Microbial mineral weathering for nutrient acquisition releases arsenic. *Appl. Environ. Microbiol.* **75**, 2558–2565 (2009).

(164) Hedrich, S., Guézennec, A. G., Charron, M., Schippers, A. & Joulian, C. Quantitative monitoring of microbial species during bioleaching of a copper concentrate. *Front. Microbiol.* **7**, 1–11 (2016).

(165) Bray, D. Critical Point Drying of Biological Specimens for Scanning Electron Microscopy. in *Williams, J.R., Clifford, A.A. (eds) Supercritical Fluid Methods and Protocols. Methods In Biotechnology* **13**, 235–243 (Humana Press, 2000).

(166) Staudigel, H., Chastain, R. A., Yayanos, A. & Bourcier, W. Biologically mediated dissolution of glass. *Chem. Geol.* **126**, 147–154 (1995).

(167) Thorseth, I. H., Torsvik, T., Furnes, H. & Muehlenbachs, K. Microbes play an important role in the alteration of oceanic crust. *Chem. Geol.* **126**, 137–146 (1995).

(168) Bach, W. & Edwards, K. J. Iron and sulfide oxidation within basalt ocean crust: Implications for chemolithoautotrophic microbial biomass production. *Geochim. Cosmochim. Acta* **67**, 3871–3887 (2003).

(169) Kraemer, S. M. Iron oxide dissolution and solubility in the presence of siderophores. *Aquat. Sci.* **66**, 3–18 (2004).

(170) Thorseth, I. H., Furnes, H. & Tumyr, O. Textural and chemical effects of bacterial activity on basaltic glass: an experimental approach. *Chem. Geol.* **119**, 139–160 (1995).

(171) Templeton, A. S., Knowles, E. J., Eldridge, D. L., Arey, B. W., Dohnalkova, A. C., Webb, S. M., Bailey, B. E., Tebo, B. M. & Staudigel, H. A seafloor microbial biome hosted within incipient ferromanganese crusts. *Nat. Geosci.* **2**, 872–876 (2009).

(172) Cockell, C. S., van Calsteren, P., Mosselmans, J. F. W., Franchi, I. A., Gilmour, I., Kelly, L., Olsson-Francis, K. & Johnson, D. Microbial endolithic colonization and the geochemical environment in young seafloor basalts. *Chem. Geol.* **279**, 17–30 (2010).

(173) Ward, M. B., Kapitulčinová, D., Brown, A. P., Heard, P. J., Cherns, D., Cockell, C. S., Hallam, K. R. & Ragnarsdóttir, K. V. Investigating the role of microbes in mineral weathering: Nanometre-scale characterisation of the cell-mineral interface using FIB and TEM. *Micron* **47**, 10–17 (2013).

(174) Davison, W. & Seed, G. The kinetics of the oxidation of ferrous iron in synthetic and natural waters. *Geochim. Cosmochim. Acta* **47**, 67–79 (1983).

(175) Liermann, L. J., Barnes, A. S., Kalinowski, B. E., Zhou, X. & Brantley, S. L. Microenvironments of pH in biofilms grown on dissolving silicate surfaces. *Chem. Geol.* **171**, 1–16 (2000).

(176) Paul, A. & Zaman, M. The relative influences of Al_2O_3 and Fe_2O_3 on the chemical durability of silicate glasses at different pH values. *J. Mater. Sci.* **13**, 1499–1502 (1978).

(177) Kumar, B. Redox State of Iron and Its Related Effects in the $Ca0-P_205-Fe_203$ Glasses. *J. Am. Ceram. Soc.* **74**, 226–228 (1991).

(178) Rosso, K. M., Zachara, J. M., Fredrickson, J. K., Gorby, Y. A. & Smith, S. C. Nonlocal bacterial electron transfer to hematite surfaces. *Geochim. Cosmochim. Acta* **67**, 1081–1087 (2003).

(179) Herrera, A., Cockell, C. S., Self, S., Blaxter, M., Reitner, J., Arp, G., Droese, W., Thorsteinsson, T. & Tindle, A. Bacterial colonization and weathering of terrestrial obsidian in Iceland. *Geomicrobiol. J.* **25**, 25–37 (2008).

(180) Bagshaw, E. A., Cockell, C. S., Magan, N., Wadham, J. L., Venugopalan, T., Sun, T., Mowlem, M. & Croxford, A. J. The Microbial Habitability of Weathered Volcanic Glass Inferred from Continuous Sensing Techniques. *Astrobiology* **11**, 651–664 (2011).

(181) Callac, N., Rommevaux-Jestin, C., Rouxel, O., Lesongeur, F., Liorzou, C., Bollinger, C., Ferrant, A. & Godfroy, A. Microbial colonization of basaltic glasses in hydrothermal organic-rich sediments at Guaymas Basin. *Front. Microbiol.* **4**, 1–20 (2013).

(182) Einen, J., Kruber, C., Thorseth, I. H. & Torsvik, V. Microbial colonization and alteration of basaltic glass. *Biogeosciences Discuss.* **3**, 273–307 (2006).

(183) McEldowney, S. & Fletcher, M. Effect of growth conditions and surface characteristics of aquatic bacteria on their attachment to solid surfaces. *J. Gen. Microbiol.* **132**, 513–523 (1986).

(184) Pirbadian, S., Barchinger, S. E., Leung, K. M., Byun, H. S., Jangir, Y., Bouhenni, R. A., Reed, S. B., Romine, M. F., Saffarini, D. A., Shi, L., Gorby, Y. A., Golbeck, J. H. & El-Naggar, M. Y. Shewanella oneidensis MR-1 nanowires are outer membrane and periplasmic extensions of the extracellular electron transport components. *Proc. Natl. Acad. Sci.* **111**, 12883–12888 (2014).

(185) Eick, M. J., Grossl, P. R., Golden, D. C., Sparks, D. L. & Ming, D. W. Dissolution kinetics of a lunar glass simulant at 25°C: The effect of pH and organic acids. *Geochim. Cosmochim. Acta* **60**, 157–170 (1996).

(186) Goudie, A. S. & Viles, H. A. Weathering and the global carbon cycle: Geomorphological perspectives. *Earth-Science Rev.* **113**, 59–71 (2012).

(187) Michelin, A., Burger, E., Rebiscoul, D., Bruguier, F., Drouet, E., Dillmann, P. & Gin, S. Silicate Glass Alteration Enhanced by Iron: Origin and Long-Term Implications. *Environ. Sci. Technol.* **47**, 750–756 (2013).

(188) Virgo, D. & Mysen, B. O. The Structural State of Iron in Oxidized vs. Reduced Glasses at 1 Atm: A 57Fe Mössbauer Study. *Phys. Chem. Miner.* **12**, 65–76 (1985).

(189) Zhang, H. L., Hirschmann, M. M., Cottrell, E., Newville, M. & Lanzirotti, A. Structural environment of iron and accurate determination of Fe3+/ΣFe ratios in andesitic glasses by XANES and Mössbauer spectroscopy. *Chem. Geol.* **428**, 48–58 (2016).

(190) Mysen, B. O., Virgo, D. & Kushiro, I. The structural role of aluminum in silicate melts-a Raman spectroscopic study at 1 atmosphere. *Am. Mineral.* **66**, 678–701 (1981).

(191) Oelkers, E. H. & Gislason, S. R. The mechanism, rates and consequences of basaltic glass dissolution: I. An experimental study of the dissolution rates of basaltic glass as a function of aqueous Al, Si and oxalic acid concentration at 25°C and pH ، 3 and 11. *Geochim. Cosmochim. Acta* **65**, 3671–3681 (2001).

(192) Parruzot, B., Jollivet, P., Rébiscoul, D. & Gin, S. Long-term alteration of basaltic glass: Mechanisms and rates. *Geochim. Cosmochim. Acta* **154**, 28–48 (2015).

(193) Conradt, R. Chemical Durability of Oxide Glasses in Aqueous Solutions : A Review. **735**, 728–735 (2008).

(194) Furrer, G. & Stumm, W. The coordination chemistry of weathering : I . Dissolution kinetics of Al2O3 and BeO. *Geochim. Cosmochim. Acta* **50**, 1847–1860 (1986).

(195) Yue, Y. Z., Christiansen, J. & Jensen, S. L. Determination of the fictive temperature for a hyperquenched glass. *Chem. Phys. Lett.* **357**, 20–24 (2002).

(196) Pederson, L. R., Buckwalter, C. Q. & Mcvay, G. L. The Effects of Surface Area to Solution Volume on Waste Glass Leaching. *Nucl. Technol.* **62**, 151–158 (1983).

(197) Cooper, R. F., Fanselow, J. B. & Poker, D. B. The mechanism of oxidation of a basaltic glass: Chemical diffusion of network-modifying cations. *Geochim. Cosmochim. Acta* **60**, 3253–3265 (1996).

(198) Stockmann, G. J., Wolff-boenisch, D., Gislason, S. R. & Oelkers, E. H. Do carbonate precipitates affect dissolution kinetics ? 1 : Basaltic glass. *Chem. Geol.* **284**, 306–316 (2011).

(199) Drever, J. I. & Vance, G. F. Chapter 6 Role of Soil Organic Acids in Mineral Weathering Processes. in *Organic Acids in Geological Processes* (ed. Pittman, E. D.) 138–161 (Springer, 1994).

(200) Giuli, G., Paris, E., Hess, K. U., Dingwell, D. B., Cicconi, M. R., Eeckhout, S. G., Fehr, K. T. & Valenti, P. XAS determination of the Fe local environment and oxidation state in phonolite glasses. *Am. Mineral.* **96**, 631–636 (2011).

(201) Perez, A., Rossano, S., Trcera, N., Verney-Carron, A., Huguenot, D., van Hullebusch, E. D., Catillon, G., Razafitianamaharavo, A. & Guyot, F. Impact of iron chelators on short-term dissolution of basaltic glass. *Geochim. Cosmochim. Acta* **162**, 83–98 (2015).

(202) Waff, H. S. The structural role of ferric iron in silicate melts. *Can. Mineral.* **15**, 198–199 (1977).

(203) Gautier, J.-M., Oelkers, E. H. & Schott, J. Are quartz dissolution rates proportional to B.E.T. surface areas ? *Geochim. Cosmochim. Acta* **65**, 1059–1070 (2001).

(204) Briese, L., Arvidson, R. S. & Luttge, A. The effect of crystal size variation on the rate of dissolution – A kinetic Monte Carlo study. *Geochim. Cosmochim. Acta* **212**, 167–175 (2017).

(205) Bunker, B. C. Molecular mechanisms for corrosion of silica and silicate glasses. **179**, 300–308 (1994).

(206) Cama, J. & Ganor, J. The effects of organic acids on the dissolution of silicate minerals : A case study of oxalate catalysis of kaolinite dissolution. **70**, 2191–2209 (2006).

(207) Johnson, S. B., Yoon, T. H., Slowey, A. J. & Brown, G. E. Adsorption of Organic Matter at Mineral / Water Interfaces : 3 . Implications of Surface Dissolution for Adsorption of Oxalate. *Langmuir* **20**, 11480–11492 (2004).

(208) Chemtob, S. M. & Rossman, G. R. Timescales and mechanisms of formation of amorphous silica coatings on fresh basalts at Kīlauea Volcano, Hawai'i. *J. Volcanol. Geotherm. Res.* **286**, 41–54 (2014).

(209) Crovisier, J. L., Honnorez, J., Fritz, B. & Petit, J. C. Dissolution of subglacial volcanic glasses from Iceland: laboratory study and modelling. *Appl. Geochemistry* **7**, 55–81 (1992).

(210) Panias, D. & Paspaliaris, I. Calculated Solubility of Trivalent Iron and Aluminum in Oxalic Acid Solutions at 25 ° C . *Can. Metall. Q.* **40**, 421–432 (2001).
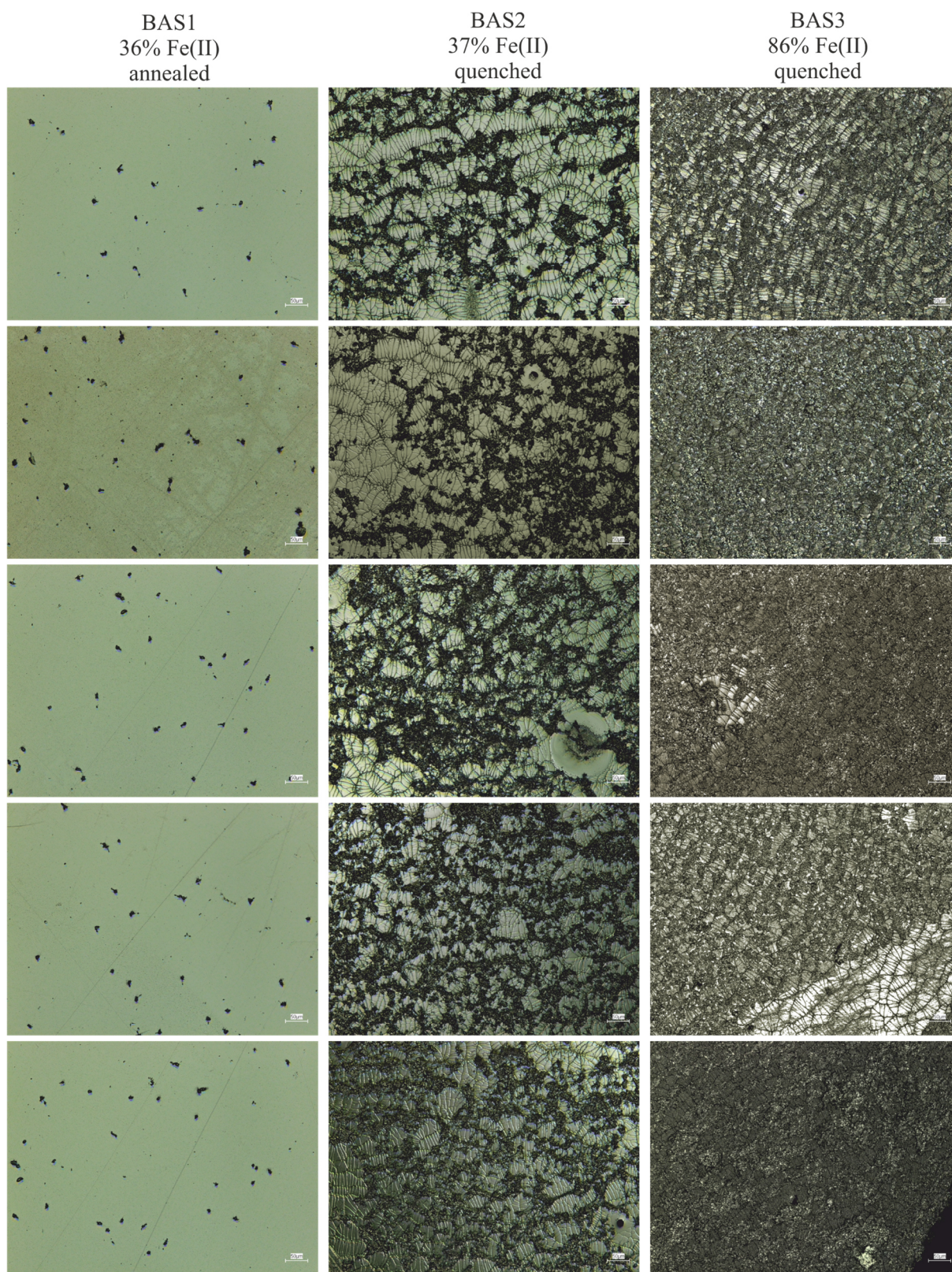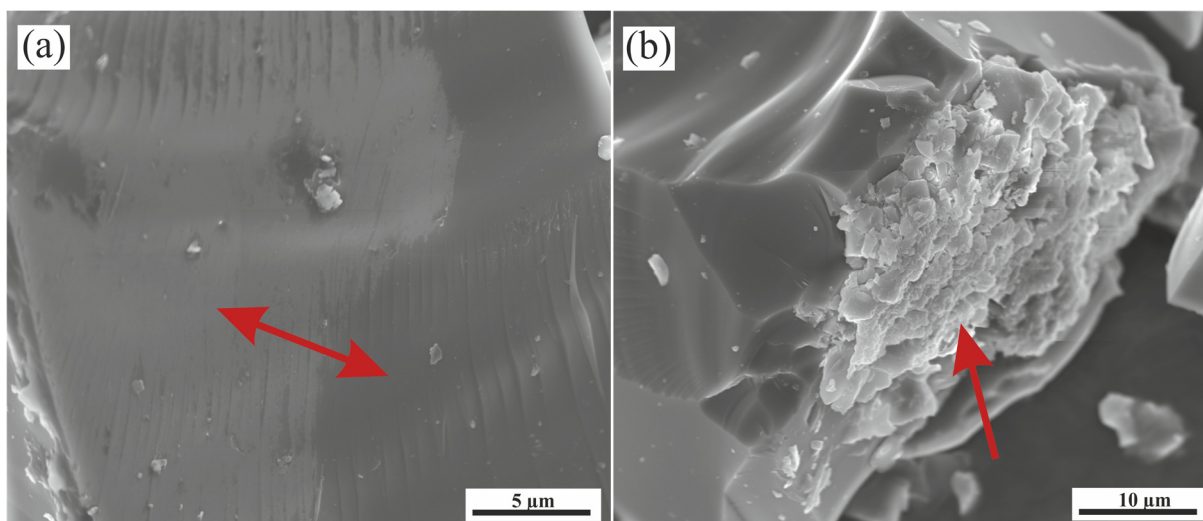
Supplemental Figures
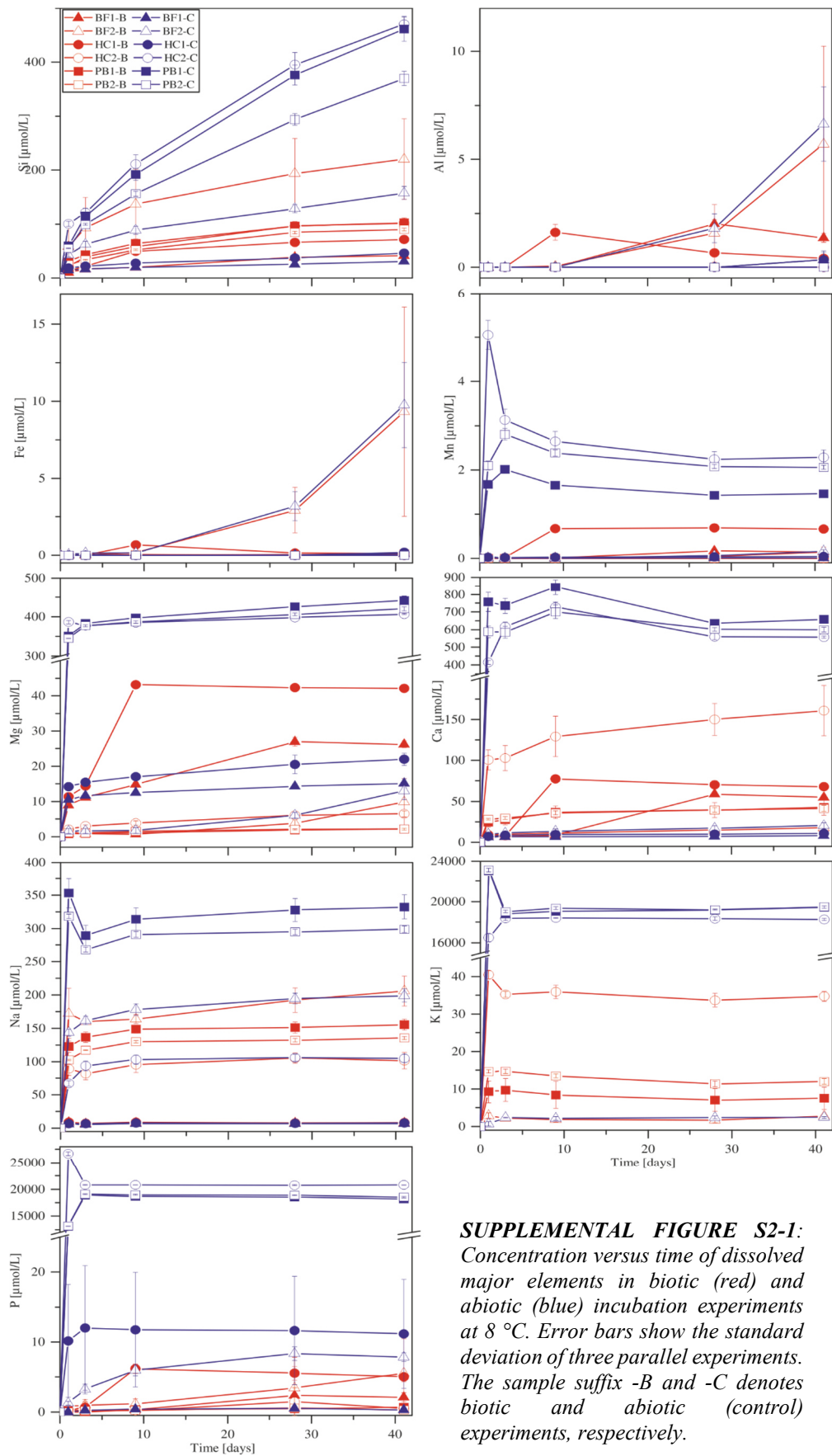
SUPPLEMENTAL FIGURE S2-1: *Concentration versus time of dissolved major elements in biotic (red) and abiotic (blue) incubation experiments at 8 °C. Error bars show the standard deviation of three parallel experiments. The sample suffix -B and -C denotes biotic and abiotic (control) experiments, respectively.*
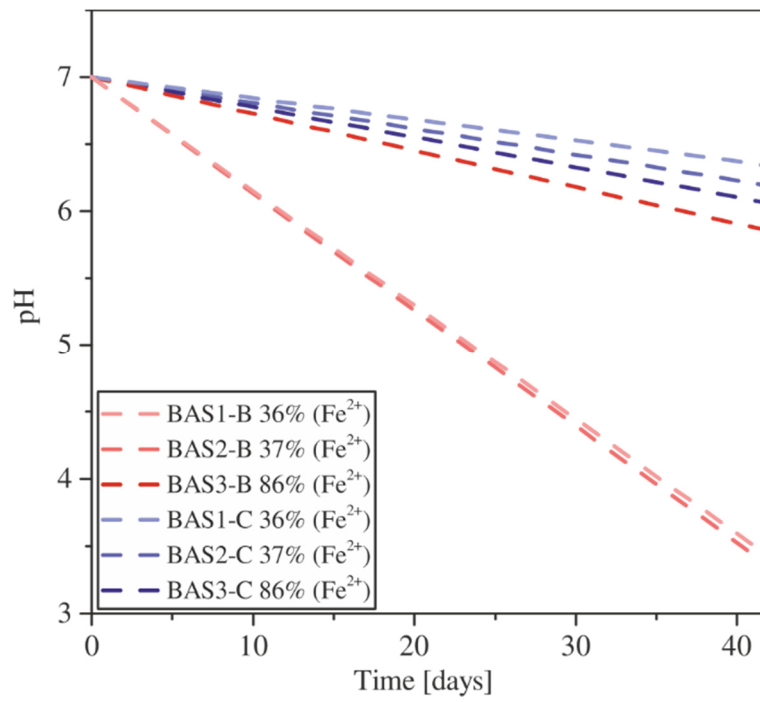
SUPPLEMENTAL FIGURE S2-2: *pH evolution for biotic (red) and abiotic (blue) colonization experiments at 30 °C. The sample suffix -B and -C denotes biotic and abiotic (control) experiments, respectively.*

SUPPLEMENTAL FIGURE S2-3: *Surface morphologies of synthetic basaltic glasses (from left to right: BAS1 - BAS2 - BAS3). The number of cells adhering to the glass surfaces increases with increasing residual stress.*

SUPPLEMENTAL FIGURE S3-1*: Scanning electron micrographs of percolation experiments with synthetic basaltic glasses. **(a)** basalt glass B-OQ altered at pH 2 with the addition of 1 mM oxalic acid for 388 h. Part of the surface is covered with a nm thick alteration layer (light shining; red arrow). The layer seemed to be scratched and not fully intact. **(b)** basalt glass B-RQ altered at pH 2 for 388 h. A conglomerate of small particles enriched in SiO₂ adheres to the surface of the basalt glass (red arrow).*
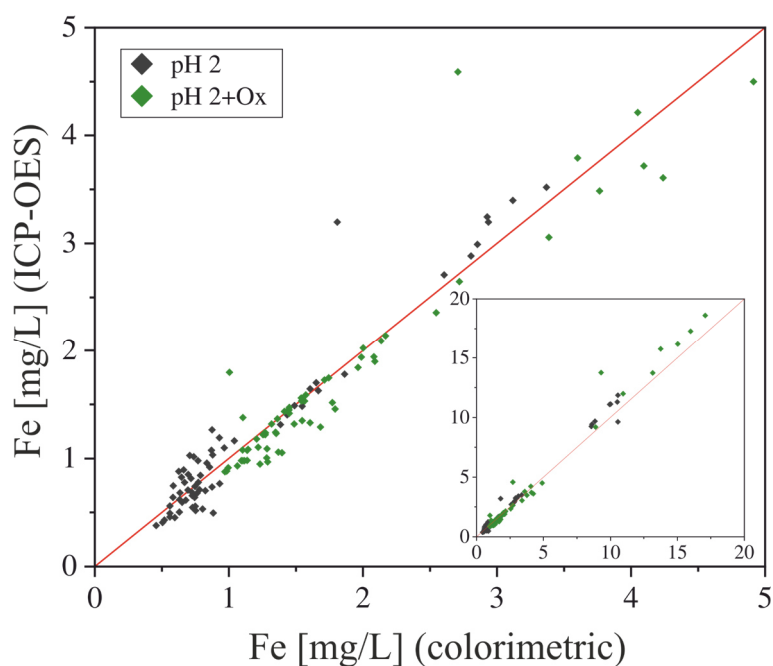
SUPPLEMENTAL FIGURE S3-2*: Comparison of dissolved Fe concentrations measured by spectrophotometrically vs ICP-OES. Concentrations < 5 mg/L Fe are enlarged. The full data points are shown in the reduced plot. Red line shows a ratio of 1:1 for Fe concentrations measured spectrophotometrically and by ICP-OES.*

Curriculum Vitae

❖ Personal Details

Marius Stranghöner

25.11.1990 in Herford, German citizenship

❖ Work experience

| 08/2016 – today | **Research assistant** |
| | Institut für Mineralogie, Leibniz Universität Hannover, Germany |

| 11/2011 – 10/2015 | **Student assistant** |
| | Institut für Mineralogie, Leibniz Universität Hannover, Germany |

❖ Education

08/2016 – today	**PhD Student**
	Institut für Mineralogie, Leibniz Universität Hannover, Germany
	Thesis: „Alteration of Subsurface Basaltic Rocks and Glasses: Implications of Environmental, Chemical and Structural Properties on Fe Mobilization"

10/2013 – 10/2015	**Master´s studies in Geoscience with focus on Mineralogy/Geochemistry**
	Leibniz Universität Hannover, Germany
	Thesis: „Investigations on the iron specification in lithium iron Phosphate Glasses"

10/2010 – 09/2013	**Bachelor´s studies in Geoscience**
	Leibniz Universität Hannover, Germany
	Thesis: „Experimentelle Bestimmung von Phasenbeziehungen in trachytischen Schmelzen"

| 08/2007 – 06/2010 | **Abitur** |
| | Friedrichs-Gymnasium Herford, Germany |

List of Publications

Journals (peer reviewed)

Stranghoener, M., Schippers, A., Dultz, S., Behrens, H. (2018): Experimental microbial alteration and Fe mobilization from basaltic rocks of the ICDP HSDP2 drill core, Hilo, Hawaii. Front. Microbiol. 9:1252. doi:10.3389/fmicb.2018.01252.

Conference Abstracts

Stranghoener, M., Dultz, S., Behrens, H., Schippers, A., (2019): Implications of subsurface basaltic rock alteration on the supply of soluble Fe to ocean surface waters – a study on ICDP site Hawaii, Annual ICDP/IODP meeting Köln.

Stranghoener, M., Schippers, A., Dultz, S., Behrens, H. (2018): Microbially mediated alteration and Fe mobilization from basaltic rocks of the HSDP2 drill core, Hilo, Hawaii, Annual ICDP/IODP meeting Bochum.

Stranghoener, M., Behrens, H., Welsch, A. M. (2017): Iron specification in lithium iron phosphate glasses. 12th Pacific Rim Conference on Ceramic and Glass Technology, Hilo, Big Island (Hawaii)

Stranghoener, M., Behrens, H., Dultz, S., Schippers, A. (2017): Interface driven Fe transfer from volcanic rocks of ICDP site Hawaii to ocean surface waters, Annual ICDP/IODP meeting Braunschweig.